Old Dominion University

ODU Digital Commons

Spring 2010

Cellular Immunity in Mouse Models of Viral Encephalitis

Christina Dawn Steel
Old Dominion University

Recommended Citation

CELLULAR IMMUNITY IN MOUSE MODELS OF VIRAL

ENCEPHALITIS

by

Christina Dawn Steel

B.S., 2001, Radford University

B.A., 2001, Radford University

A Dissertation Submitted to the Faculty of Eastern Virginia Medical School and

Old Dominion University in Partial Fulfilment of the

Requirement for the Degree of

DOCTOR OF PHILOSOPHY

BIOMEDICAL SCIENCES

EASTERN VIRGINIA MEDICAL SCHOOL AND

OLD DOMINION UNIVERSITY

May 2010

Approved by:

_____
Richard P. Ciavarra (Director)

Julie A. Kerry (Member)

_____
Christopher J. Osgood (Member)

_____
Edward M. Johnson (Member)

ABSTRACT

CELLULAR IMMUNITY IN MOUSE MODELS OF VIRAL ENCEPHALITIS

Christina Dawn Steel

Eastern Virginia Medical School and Old Dominion University, 2010

Director: Dr. Richard P. Ciavarra

Evidence is presented herein that intranasal application of vesicular stomatitis virus (VSV) caused acute infection of the murine central nervous system (CNS) with associated morbidity and significant mortality in mice. However, VSV encephalitis was not invariably fatal, suggesting that the CNS contained a professional antigen-presenting cell (APC) capable of inducing or propagating a protective antiviral immune response. To examine this possibility, we administered VSV via the intranasal route and then characterized the cellular elements that infiltrate the brain as well as the activation status of resident microglia, cells widely believed to represent the major APC population in the CNS. To exclude a contribution of peripheral dendritic cells (DCs), a population with documented APC activity *in vivo* and capable of infiltrating the inflamed CNS, studies were conducted in a conditional ablation transgenic mouse model that allowed for the selective depletion of these cells with diphtheria toxin (DT). Microglia isolated from infected brains rapidly upregulated expression of major histocompatibility complex (MHC) class I antigens, program death receptor 1 (PD-1) and underwent a microgliosis indicating virus-induced activation and expansion. Peripheral blood cells started to infiltrate the virus infected brain around days 4-5, peaked on day 8 and achieved basal trace levels at 21 days post infection. The infiltrate was composed primarily of myeloid cells ($CD45^{high}CD11b^+$), $CD4^+$ and $CD8^+$ T cells; the latter subset containing cells specific for the immunodominant VSV nuclear protein epitope. Although the $CD45^{high}CD11b^+$ phenotype suggests that these cells are macrophages, subsequent 4-5-color flow cytometry demonstrated that this was primarily a granulocytic response ($CD45^{high}CD11b^+Gr-1^+F4/80^-$). The T cell infiltrate correlated temporally with a rapid and sustained upregulation of class I expression on microglia, whereas class II expression was markedly delayed. Ablation of peripheral DCs profoundly inhibited the inflammatory response as well as infiltration of virus-specific $CD8^+$ T cells and this correlated with inefficient viral clearance in the brain and

increased morbidity/mortality. Unexpectedly, the VSV-induced interferon-gamma (IFN-γ) response in the CNS remained intact in mice rendered deficient of DCs suggesting that a resident brain cell produced this cytokine. In summary, these studies expanded prior work on the changes in resident microglia and the composition of brain leukocytes in the encephalitic brain. In addition, data demonstrated that peripheral DCs play an essential role *in vivo* in the inflammatory and certain components of the adaptive primary antiviral immune response in the CNS and as a result, modulate viral clearance and survivability for this pathogen.

Because macrophages may also function as APCs *in vivo*, we used two different approaches to ablate peripheral macrophages *in vivo* to examine their role in VSV encephalitis and viral clearance in the CNS. Chemical ablation of macrophages using AP20187 in the MAFIA (macrophage fas-induced apoptosis) conditional ablation model did not diminish microglia numbers or activation and failed to alter the cellular composition of the infiltrate. In contrast, ablation of phagocytic cells by intravenous liposome-encapsulated clodronate administration markedly suppressed the influx of leukocytes into the brain including CD8$^+$ VSV-specific T cells and enhanced morbidity/mortality despite normal viral clearance from the brain. Intracerebroventricular (ICV) infusion of clodronate did not impair VSV encephalitis and eliminated a role for brain perivascular macrophages (PVM) and/or meningeal macrophages as contributors to viral clearance or antigen presentation.

In summary, VSV encephalitis was characterized by i) microglial activation and expansion, ii) a prominent and early myeloid infiltrate dominated by granulocytes with smaller contributions of CD11c+ DCs and macrophages, iii) a lymphoid infiltrate of CD4$^+$ and CD8$^+$ T cells including a subset specific for the immunodominant nuclear protein epitope and iv) the absence of significant numbers of pDCs, B cells, NK and NK T cells. A role for peripheral DCs in the development of innate and adaptive antiviral immunity in the CNS, viral clearance and survivability was demonstrated *in vivo* using a conditional ablation mouse model. Enhanced VSV encephalitis was observed following depletion of circulating or brain-resident macrophages in the MAFIA transgenic model and following ICV infusion of liposome-encapsulated clodronate. These data suggest that macrophages enhance pathogenesis during viral infections of the CNS.

The way to do research is to attack the facts at the point of greatest astonishment.

~Celia Green, The Decline and Fall of Science, 1972

ACKNOWLEDGMENTS

I would first like to express my gratitude to my doctoral advisor, Dr. Richard Ciavarra, for his support and guidance in developing and conducting these studies and resulting publications. Without his mentorship, patience, and assistance, I would not have been able to accomplish this journey of personal and scientific discovery. His kindness and willingness to provide second, third, and fourth chances helped me persist despite the difficulties. The assistance of my co-workers, Ms. Amber Stephens, Ms. Suzanne Hahto, and Dr. Nazita Yousefieh, provided invaluable help during the course of these studies. I would also like to thank the laboratories of Dr. Ann Campbell, Dr. Edward Johnson, and Dr. Julie Kerry, for the use of equipment that was critical to the completion of these studies. I would particularly like to thank Dr. Julie Kerry for her critical reading of my first submission of this dissertation; without her comments and suggestions for revision, I would not have noticed the patterns in my data that finally enabled me to develop a model for CNS infection. Dr. Victoria Cavanaugh provided training on some of the mouse techniques used to treat mice during the course of these studies. Dr. Woong-Ki Kim provided outstanding support and training with use of the flow cytometer, and also performed the immunohistochemical studies presented herein. I extend my gratitude to Dr. Charles Kugler, my undergraduate advisor, who inspired my interest in Biology.

For their personal support, I would like to thank Mr. Richard Ryburn and Mrs. Sharon Rust-Ryburn for their emotional support and for believing in me. I owe particular thanks to Mr. Ryburn for his help in reconciling some diverse data into an integrated model of antiviral immunity. My parents, Mr. Mark Steel and Mrs. Diane Steel, encouraged me to pursue my education. Finally, I thank my friend Ms. Carrie Sullivan, who helped me with coffee when needed.

TABLE OF CONTENTS

LIST OF TABLES

LIST OF FIGURES

CHAPTER I

INTRODUCTION

The immunological response to viral infection is complex and highly choreographed. The central nervous system (CNS) has long been held as an immunologically privileged site because of its inability to eliminate antigenic stimuli in the parenchyma. Immunological privilege is largely attributed to the blood-brain barrier (BBB) (Galea et al., 2007a) and the absence of a classical lymphatic system. However, this view of the CNS as an immunocompromised site is rapidly changing. More recent studies indicate that BBB permeability is altered in response to injury or infection and permits the infiltration of peripherally-derived leukocytes. Some areas of the brain are not protected by the BBB (meninges, choroid plexus, circumventricular organs and ventricles (Farina et al., 2007; Galea et al., 2007a). Several studies have demonstrated the presence of small populations of peripherally-derived leukocytes that patrol the naïve CNS (Bechmann et al., 2007; Galea et al., 2007a). Finally, many cells of the CNS possess some intrinsic immunological capacity (Hart and Fabry, 1995). Thus, it is more appropriate to consider the CNS an unique immunological microenvironment. The immune response of the CNS must be orchestrated differently from in the periphery of an animal; inflammation and cytotoxicity in the brain would result in loss of critical neurons and other cell types. These cells do not repopulate quickly or well; their loss represents a devastating impact on survival. Therefore, understanding how the immune response in the CNS differs from that of the periphery represents an unique challenge and an important topic of study.

To date, most research in CNS immunity has focused on demyelinating diseases such as experimental autoimmune encephalomyelitis (EAE) and persistent infections such as Theiler's murine encephalomyelitis virus (TMEV), primarily with regard to development of treatments for multiple sclerosis. Although these studies provide insights into the general inflammatory and adaptive immune responses in the CNS, they may not accurately reflect the events during acute viral infection.

The model journal for this dissertation is Glia.

More recently, several viruses capable of producing acute infections in the CNS of mice have been studied, including lymphocytic choriomeningitis virus (LCMV), rabies virus, Borna disease virus, Theiler's murine encephalitis virus, and Sindbis virus.

However, with the exception of rabies, these models do not address cytolytic infections such as VSV. Understanding neurological viral infections is critical to the treatment of several human diseases that are caused by or may include acute phases of infection. The primary cause of acute viral infections of the CNS is from arboviruses, including West Nile virus, Equine encephalitis viruses, Crimean-Congo haemorrhagic fever, Rift Valley Fever virus, Dengue, and Yellow fever (Binder and Griffin, 2003a; Binder and Griffin, 2003b). Additional viruses that may result in acute-phase infections include HIV, several herpes viruses, measles, and rabies (Nair et al., 2007; Nelson et al., 2002; Ponomarev et al., 2005a). Developing a model for antiviral immunity in the CNS could provide therapeutic targets for acute viral infections in humans as well as animals. Therefore, this work focuses on characterizing the immune response in the CNS to an acute viral infection.

At a very simplistic level, two aspects of the immune response are relevant: the innate (nonspecific) and adaptive (antigen-specific) responses. Both are involved in antiviral immunity in response to peripheral infections. The innate immune response is generally characterised by an influx of myeloid cells, including macrophages, dendritic cells, natural killer cells, and granulocytes, whose functions are to induce inflammation, recognize and destroy pathogens and to stimulate the adaptive immune response via antigen presentation and cytokine/chemokine secretion. For CNS infections, the innate immune system is rarely sufficient to clear virus (Griffin, 2003; Ireland and Reiss, 2006). The adaptive immune response is activated when the innate immune response fails to clear the antigen source, and is characterised by an infiltrating population of lymphocytes that are specific for the pathogen in question. These antigen-specific cells also recognise and destroy pathogens and infected cells and provide a pool of immunologic memory cells (Janeway et al., 2001). In all models of CNS inflammation, infection, or injury, cells from both the innate and adaptive responses have been demonstrated to enter the CNS. Their recruitment to the CNS, activation, and effector functions, however, remain poorly characterised.

In general, resolution of a viral infection follows a typical course beginning with viral replication and recruitment of nonspecific (innate) leukocytes such as granulocytes, macrophages, and dendritic cells. Dendritic cells enter the lymphatic system, secreting various cytokines that will serve to direct additional leukocytes to the infected location. Once in the draining lymph node, they present antigen to and activate lymphocytes, which rapidly migrate out of the lymph nodes and home toward the site of infection, directed by DC-secreted cytokine/chemokine gradients. Antigen-specific lymphocytes and innate leukocytes may secrete additional antiviral chemokines/cytokines, induce cell-contact-dependent apoptosis, or phagocytose infected target cells to mediate viral clearance. The next sections describe cell types and events likely to be critical to understanding antiviral immunity in the CNS.

Anatomy and biology of the brain

As previously noted, the brain is commonly considered to be immunologically privileged due to the blood-brain barrier (BBB). Until recently, it was held that the BBB represented a nearly impenetrable barrier through which only select substances may pass. Although the brain is generally considered to be a single organ, it possesses at least three distinct microenvironments defined by proximity to the blood-brain barrier (BBB): the parenchyma of the brain (protected by the BBB), the perivascular spaces on the border between the peripheral circulatory system and the BBB, and areas of the brain are not protected by the BBB (meninges, choroid plexus, circumventricular organs and ventricles (Farina et al., 2007; Galea et al., 2007a). The history of the BBB and its more modern view are thoroughly reviewed in (Bechmann et al., 2007). More recent studies indicate that BBB permeability is altered in response to injury or infection and permits the infiltration of peripherally-derived leukocytes (Archambault et al., 2005; Galea et al., 2007b; Komatsu et al., 1999; Lees et al., 2006; Nag, 2003; Pardridge, 1999; Persidsky, 1999; Persidsky et al., 1999). Several studies have demonstrated the presence of small populations of peripherally-derived leukocytes that patrol the naïve CNS (Bechmann et al., 2007; Galea et al., 2007a).

Parenchymal cell types

Many cells of the CNS possess some intrinsic immunological capacity (Hart and Fabry, 1995). In the CNS parenchyma, there are three primary cell types: neurons, astrocytes, and glial cell types. Neurons are generally considered to be immunologically quiescent cells, but a handful of studies imply that they may be able to directly participate in antiviral immunity, though their roles are unclear (Delhaye et al., 2006; Neumann, 2001). Astrocytes are generally considered to be support scaffold cells for neurons, and the end-feet of astrocytes form the basement membrane of the BBB (Bechmann et al., 2007). Their potential role in antiviral immunity has been more thoroughly investigated than for neurons. Independent of their structural role in forming the BBB, astrocytes react to infections of the CNS. They have been shown to produce nitric oxide (a common cytotoxic/antiviral mechanism for viral clearance) (Barna et al., 1996), as well as several cytokines and chemokines involved in immunity (refer to Appendix B), most of which are chemotactic for monocytes and macrophages (Barna et al., 1996; Constantinescu et al., 1996; Dong and Benveniste, 2001; Farina et al., 2007; Pardridge, 1999; Persidsky et al., 1999; Speth et al., 2007). Further evidence indicates that astrocytes may be able to present antigen (Aloisi et al., 1998; Barna et al., 1996; Farina et al., 2007; Persidsky et al., 1999; Speth et al., 2007), though these data are primarily based on *ex vivo* culture studies and may not reflect *in vivo* capacity. Of the resident CNS cells with immunological capacity, microglia are widely regarded as the most critical and represent approximately 10-20% of the brain parenchyma (Havenith et al., 1998; Lawson et al., 1990; Rock et al., 2004; Santambrogio et al., 2001; Town et al., 2005). They are also thought to provide a liaison between the immune and nervous systems (Ponomarev et al., 2005a; Ponomarev et al., 2005b). The origin of microglia is a hotly debated issue. Some studies indicate that they derive from monocyte precursors and migrate to the CNS during embryonic development, with poor subsequent repopulation from the periphery (Neumann, 2001; Town et al., 2005). However, others have demonstrated that some peripheral monocyte/macrophage cells from the periphery assume a microglial-like morphology and phenotype upon entry to the CNS following trauma or infection (Flugel et al., 2001; Town et al., 2005). Despite their shrouded origins, microglia are phenotypically characterised by an uniquely low to intermediate expression of CD45 (Ponomarev et al., 2005a; Ponomarev et al., 2005b) and CD11b (Ponomarev et al., 2005b) and have a characteristic ramified

morphology when resting (Ponomarev et al., 2005b; Santambrogio et al., 2001; Town et al., 2005). CD45 is an antigen widely expressed on leukocytes. Early characterization of this molecule revealed a role *in vitro* for macrophage adhesion (Roach et al., 1997). Microglia also express common macrophage markers such as CD11b, (commonly referred to as Mac-1, an α-integrin associated with cellular adhesion and is expressed on a wide variety of leukocytes) and F4/80 (which is expressed at low levels on microglia and high levels on macrophages). The biological function of the F4/80 target (an epidermal growth factor membrane protein) in immunity remains unclear (van den Berg and Kraal, 2005). Resting microglia are CD11c⁻ (also an α-integrin variant, common to DCs), and are slightly smaller than peripheral $CD45^{high}$ leukocytes (Ford et al., 1995). Microglia have been shown to respond (via activation and/or proliferation) to a wide variety of CNS events, including injury, ischaemia, autoimmune disorders, infection, and even aging (Ackman et al., 2006; Aloisi, 2001; Barna et al., 1996; Bulloch et al., 2008; Cosenza-Nashat et al., 2006; Getts et al., 2008; Hickey, 2001; Juedes and Ruddle, 2001; Katz-Levy et al., 1999; Lalancette-Hebert et al., 2007; Mack et al., 2003; Miller et al., 2007; Morris et al., 1997; Nair et al., 2007; Nelson et al., 2002; Persidsky et al., 1999; Ponomarev et al., 2005b; Raivich et al., 1994; Reichmann et al., 2002; Rock et al., 2004; Schilling et al., 2003; Stichel and Luebbert, 2007; Stoll and Jander, 1999; Stoll et al., 1998; Town et al., 2005; Watanabe et al., 1999) . On infection, the microglia become activated (Ponomarev et al., 2005a; Ponomarev et al., 2005b), upregulating several cell surface antigens, including MHC II, CD80, and CD40 (Ponomarev et al., 2005a; Ponomarev et al., 2005b), and assume a more spheroid shape. Microglia are also potent producers of a wide variety of cytokines and chemokines, depending on the stimulus (again, refer to Appendix B) (Aloisi, 2001; Nelson et al., 2002; Neumann, 2001; Olson and Miller, 2004; Persidsky, 1999; Prat et al., 2001; Rock et al., 2004; Speth et al., 2007; Walker et al., 2006; Wang and Suzuki, 2007). Thus, clarifying the role of microglia in antiviral immunity of the CNS will be an important focus of this work.

Perivascular cell types

The perivascular spaces were initially termed lymphatic clefts by Goldman (Bechmann et al., 2007). This is an apt description, given the diversity of cell types that may be found in these regions. Current studies have clearly demonstrated localization of macrophages to these regions, which may

produce a localized region architecturally similar to lymphoid tissue (also known as tertiary lymphoid regions, (Galea et al., 2007a; Persidsky, 1999). Additional relevant cellular elements (DC, T cells, macrophages) that reside there may be sufficient to drive T cell activation and clonal expansion (Bechmann et al., 2007; Fischer and Reichmann, 2001; Matyszak and Perry, 1996; Newman et al., 2005). The brain also contains two strategically located macrophage populations, perivascular macrophages (PVM) and meningeal macrophages (MM), which represent the major macrophage populations resident in the brain. Several recent studies have demonstrated that macrophages residing in the perivascular spaces in the CNS play a key role in mediating the antiviral immune response and may be more important than microglia for antiviral immunity (Fabriek et al., 2005; Kim et al., 2006; Perry, 1998; Persidsky, 1999; Polfliet et al., 2001b), although not all models agree (Galea et al., 2007b; Williams et al., 2001). Perivascular and meningeal macrophages are continuously repopulated from the periphery (Kim et al., 2006; Neumann, 2001; Stoll and Jander, 1999; Williams et al., 2001). Their function(s) in the CNS, however, remains poorly defined.

Infiltrating cell types

Several studies have demonstrated the presence of small populations of peripherally-derived leukocytes that patrol the naïve CNS (Bechmann et al., 2007; Galea et al., 2007a). Virtually all immune effector cells have been demonstrated to enter the CNS following injury or infection. These include both the nonspecific macrophages, dendritic cells, and natural killer cells, and granulocytes as well as adaptive, specific T cells and B cells (Bi et al., 1995a; Glabinski and Ransohoff, 1999; Persidsky, 1999; Rubin and Staddon, 1999). Therefore, it will be critically important to first determine which cell types are detectable in the CNS of virally infected animals for our own model.

Vesicular stomatitis virus

Vesicular stomatitis virus (VSV) is a neurotrophic ssRNA virus of the Vesiculovirus genus in the Rhabdoviridae family and is the prototypic virus of this family that includes rabies virus. This virus is used as a model for nearly all negative-sense ssRNA viruses, including measles. Currently, VSV is widely used

in laboratories due to its simple genome encoding only five proteins, leading to ease of manipulation. The glycoprotein (G) allows for fusion with the host cell membrane, thus permitting viral entry. The acid environment of endocytic vesicles results in the release of the negative-sense ssRNA, which is transcribed to a positive-sense RNA strand by the VSV-L polymerase in conjunction with the phosphoprotein (VSV-P). As the host cells produce new transcripts and proteins, the matrix proteins (VSV-M) assemble into new virions encapsulating the viral genome and copies of the encoded proteins. The nucleocapsidprotein (N) coats the viral genome and associates with the matrix proteins during assembly. The nucleoprotein also includes the immunodominant epitope for antiviral recognition by $CD8^+$ cytotoxic T lymphocytes (CTLs)(Puddington et al., 1986). VSV produces a cytolytic infection that has been well-characterised with regard to innate (nonspecific), biochemical (cytokine and chemokine), cellular (lymphocyte), and humoral (antibody-mediated) immune responses in mice (Buckler and Baron, 1966; Ciavarra and Burgess, 1988; Ciavarra and Tedeschi, 1994; Gobet et al., 1988). Following systemic infection, immunocompetent mice rapidly clear VSV from peripheral organs, produce IgM and neutralizing IgG antibodies and mount a robust CTL response although viral antigens persist for weeks in peripheral tissues (Battegay et al., 1996; Turner et al., 2007). When VSV is delivered via the intranasal route, it initially infects and replicates in olfactory receptor neurons and is then transmitted via the olfactory nerve to the central nervous system (CNS) within 12-24 hours (Forger et al., 1991; Plakhov et al., 1995). VSV replicates invasively in the olfactory bulb (OB) penetrating deeper layers of this structure, reaching the OB ventricle by days 4-5 post infection producing focal cytopathology. Depending on the dose and strain, virus can enter the ventricles causing inflammation and necrosis around the ventricles and travel caudally to the hindbrain by day 8 post infection. VSV does not use the trigeminal nerve for entry into the brain, as the trigeminal ganglion remains virus-free following intranasal infection (Reiss et al., 1998).

Fig. 1 offers a visual map to VSV progression through the brain during infection. Although VSV infection of the CNS is associated with a high rate of morbidity and mortality, surviving mice completely clear infectious virus from the brain around days 10-12. We previously demonstrated that approximately one-third of mice acutely depleted of DC *in vivo* and infected peripherally with vesicular stomatitis virus (VSV) developed persistent brain infections (Ciavarra et al., 2006), characterised by a failure to clear VSV

from the CNS accompanied by weight loss, hindlimb paralysis, extreme morbidity and mortality. Because it was impossible to predict which mice supported CNS infections prior to euthanasia, we moved to an intranasal mode of VSV application that allowed us to achieve reproducible CNS infections in all mice.

The susceptibility to and kinetics of VSV infection in the CNS were first described by the laboratories of Dr. Carol Reiss, and varied with mouse strain and gender (Barna et al., 1996; Forger et al., 1991). The work of Huneycutt et al. demonstrated that VSV antigen was detectable in the olfactory bulb as early as 12 hours post-infection and spread caudally through the forebrain by 7 days post-infection, with only a few areas of the midbrain demonstrating antigen reactivity (Huneycutt et al., 1994). Previous studies by Reiss and colleagues demonstrated a high rate of morbidity/mortality in this model that correlated with high titres of VSV at 7 days post-infection and loss of the BBB function late in the infection. Surviving mice efficiently cleared VSV from the CNS, suggesting that the host can mount an efficient antiviral immune response in the CNS (Barna et al., 1996; Huneycutt et al., 1994; Plakhov et al., 1995). These data was further supported by immunohistochemical studies that demonstrated a VSV-induced CNS infiltrate composed primarily of macrophages and lymphocytes (Bi et al., 1995a).
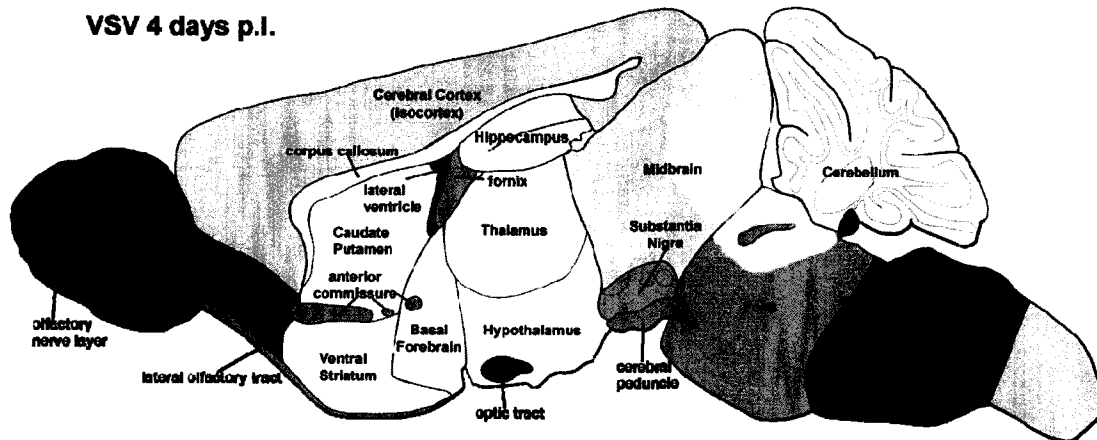
Fig. 1. *Kinetics of VSV spread through the CNS of intranasally infected mice.*

This figure represents the caudal spread of VSV through the CNS following intranasal application of virus based on immunohistochemical results for the immunodominant VSV epitope (N_{52-59}) defined by Reiss et al. (Bi et al., 1995a). VSV antigen is detectable as early as 12 hours post-infection and spreads caudally through various midbrain structures by 8 days post-infection. Mice that survive infection typically clear infection by 10-12 days post infection. Areas unaffected by virus are rendered in white. Image modified from "The Gene Expression Nervous System Atlas (GENSAT) Project, NINDS Contracts N01NS02331 & HHSN271200723701C to The Rockefeller University (New York, NY). (2008)"

Antigen presentation

Dendritic cells (DC) continuously circulate throughout peripheral tissues as sentinels, sampling the environment for foreign antigens (Andrews et al., 2003). These cells are currently held as the most crucial and specialised antigen-presenting cell (APC) (Lipscomb and Masten, 2002; Matyszak and Perry, 1996; Megjugorac et al., 2004; Pozzi et al., 2005; Probst and van den Broek, 2005; Randolph et al., 2005). On encounter with foreign antigen, they migrate to various lymphoid tissues where they present antigen to naïve T and B cells (Bjorck, 2001; Lipscomb and Masten, 2002; Matyszak and Perry, 1996; Randolph et al., 2005). The current immunological paradigm holds DC as the exclusive cell type capable of activating a naïve T cell (Abbas and Sharpe, 2005; Probst and van den Broek, 2005; Serbina and Pamer, 2003). Thus, they represent a bridge between the innate and adaptive immune responses.

On encounter with foreign antigen, DCs migrate to various lymphoid tissues where they present antigen to naïve T and B cells (Bjorck, 2001; Lipscomb and Masten, 2002; Matyszak and Perry, 1996; Randolph et al., 2005). The current immunological paradigm holds DC as the exclusive cell type capable of activating a naïve T cell (Abbas and Sharpe, 2005; Probst and van den Broek, 2005; Serbina and Pamer, 2003). Several subsets of DC exist, including the myeloid (CD8α-) and lymphoid (CD8α+) DC and plasmacytoid DC (pDC) (Andrews et al., 2003; Kronin et al., 2000; Lipscomb and Masten, 2002; Megjugorac et al., 2004; Town et al., 2005). Plasmacytoid DC are highly specialised and are often referred to as interferon-producing cells (IPC) for their unique ability to produce large amounts of Type 1 interferon (IFN-α/β) in response to pathogens (2003; Andoniou et al., 2005; Andrews et al., 2003; Barchet et al., 2002; Bjorck, 2001; Fitzgerald-Bocarsly, 2002; Hornung et al., 2005; Kelsall et al., 2002; Krug et al., 2004; Lund et al., 2004; Megjugorac et al., 2004). Plasmacytoid dendritic cells express CD11c, B220, and Gr-1 (Colonna et al., 2004; Kelsall et al., 2002; Krug et al., 2004; Shortman and Liu, 2002) as well as PDCA-1 (Colonna et al., 2004; Krug et al., 2004), but do not express CD11b (Krug et al., 2004). The production of IFN-α by pDC has been confirmed by depletion with the 120G8 monoclonal antibody (mAb) in our lab (data not presented) and others (Colonna et al., 2004). Interferon α is largely regarded as a major antiviral cytokine which induces an antiviral state in resting tissues by suppressing proliferation, transcription, and

translation (Barchet et al., 2002; Dalod et al., 2002; Lund et al., 2004; Pogue et al., 2004; Stark et al., 1998).

The mechanisms by which DC direct Th1 or Th2 mediated responses are still poorly understood; most implicate the production of cytokines such as IL-2, IL-4, and IFN-γ, though some studies implicate antigen load (2003) and expression of various antigens such as CD11b (Kelsall et al., 2002). Our current studies demonstrate that dendritic cells and Type I IFN are not critical to early viral clearance. Our data and that of other researchers implies a crucial role for some marginal splenic macrophages in antiviral immunity and viral clearance (Ciavarra et al., 1997; Ciavarra et al., 2005; Claassen et al., 1995; Claassen et al., 1998; Oehen et al., 2002). One possible explanation for the observed differences is casually noted in a recent article by Pozzi et al. (Pozzi et al., 2005), which suggests that macrophages may be crucial to antiviral immunity after stimulation by T cells rather than playing a role in T cell activation.

Several studies suggest that during CNS inflammation, activated DCs migrate to the cervical lymph nodes (Bailey et al., 2007; Dimier-Poisson et al., 2006; Galea et al., 2007a; Hatterer et al., 2006; Plakhov et al., 1995; Schwob et al., 2001; Velge-Roussel et al., 2000), where they activate naïve lymphocytes, which then emigrate to the site of inflammation. The origin of these cells, whether peripherally-derived or brain-resident, is still contentious. Most research has not convincingly demonstrated the presence of DC in naïve brain parenchyma (Lauterbach et al., 2006; Matyszak and Perry, 1996; Perry, 1998; Serafini et al., 2000), although they are readily detected in areas unprotected by the BBB (Bailey et al., 2007; Fischer and Reichmann, 2001; Karman et al., 2006; Lauterbach et al., 2006; Matyszak and Perry, 1996; McMenamin, 1999; Miller et al., 2007; Newman et al., 2005; Perry, 1998; Serafini et al., 2000; Serot et al., 2000; Serot et al., 1997; Serot et al., 1998). Only a handful of recent studies, such as those by Fabry et al. and Bulloch et al. (Bulloch et al., 2008; Karman et al., 2006), have demonstrated DCs in the naïve CNS parenchyma. These studies further indicate that either resident or infiltrating DCs provide APC function essential for propagation of innate and adaptive immunity in the CNS. It should be noted that identification of DCs in the CNS relies on a phenotypic rather than a functional definition for DCs; many of these studies also note that another population of CNS-resident cells may fulfil the role of APC.

Microglia are phenotypically highly similar to DC (Ponomarev et al., 2005a; Ponomarev et al., 2005b; Shortman and Liu, 2002), but express CD45 (Ponomarev et al., 2005a; Ponomarev et al., 2005b) and CD11b (Ponomarev et al., 2005b) at low to intermediate levels. More recent studies on the function of CD45 have revealed additional roles in T and B cell activation (Saunders and Johnson) via enhanced T cell receptor (TCR) signalling, particularly for B-cell activating T helper 2 lymphocytes (Thauland et al., 2008). On infection, the microglia become activated (Ponomarev et al., 2005a; Ponomarev et al., 2005b), upregulating several cell surface antigens, including MHC II, CD80, and CD40 (Ponomarev et al., 2005a; Ponomarev et al., 2005b). MHC II is the primary means of antigen presentation to naïve $CD4^+$ T cells. CD80 (B7-1) provides necessary costimulatory signals in conjunction with CD28 or CD152 (CTLA-4) for full $CD8^+$ T cell activation, while CD40 binds with CD154 (CD40L) to provide costimulation leading to full activation of $CD4^+$ T cells. Resting expression of CD45 and CD11b, along with upregulation of MHC II, CD80, and CD40 imply that microglia are capable of acquiring APC capacity and may be able to initiate and/or propagate the adaptive immune response in the CNS (Fischer and Reichmann, 2001; Juedes and Ruddle, 2001; Mack et al., 2003; Persidsky et al., 1999; Ponomarev et al., 2005a; Ponomarev et al., 2005b; Shortman and Liu, 2002). Activated microglia can present antigen to $CD4^+$ T cells and secrete various chemokines (Persidsky et al., 1999) that help recruit activated leukocytes of monocyte origin.

Although a peripheral immune system model would predict that the draining CLNs are the primary site for T cell activation, it is possible that the perivascular regions could fill this role for the CNS. Because of their strategic location and the observation that $CD8^+$ T cell infiltration is markedly enhanced by cognate antigen recognition (Galea et al., 2007b), they are ideally suited to function as APCs. Perivascular macrophages have been shown to express MHC II and present antigen (Fabriek et al., 2005; Fischer and Reichmann, 2001; Griffin, 2003; Perry, 1998; Polfliet et al., 2001b; Stoll and Jander, 1999; Williams et al., 2001). Their unique location at entry points to the CNS (vascular spaces) makes them attractive targets as an *in situ* APC.

Dendritic cells have not yet been shown to play a major role in CNS immunity (Matyszak and Perry, 1996), especially in regard to viral infections, although they have been shown to enter the cerebrospinal fluid (CSF) in response to bacterial infections (Matyszak and Perry, 1996; Pashenkov et al.,

2002; Ponomarev et al., 2005b) and may penetrate the CNS during inflammation, independently of T cells (Reichmann et al., 2002). These studies may be questionable due to the difficulty in differentiating between activated microglia and dendritic cells based on the expression of cell surface antigens. Identification of the true APC in CNS infections is therefore a controversial area given the conflicting data for DCs and/or microglia as APCs.

Leukocyte extravasation into the CNS

T cells, DCs, granulocytes, and macrophages are recruited to the CNS during active infections (Bi et al., 1995a; Glabinski and Ransohoff, 1999; Persidsky, 1999; Rubin and Staddon, 1999). Although the precise mechanisms by which cells extravasate through the vascular endothelium and enter the CNS are not fully understood, several intracellular adhesion molecules (ICAMs) such as CD11a (LFA-1), CD11b (Mac-1) and CD49d (VLA-4) seem to play a role in homing to and penetration of the BBB (Persidsky, 1999). CD49d seems to be required for BBB penetration in some studies (Glabinski and Ransohoff, 1999). Notably, these antigens are all upregulated on activated lymphocytes.

Additionally, the loss of BBB integrity during VSV encephalitis may play a role in leukocyte infiltration into the inflamed CNS. The normal BBB is composed of tight junctions between endothelial cells surrounded by a basement membrane and flanked by pericytes and astrocytic end feet (Miller, 1999). Astrocyte degradation and BBB failure is proposed to be contingent on large numbers of T cells infiltrating the CNS in (Bechmann et al., 2007). Critical to maintaining these tight junctions are three classes of proteins: the cadherins, selectins, and integrins. In the resting CNS, integrins are expressed at relatively low levels, which increase markedly in response to inflammation (Miller, 1999) and bind with ICAMs to promote leukocyte adhesion, a first step in CNS penetrance. Cytokines and chemokines have been shown to cross the BBB and may impact BBB integrity (Rubin and Staddon, 1999). Research has implicated a crucial role for nitric oxide and IL-12 in the breakdown of the BBB (Komatsu et al., 1999). Other cytokines, such as IL-1β, IFN-γ, CXC, and TNF-α, have also been correlated with weakening of the BBB (Pardridge, 1999). Further degradation of the BBB may be accomplished with matrix metalloproteinases (MMPs), which can degrade the basement membrane (particularly MMP-3 and MMPs-2 and -9, the type

IV collagenases) and may actively participate in inflammation by interacting with E-cadherin, IL-1β, pro-TNFα, and osteopontin to recruit leukocytes (Agnihotri et al., 2001; Gearing et al., 1995; Noe et al., 2001). Many of these inflammatory mediators are produced by monocytic cells. Perhaps not surprisingly, microglia have also been shown to produce these critical cytokines and MMPs (Kawanokuchi et al., 2006; Suzuki et al., 2005; Walker et al., 2006; Wang and Suzuki, 2007), although their contribution during acute viral encephalitis has not been established.

Mechanisms of viral clearance

Macrophages are phagocytic, and in many models they mediate viral clearance. Our previous studies in the peripheral immune system indicate that they play a key role in clearance of VSV in immunocompetent mice (Ciavarra et al., 2006). In contrast, most acute viral infections of the CNS appear to be cleared by IFN-γ dependent action of T cells, in particular, CD8$^+$ CTL (reviewed in (Griffin, 2003)). In the CNS, interferon γ (IFN-γ) has been shown to inhibit viral replication and in some models is required for viral clearance (Komatsu et al., 1996; Parra et al., 1999). Furthermore, *in vitro* studies have shown that IFN-γ can inhibit VSV replication (Binder and Griffin, 2001; Chesler and Reiss, 2002; Komatsu et al., 1996; Komatsu et al., 1999). Not surprisingly, microglia have been shown to produce IFN-γ (Kawanokuchi et al., 2006; Parra et al., 1999; Shaked et al., 2005; Wang and Suzuki, 2007) under a wide variety of conditions. IL-12 and TNF-α have also been shown to play key roles in mediating viral clearance in both *in vitro* and *in vivo* models (Chesler and Reiss, 2002; Komatsu et al., 1997; Komatsu et al., 1996; Komatsu et al., 1999; Lauterbach et al., 2006; Parra et al., 1999; Patterson et al., 2002), and again, these cytokines have been shown to be produced by microglia. Therefore, microglia may also play a key role in mediating viral clearance from the infected CNS.

Current model of antiviral immunity in the CNS

Cumulatively, the current model for viral clearance from the CNS indicates that DCs encounter antigen (either from the CNS or from the nasal mucosa) and migrate to the draining cervical lymph nodes. Here, they activate naïve T cells, particularly CD8$^+$ CTL. These cells appear to first migrate to the

perivascular spaces, where they require secondary stimulation by perivascular-resident APCs (Bechmann et al., 2007). Following this stimulation, BBB integrity declines (due to viral pathogenesis, contact-mediated or cytokine-mediated disruption), these lymphocytes migrate into the brain parenchyma (Bechmann et al., 2007), where they mediate viral clearance in an IFN-γ dependent manner. To evaluate this model, we intranasally infected mice with vesicular stomatitis virus (VSV) in order to produce viral infection of the brain. We next depleted mice of several critical cell populations to assess their contribution to antiviral immunity of the CNS.

CHAPTER II

SPECIFIC AIMS

The primary objective of this research was to develop a model for the primary immune response to acute viral infections of the central nervous system (CNS). This model must address the critical facets of the immune response: antigen presentation and lymphocyte activation, leukocyte migration and extravasation into the brain, and viral clearance. Several target cell populations exist that may be critical to mediating CNS immunity, including dendritic cells, microglia, macrophages, and antigen-specific lymphocytes. Therefore, we employed several depletion strategies to target each of these cell populations and clarify their relative contribution to antiviral immunity of the CNS. Concurrently, we assayed various cytokines and chemokines known to affect the course and development of antiviral immunity. For this model, we induced acute viral infection of the brain via intranasal application of vesicular stomatitis virus. VSV is a simple, well-characterised rhabdovirus that is rapidly cleared from the CNS of immunocompetent mice but replicates in immunocompromised mice, leading to morbidity and mortality.

Specific Aim 1: Characterisation of the inflammatory response in the CNS.

Several models of viral infection of the CNS exist, but very few address acute cytolytic (rather than persistent or lysogenic) viral infections. Our model of acute infection with VSV has previously been documented for particular strains of mice (Balb/c and C57BL/6). However, the exact cell types involved in the primary response may be dependent on multiple factors, including mouse strain, gender, and viral dosage. Thus, it is critical to first characterise the normal cellular and molecular immune response in our mice (Balb/c x C57BL/6 offspring, henceforth referred to as CB6F1). These experiments are discovery-driven rather than hypothesis-driven; however, we predict that the cellular and chemokine/cytokine responses should agree with published data. We will pay particular attention to microglia throughout these studies; because they are phenotypically similar to both DCs and macrophages, their role in antiviral immunity in the CNS is unclear and they may be inhibited or depleted by the techniques that follow. These

studies will provide a basis for identifying dysregulated immune responses, either cellular or molecular, in subsequent studies.

Specific Aim 2: Assess the role of dendritic cells in the inflammatory response of the CNS

Our previous studies demonstrated that one-third of dendritic cell-depleted mice develop persistent brain infections following peripheral infection. These observations led directly to our interest in dendritic cells (DCs) as key regulators of the antiviral immune response of the CNS. Our data imply a novel role for DCs in controlling CNS infections. To date, DCs have not been shown to be involved in mediating viral clearance in the CNS. Their primary role in an immune response, whether peripheral or in the CNS, is antigen presentation to naïve lymphocytes. Therefore, **we hypothesise that circulating peripheral DCs serve as the primary antigen-presenting cell (APC) for the CNS**. To test this hypothesis, we will selectively deplete mice of DCs using a transgenic mouse strain whose DCs are susceptible to diphtheria toxin and intranasally infect depleted mice with VSV to induce CNS inflammation. If the hypothesis is correct, we predict that loss of DCs will impair lymphocyte activation and subsequent infiltration into the brain without disruption of nonspecific cell types such as macrophages and granulocytes. Because lymphocytes appear to be the crucial mediators of viral clearance in the CNS, **we can extend this hypothesis such that loss of DCs, and subsequent loss of lymphocytes, will result in impaired viral clearance within the CNS, leading to increased morbidity and mortality**. We will concurrently observe the various leukocyte subsets (including microglia) and cytokine/chemokine production for loss of function relative to immunocompetent mice as revealed by Aim 1. Within this context, we should be able to explain the mechanistic failure underlying our previous observations of increased morbidity and mortality in our peripheral studies (a secondary objective of these studies).

Specific Aim 3: Assess the role of macrophages in the inflammatory response of the CNS.

Our previous results in peripheral models of VSV infection and macrophage depletion provided strong evidence that macrophages were direct mediators of viral clearance. There is also ample evidence from other models that macrophages can and do serve as functional APCs. Two significant pools of

macrophages exist: circulating macrophages and the brain-resident perivascular macrophages. Therefore, we propose **two alternative hypotheses to those presented in Aim 2: first, that macrophages (either peripheral or CNS-resident) serve as functional APCs; and second, that macrophages directly mediate viral clearance in the CNS.** To test these hypotheses, several depletion strategies will be employed to selectively target either circulating macrophages for depletion (MAFIA transgenic mice and intravenous administration of clodronate-bearing liposomes) or perivascular macrophages (intracerebroventricular administration of clodronate-bearing liposomes). If macrophages serve as functional APCs, then we predict that lymphocyte activation and infiltration into the CNS would be normal despite the loss of DCs in Aim 2, and impaired in macrophage-depleted mice. Macrophage-depleted mice should therefore also exhibit increased morbidity and mortality due to loss of antiviral lymphocytes. If the role of macrophages is strictly limited to viral clearance, we would predict normal clearance in mice depleted of DCs (Aim 2) with corresponding health of mice, whereas macrophage-depleted mice should exhibit increased pathogenesis, morbidity, and mortality. Again, we will monitor the various leukocyte subsets (including microglia) and cytokine/chemokine production for loss of function relative to immunocompetent mice as revealed by Aim 1.

CHAPTER III

METHODOLOGY

Mice

MAFIA transgenic mice

A transgenic mouse line (MAFIA, macrophage Fas-induced apoptosis, strain C57BL/6J-Tg (Csf1r-EGFP-NGFR/FKBP1A/TNFRSF6) 2Bck/J, Jackson Laboratories, Bar Harbor, ME (Burnett et al., 2004) was used for macrophage depletion studies. These mice constitutively co-express enhanced green fluorescent protein (EGFP) and a fas-mediated suicide gene under the control of a macrophage-specific promoter for *c-fms* (gene for colony-stimulating factor 1 receptor, CSFR1). Intravenous injection with AP 20187 dimeriser (Ariad Pharmaceuticals, Cambridge, MA) cross-links the transgenic, cytoplasmic fas proteins induces apoptosis and ultimately results in the peripheral depletion of macrophages. Breeding mice were obtained from Jackson Laboratories and maintained in the mouse colony at EVMS. MAFIA mice were bred in the animal facility using MAFIA x MAFIA crosses, as recent communications with Jackson Laboratories and Sandra Burnett (Brigham Young University, Provo, UT) indicated problems with MAFIA x WT crosses. To phenotype MAFIA mice, a drop of blood was obtained by a tail prick with a sterile lancet dipped in heparin, collected from the tail with a sterile, heparin-lined 200 μL pipette tip, and transferred to a sterile, heparin-lined microcentrifuge tube. Blood samples were then suspended in 200 μL flow cytometry wash buffer, and examined for EGFP expression by flow cytometry. Male or female mice were used for experiments at 6-8 weeks of age. Non-transgenic progeny were used as controls.

Experimental conditions for these mice required intravenous injection of the AP20187 (Ariad Pharmaceuticals, Inc., Cambridge, MA) dimeriser at a dose of 20 mg/kg. These injections were administered via the lateral tail vein after heating the tail to dilate the vein for approximately one minute and swabbing the injection site with a 70% isopropyl alcohol pad (BD Biosciences, San Diego, CA). Alternatively, injections were administered via the retro-orbital venous sinus under 2% isoflurane anaesthesia in accordance with EVMS IACUC approved protocol #06-016. Mice were euthanized by CO_2 asphyxiation.

CD11c/DTR transgenic mice

Breeding mice were obtained from Jackson Laboratories (strain C.FVB-Tg(Itgax-DTR/EGFP)57Lan/J). Male CD11c/DTR mice were bred with female C57BL/6 mice (Jackson Laboratory) to obtain CB6F1/DTR progeny that expressed H-$2^{d/b}$ haplotype MHC I (H-2^b is required for antigen-specific tetramer studies). These mice express the simian diphtheria toxin receptor (DTR) fused with green fluorescence protein (GFP) under the control of the CD11c promoter. Expression of CD11c is most highly expressed in the dendritic cell populations in mice (Jung et al., 2002). Although CD11c is expressed at significantly lower levels on other cell types (activated T cells, microglia, monocyte/macrophage populations), this is primarily noted during active infections and not typical of resting conditions. The simian DTR has a higher affinity for DT than the endogenous murine receptor. Therefore, DC can be selectively depleted in these mice by the administration of DT (Jung et al., 2002).

Genotyping of the mice was performed at 10-14 days of age. The tails of pups were anaesthetised with ice, and then the distal 0.5-1 cm of the tail was quickly amputated using a sterile razor blade. Pressure was applied to the tail until bleeding stopped and pups were hand-warmed to prevent hypothermia. Tail sections were halved and stored in sterile microcentrifuge tubes. Tail sections were subsequently minced and suspended in 250 μL QuickExtract solution (Epicentre Biotechnologies, Madison, WI), vortexed for 15 seconds, heated at 65°C for 6 minutes, vortexed again for 15 s, and heated at 98°C for 2 minutes. DNA was diluted at a 1:8 ratio, and quantitation was performed by spectrophotometry at 260 and 280nm. The DNA concentration was calculated and 40-80ng DNA was used in subsequent PCR reactions. Mice were genotyped for transgene expression by multiplex PCR reactions using established primers for DTR (DTR1, forward 5' GGG ACC ATG AAG CTG CTG CCG 3'; DTR2, reverse, 5' TCA GTG GGA ATT AGT CAT GCC 3') (Jung et al., 2002). Control reactions were performed using primers for the TCR-δ chain (TCRd1, forward 5' CAA ATG TTG CTT GTC TGG TG 3', TCRd2, reverse 5' GTC AGT CGA GTG CAC AGT TT 3'). Primer pairs were purchased from Integrated DNA Technologies, Coraville, IA. PCR reactions were performed with 3.66 μL nuclease-free water, 1.2 μL 10X PE Buffer II, 0.96 μL 25 mM MgCl$_2$, 0.96 μL 2.5 mM dNTP, 0.45μL each 20μM DTR1 and DTR2 primers, 0.3 μL each 20 μM TCRd1 and TCRd2 primers, 0.15 U/μL Taq polymerase, and 40-80ng DNA. PCR amplification was performed with an

initialisation step of 94°C for 3 minutes followed by 35 cycles as follows: denaturation, 94°C, 30 s; annealing, 62°C, 60 s; elongation, 72°C, 30 s. A final elongation step at 72°C for 2 minutes ended the PCR reaction. Products were held at 4°C overnight. PCR fragments were resolved on a 1% agarose gel at 100 V for approximately 40 minutes with 1X GelStar nucleic acid stain (Lonza Rockland, Inc., Rockland, ME). Bands at 600 bp indicated the presence of the DTR transgene; bands at 200 bp were indicative of the internal TCR-δ control. Mice lacking the transgene were used as non-DTRTg, wild type controls. Male and female adult mice ages 6-8 weeks were used for all experiments.

Experimental conditions for these mice required intraperitoneal injections of diphtheria toxin (DT). Each lot of diphtheria toxin (Sigma, St. Louis, MO) was titrated to give optimal depletion of DC while maintaining the health and safety of the animals. Mice were weighed immediately prior to injections of DT and the determined dose administered per gram body weight. DT was administered one day before and after viral infections in accordance with EVMS IACUC approved protocol #06-016. Mice were euthanized by CO_2 asphyxiation.

N15 TCRTg Mice

N15 TCR Tg RAG-2$^{-/-}$ H-2^b mice (Rag2^{tm1} TgN (N15)) were obtained from Taconic (Taconic Farms Inc., Germantown, NY) in cooperation with and courtesy of Dr. Ellis L. Reinherz (Harvard Medical School, Boston, MA) and maintained in sterile microisolators. The transgenic α and β TCR chains on MHC I$^+$ (CD8$^+$) T cells are specific for the VSV nucleoprotein octapeptide N$_{52-59}$ specific (Ghendler et al., 1997). Thus, virtually all CD8$^+$ T cells in this mouse strain are specific for the immunodominant epitope of VSV. Gloves were washed with 70% ethanol prior to handling each cage of mice, and all animal manipulations were performed in a biosafety hood. Mice were bred in-house as N15 x N15 crosses. Mouse phenotype was confirmed by multicolour flow cytometry performed on a drop of blood obtained from the lateral tail vein (as described for MAFIA mice) and staining with FITC-α-TCR-Vβ (specific for the transgenic TCR type), PE-α-CD45R (B220), and PE-Cy7-α-CD8a, as recommended by by Dr. Reinherz. All antibodies were purchased from eBioscience. Mice were determined to have a predominantly CD8$^+$TCR-Vβ$^+$ phenotype and were lacking in CD4$^+$ cells and CD45R$^+$ cells. Mice were

used in accordance with EVMS IACUC approved protocol #06-016 and were euthanized by CO_2 asphyxiation.

Clodronate Liposomes

Preparations of liposome encapsulated dichloromethylene bisphosphonate (clodronate, CL2MDP) were a kind gift of Roche Diagnotics GmbH, Mannheim, Germany and were injected intravenously into mice at 200 µL/mouse via the retro-orbital venous sinus under 2% isoflurane anaesthesia in accordance with EVMS IACUC approved protocol #06-016.

MGBG

Methylglyoxal bis(guanylhydrazone) (MGBG) was provided as a gift from Pathologica, LLC (San Francisco, CA) in collaboration with Dr. Michael McGrath and Dr. Jeremy Blitzer. MGBG was diluted in PBS and administered intraperitoneally to mice at a dosage of 15 mg/kg three times weekly beginning 24 hours prior to infection. It should be noted that the supply of MGBG was sufficient for only a single experiment, and IACUC approval covered only one pilot study to assess the efficacy of this depletion technique.

Surgical Treatment of Mice

Mice were initially induced to a surgical plane of anaesthesia under 5% isoflurane. For retro-orbital injections, mice were removed from anaesthesia and injected via the retro-orbital venous sinus as previously described. Because these injections required only a few seconds to administer, mice did not require additional anaesthesia beyond induction and recovered rapidly.

For intracerebroventricular injections of CL2MDP, mice were given children's ibuprofen in drinking water (100 mg/L) *ad libitum* 3 days before and after surgery. Mice were monitored twice daily for 3 days following surgery. All surgical procedures were performed in collaboration with Dr. Larry Sanford (EVMS) by Dr. Laurie Wellman and Dr. Xianling Liu. Following induction, mice were weighed and the surgical site prepared by shaving, swabbing with betadine, and finally swabbing with 70% ethanol. Mice

given subcutaneous injections of potassium penicillin (100 IU/g body weight, 100 μL) and gentamicin (0.005 mg/g body weight, 100 μL) prior to surgery, then placed in a stereotaxic frame. An incision was made along the coronal suture and the scalp was retracted. The position of the left lateral ventricle was determined relative to the bregma with stereotaxic coordinates as follows: AP (anterior-posterior) -0.5 mm, ML (medial-lateral) -1.0 mm, and DV (dorsal-ventral) -2.0mm. A small hole was drilled into the skull and CL2MDP was infused at a rate of 0.67 μL/min for 12 min (8 μL per mouse). The skull was filled with bone wax and the scalp sutured. Mice were allowed to recover and were monitored every 15 minutes for the first 3 hours post-operative, then twice daily for the next 3 days. All surgeries were performed in accordance with EVMS approved IACUC protocol #05-017.

Vesicular Stomatitis Virus (VSV)

Wildtype vesicular stomatitis virus (VSV, Indiana serovar) was provided by Dr. Philip Marcus, University of Connecticut, and was grown and assayed in confluent monolayers of Vero cells and virus titers determined by standard plaque assays (Marvaldi et al., 1977; Sekellick and Marcus, 1979). For peripheral infections, mice were infected with VSV by a single i.p. injection of $2x10^7$ PFU. For infections of the CNS, dosages of virus varied based on mouse strain and gender: female mice on the C57BL/6 background received $2x10^6$ PFU intranasally (i.n.) in a 20 μL volume, while female Balb/c or CB6F1 mice received $2x10^5$ PFU i.n in a 10 μL volume. Male mice received a lower dose (25% of the dose given to female mice) of $5x10^5$ or $5x10^4$ PFU for C57BL/6 or Balb/c and CB6F1 mice, respectively, in a 10 μL volume. These dosages yielded similar morbidity across all strains and genders.

During these studies, changes in animal husbandry protocols resulted in abnormal responses to our typical virus infection models. Specifically, protocols changed to require ventilation fans in the animal cage transfer workstations to be continuously on. Animals that were born before this change in protocol subsequently exhibited enlarged lymph nodes despite a lack of viral infection and were not used for these experiments. However, animals born after this protocol change showed increased resistance to VSV infection. *A twofold higher dose of virus was required to induce similar levels of morbidity and leukocyte*

infiltrate into the CNS of infected animals. Additional alterations in the immune response, if any, were not detectable in our models. Viral doses used for each experiment are noted in the figure legends.

Organ and Tissue Harvest

Whole blood was isolated from CO_2 euthanized mice by cardiac puncture with a 28 ½ gauge insulin syringe that was lined with heparin to prevent clotting. Blood was collected into heparin-lined 1.2 mL microcentrifuge tubes. For collection of plasma, blood samples were centrifuged and the supernatant drawn off and stored in 600 µL microcentrifuge tubes at -80°C. For experiments using whole blood in flow cytometry, 200 µL whole blood was aliquotted per flow cytometry tube and lysed with 1X PharmLyse buffer (BD Biosciences, San Diego, CA) to lyse red blood cells. Flow cytometry staining was performed in the PharmLyse buffer for these experiments.

Peritoneal exudate cells (PEC) were obtained by lavage of the peritoneal cavity with 10-20 mL PBS. PEC were filtered through 0.4µm nylon mesh cell strainers and centrifuged at 280 xg for 8 minutes.

Spleens were harvested from mice and ground through a 0.4µm nylon mesh cell strainer with a glass pestle until remaining connective tissue was white and gelatinous in appearance. Cell suspensions were filtered through a second nylon mesh filter and centrifuged at 280 xg for 8 minutes to pellet cells. Cells were resuspended in 1X PharmLyse buffer at a density of 1 mL/spleen and incubated at room temperature for approximately 10 minutes. Cells were again centrifuged at 280 xg for 8 minutes. For experiments requiring enrichment of dendritic cells, spleens were removed from mice and injected with 400U/mL collagenase D (Sigma, St. Louis, MO), then minced and incubated in 100U/mL collagenase D for 30 minutes at 37°C. Digested tissue was filtered through 0.4µm nylon mesh cell strainers and centrifuged at 280 xg for 8 minutes to pellet cells. Red blood cells were lysed as described above.

Lungs were removed from mice and digested with either collagenase D as described for spleens, or minced and digested with tumour digestion solution (1 mg/mL collagenase I, 0.1 mg/mL DNAse I, and 2.5 U/mL hyaluronidase, Sigma, St. Louis, MO) in 10 mM HEPES buffer supplemented with 142 mM sodium chloride, 0.67mM potassium chloride, and 0.67 mM calcium chloride. Tissue was scrubbed through a nylon mesh cell strainer with a glass pestle until remaining connective tissue was white and gelatinous in

appearance. Cells were centrifuged and subjected to red blood cell lysis as described above. Alternatively, lungs were homogenised in a 5 mL glass Tenbroek homogeniser at 0.5 mL PBS/lung, followed by discontinuous Percoll centrifugation on a 70%-35%-0% gradient at 1200 xg for 45 minutes at 20°C.

Bone marrow was obtained by careful dissection of both femurs from mice. Bone marrow was flushed from the femurs using 0.5mL RPMI via a 18 ½ gauge syringe. Cells were filtered through a 0.4 μm nylon mesh cell strainer and red blood cells lysed as described above.

Brains were removed by decapitation of mice. The skulls were cut along the sagittal and lamboidal sutures, and the skull bone carefully lifted from the brain with forceps. The brain was gently lifted from the posterior skull with forceps and placed in PBS. Brains were homogenised in 2 mL PBS with a 5 mL glass Tenbroek homogeniser using 20 strokes per brain. The homogenate was centrifuged at 280 xg for 8 minutes and the supernatant stored for future use. Leukocytes were isolated by resuspending the pellet in 70% Percoll for discontinuous Percoll centrifugation on a 70%-35%-0% gradient at 1200 xg for 45 minutes at 20°C.

Additional tissues that were investigated were handled similarly to the non-enzymatic preparation of the spleen. For some experiments, tissues were stored for future determination of viral titres at 0.1 g tissue/mL RPMI at -80°C.

Tissue slices for immunohistochemistry were obtained prior to other processing and mounted in OCT cut face up, then flash-frozen in liquid nitrogen and stored at -80°C. For immunohistochemistry of brain tissue, the right atrium of a euthanized mouse was nicked, and 30 mL of 10% buffered formalin was slowly (approximately 1 mL/minute) perfused into the left atrium of the mouse using an 18 ½ gauge syringe, followed by an additional 30 mL ice-cold PBS. For some experiments requiring both flow cytometry and immunohistochemistry, perfusion with formalin was omitted and only PBS was used.

Cell density was determined by Coulter counter or by haemocytometer counting with Trypan blue exclusion.

Flow Cytometry

Single-cell suspensions were prepared as described in Organ and Tissue Harvest. Two million cells were aliquotted to each flow cytometry tube. MHC class I tetramers specific for the immunodominant epitope VSV nucleoprotein VSV-N$_{52-59}$ (NIH Tetramer Core Facility, Emory University, Atlanta, GA) were conjugated to allophycocyanin (APC), and were added to cells, then incubated for 30 minutes at room temperature. Volumes of stock fluorochrome-conjugated antibodies were calculated for optimal concentrations based on manufacturer's recommendations (see Appendix A: Antibodies for details) and diluted to 50 μL per flow cytometry tube. Antibody cocktails were added to cells and incubated for 30 minutes at 4°C. Biotinylated antibodies were included in the antibody cocktails, and a second incubation was carried out with streptavidin-fluorophore conjugates (also listed in antibody table) at 4°C for 30 minutes. Unconjugated, purified antibodies were added separately from cocktails, incubated 30 minutes at 4°C, and followed with an anti-host biotinylated antibody (also separate from cocktail) for 30 minutes at 4°C, and finally incubated for 30 minutes at 4°C with streptavidin-fluorophore. Washes were performed between each incubation step by diluting the cell-antibody cocktail solution with 2 mL flow cytometry wash buffer (PBS +1% goat serum and 0.1% sodium azide) and centrifugation for 8 minutes at approximately 300 xg. Following all incubations, three washes were performed prior to resuspension in 200 μL flow cytometry wash buffer for data acquisition. In some instances, cells were resuspended in 1% paraformaldehyde in PBS and stored at 4°C for later acquisition; these samples were subsequently washed 3 times in flow cytometry wash buffer and resuspended in 200 μL flow cytometry wash buffer prior to acquisition.

Instrument compensation was performed by preparing experimental samples with a single fluorophore-conjugated antibody per tube (typically, the most highly expressed marker was chosen) and adjusting instrument settings to yield optimal acquisition conditions.

Determination of Viral Titres (PFU Assay)

Vero cells were cultured and grown to confluence in complete tissue culture media (RPMI supplemented with 10% FBS, 1% penicillin-streptomycin, 1% amphotericin-B, and 1% L-glutamine

(Cellgro Mediatech, Manassas, VA) at 37°C and 5% CO_2 and passaged every 2-3 days at a 1:3 dilution following dissociation with Trypsin-EDTA (Cellgro Mediatech) and gentle agitation. Tissues stored for determination of viral titre by plaque-forming unit (PFU) assay were thawed in a 37°C water bath, then subjected to 3 rapid freeze-thaw cycles using dry ice and a 37°C water bath to release virus. Serial tenfold dilutions were prepared from the supernatants of the frozen/thawed tissues and VSV stock. Each well of the 6-well tissue culture plates was coated with 200 µL attachment solution (RPMI supplemented with 6% FBS and 15 µg/mL diethylaminoethyl (DEAE) dextran) followed by 100 µL tissue supernatant or VSV. Plates were tilted gently to coat wells evenly, and incubated for 1 hour at 37°C and 5% CO_2 with gentle tilting every 15 minutes to ensure even distribution of virus. Wells were then covered with 1.6% agarose in DMEM supplemented with 6% FBS (final concentrations) and incubated at 37°C/5% CO_2 for 48-72 hours until plaques appeared in the Vero monolayer. Wells were stained with 2 mL 0.01% neutral red in PBS (pH 7.0; prepared from stock 0.1% at pH 6.0, pH adjusted with monobasic sodium phosphate) for 2 hours at 37°C. Neutral red stain was removed by pipette and 6-well plates were incubated an additional 2 hours at 37°C prior to counting plaques (unstained areas).

ELISPOT Assay

Single-cell suspensions of splenocytes or brain cells were prepared as described above. Assays were performed according to a BD Biosciences protocol (Ernst et al., 2006). ELISPOT plates (Millipore Multiscreen HTS, Millipore, Billerica, MA) were pre-wet with 15 µL 70% ethanol and rinsed with PBS. Purified capture antibodies (IL-2, IL-4, IFN-γ; see Appendix A for details) were diluted to 2 µg/mL in PBS and plated at 100 µL/well overnight at 4°C. Plates were washed with ELISPOT wash buffer (PBS+10% goat serum and 0.05% Tween-20, Sigma) three times (200 µL/well), then blocked with complete tissue culture media for two hours at room temperature. Cells were typically plated at 1-2x10^6 cells/well in a 100 µL volume in the absence of exogenous antigen or stimulation and incubated overnight at 37°C and 5% CO_2. The following day, plates were washed once with deionised water followed by three washes with ELISPOT wash buffer. Biotinylated detection antibodies were diluted to 2 µg/mL in blocking buffer (PBS+10% FBS) and incubated two hours at room temperature. Plates were washed three times with

ELISPOT wash buffer and then incubated with streptavidin-horseradish peroxidase (Sigma) for one hour at room temperature. Plates were washed four times with ELISPOT wash buffer and two to four times with PBS to remove traces of Tween-20. ELISPOTS were developed with 3-amino-9-ethyl carbazole (AEC, Sigma) prepared by dissolving 20 mg in 1 mL N,N-dimethylformamide. The final working solution was prepared by diluting 333 µL of the AEC solution in 10 mL of 0.1 M sodium acetate and 5 µL 30% H_2O_2. ELISPOT plates were monitored for development (approximately 10 minutes) and the reaction halted by rinsing with excess deionised water. ELISPOT plates dried overnight and were manually counted under a dissecting microscope the following day.

ELISA Assay

Supernatants from brain homogenates were prepared and stored at -80°C as previously described. GM-CSF ELISA assays were conducted according to eBioscience protocols (eBioscience, 2009). Secondary lymphoid chemokine (SLC, CCL21) ELISA assays were performed according to the manufacturer's instructions (R&D Systems, Inc., Minneapolis, MN). Both protocols were similar. Corning EIA/RIA high-binding microplate wells (Corning Inc., Lowell, MA) were coated with capture antibody prepared in PBS (GM-CSF, 2 µg/mL, eBioscience; SLC, 4 µg/mL, R&D Systems) overnight at 4°C (eBioscience) or room temperature (R&D Systems). Plates were washed with ELISPOT wash buffer three times, then blocked with ELISA diluent (1% BSA in PBS) for 1 hour. Plates were again washed three times and samples (1:3 dilutions) and standards (8 pg/mL-1000 pg/mL, serial twofold dilutions) prepared in ELISA diluent were added to wells for two hours at room temperature. Plates were washed three to five times and detection antibody prepared in ELISA diluent (GM-CSF, 2 µg/mL; SLC, 50 ng/mL) was added to wells, then incubated one to two hours at room temperature (GM-CSF or SLC, respectively). Plates were washed and streptavidin-HRP (Sigma, 1 µg/mL or R&D Systems) was added to wells and incubated for 20-30 minutes at room temperature. Plates were washed five times and tetramethylbenzidine (TMB) substrate solution (Sigma) was added. Colour development was carefully monitored and the reaction was halted after 20-30 minutes by the addition of 2N H_2SO_4. Absorbance of the solution was determined at

450nm on a microplate spectrophotometer. A standard curve was plotted and the concentrations of experimental samples calculated in Microsoft Excel.

Protein Cytokine Array

The RayBio Mouse Cytokine Antibody Array C Series 1000 (Ray Biotech, Norcross, GA, Catalogue #AAM-CYT-1000) was used to assess the production of a panel of 96 cytokines in brain tissue. The assay was performed according to manufacturer's instructions with minor modifications for use with the Li-Cor Odyssey infrared detection system (Li-Cor, Lincoln, NE) (2006). Tissue samples from mouse brains were flash-frozen in liquid nitrogen and stored at -80°C for future use. Brain tissues were thawed, blotted dry on a Kimwipe, and 100 mg tissue was weighed. Tissue samples were homogenised in 1X cell lysis buffer (kit component, Ray Biotech, Norcross, GA) supplemented with EDTA-free Protease Inhibitor Cocktail III (Calbiochem, San Diego, CA, Catalogue #539134) for 20 strokes. Homogenate was then centrifuged at 10,000 xg for 5 min and the supernatant retained for use.

The protein concentration in the supernatant was determined using the Pierce BCA Protein Assay (Pierce Biotechnology, Rockford, IL, Catalogue #23227) according to manufacturer's protocols. Standards of bovine serum albumin (BSA) were prepared as described in Table 1 using cell lysis buffer and Protease Inhibitor Cocktail III as the diluent. Dilutions of samples were prepared at 1:2 and 1:10 ratios with the protease-supplemented cell lysis buffer as diluent. Standards and samples were aliquotted in triplicate to wells of a 96-well flat-bottomed plate at 25 μL/well. BCA working reagent was prepared as a 50:1 dilution of BCA Reagent A:BCA Reagent B (kit components, Pierce Biotechnology). Working reagent was added to wells (200 μL/well), the plate shaken for 30 seconds, then placed in an incubator at 37°C for 30 min. The plate was allowed to return to room temperature and the absorbance of each well was determined at 570 nm. The absorbance of triplicate wells was averaged, and a standard curve plotted based on the BCA standards. The protein concentration of the samples was calculated based on this curve and the concentration of stock protein sample solutions was adjusted to yield a concentration of 250 μg/mL with Li-Cor Odyssey blocking buffer (Li-Cor, Lincoln, NE, Catalogue #927-40000) supplemented with 0.01% Tween-20 (henceforth referred to as Li-Cor blocking buffer, Sigma).

Table 1: Preparation of BSA Standards.			
Vial	Volume of Diluent	Volume & Source of BSA	Final BSA Conc
A	0 µL	300 µL of Stock	2000 µg/mL
B	125 µL	375 µL of Stock	1500 µg/mL
C	325 µL	325 µL of Stock	1000 µg/mL
D	175 µL	125 µL of B dilution	750 µg/mL
E	325 µL	125 µL of C dilution	500 µg/mL
F	325 µL	325 µL of E dilution	250 µg/mL
G	325 µL	325 µL of F dilution	125 µg/mL
H	400 µL	325 µL of G dilution	25 µg/mL
I	400 µL	0 µL	0 µg/mL

Ray Biotech protein array membranes 3 and 4 were incubated with Li-Cor blocking buffer for 30 minutes at room temperature to block nonspecific binding. From this point forward, all incubations and washes were performed on a shaking platform. Li-Cor blocking buffer was decanted, and membranes were incubated with 1 mL of the 250 µg/mL protein samples for two hours at room temperature. Membranes were then washed three times with 2 mL of 1X Wash Buffer I (kit component, Ray Biotech) for 5 min/wash at room temperature followed by two washes (also 5 min/wash) with 1X Wash Buffer II (kit component, Ray Biotech) for 5 min at room temperature. Membranes 3 and 4 were separated and incubated with 1 mL appropriate biotinylated antibodies (prepared by reconstituting kit provided antibodies with 100 µL Li-Cor blocking buffer followed by further dilution with 2 mL Li-Cor blocking buffer) overnight at 4°C. The next day, membranes were washed as previously described. The Li-Cor IRDye 800CW-streptavidin (Li-Cor, Catalogue #926-32230) was prepared at a 1:1000 dilution in Li-Cor blocking buffer with a final concentration of 1 µg/mL. Membranes were incubated with 2 mL of the IR-streptavidin conjugate for 2 hours at room temperature. Finally, the membranes were washed four times with 1X Wash Buffer I and twice with 1X Wash Buffer II for 30 minutes/wash. Membranes were scanned on the Li-Cor Odyssey Imaging System.

Fluorescence intensity of the protein array membranes was quantified using the Li-Cor Odyssey software (Li-Cor, version 2.1). A 3-pixel region was defined around each spot and this region used for background correction. The average intensity of duplicate spots was calculated. Due to extremely high signal intensity, positive control wells may have auto-quenched and thus appear dark. These wells would typically be used to normalise signals across groups for a particular membrane. Thus, pairwise

comparisons of all cytokines were made to identify pairs of spots with consistent ratios of fluorescence across the sets of membranes as recommended by RayBiotech. The standard deviation of each ratio was calculated and used to identify spots with the most consistent ratios. Cytokine spots with differences in the standard deviation of 0.01 were determined to be the most consistent. Four cytokines (two pairs) were identified per membrane that met this criterion, and signal intensities were normalised to each of these cytokines. The normalised intensities were then averaged and compared across treatment groups.

CHAPTER IV

CHARACTERISATION OF THE INFLAMMATORY RESPONSE IN THE CENTRAL NERVOUS SYSTEM

Introduction

This chapter focuses on the initial characterisation of the primary immune response to viral (vesicular stomatitis virus, VSV) challenge in the central nervous system. Although this system has previously been investigated by Reiss et al. (Barna et al., 1996; Bi et al., 1995a; Huneycutt et al., 1994; Ireland and Reiss, 2006; Komatsu et al., 1999; Plakhov et al., 1995), their studies were conducted in Balb/c mice. Differences in the immune response for different genders and strains of mice have been reported (Barna et al., 1996; Forger et al., 1991). Our studies were conducted in the CB6F1 mouse strain (Balb/c x C57BL/6). This strain allowed us to track the antigen-specific immune response to VSV using MHC class I tetramers specific for the immunodominant VSV epitope (VSV-N_{52-59}). Therefore, it was necessary to first characterise the cellular and cytokine immune responses to intranasal application of VSV in the CB6F1 mouse. In the following studies, we phenotyped the cellular infiltrate and the CNS-resident microglia in responding to viral challenge. These studies revealed a mixed leukocyte infiltrate in the CNS in response to viral infection. We further defined the kinetics for both infiltrating and resident leukocyte populations during the primary immune response to VSV in the CNS. Finally, we characterised the protein cytokine environment found during acute viral infection. These studies revealed a complex leukocyte and cytokine response to viral infection in the CNS.

VSV encephalitis is characterized by a prominent mixed cellular infiltrate.

Previous studies with intranasal applications of VSV indicated that kinetics and morbidity varied with mouse strain and gender. Therefore, our first experiments focused on identifying the peak of inflammation in the CB6F1 mouse strain. CB6F1 mice were infected with VSV and monitored for signs of illness. Mice became ill approximately 8 days post-infection, and brains were harvested for flow

cytometric analysis at this time. This time point correlated well with previously published results by Reiss et al. regarding kinetics of infection and loss of BBB integrity. We first phenotyped the cells recruited into the brain of mice following intranasal application of VSV. Microglia were gated as $CD45^{low/int}CD11b^+$ cells (Fig. 2, box in panels a-b) which distinguished them from resident or infiltrating $CD45^{high}CD11b^+$ macrophages and $CD45^{high}CD11b^-$ lymphocytes. Microglia accounted for about 20% of cells recovered from normal, uninfected (mock-infected) mice and comprised approximately 90% of $CD11b^+$ cells. Brains from mice infected with VSV also contained a prominent population of $CD45^{high}CD11b^+$ myeloid cells and a smaller population of lymphocytes ($CD45^{high}CD11b^-$). Microglia isolated from virus-infected, but not mock-infected brains, expressed MHC class II molecules suggesting an activated state (panels c-d). Mock-infected mice contained only trace numbers of conventional ($CD11c^+PDCA-1^-$) and pDCs ($CD11c^+PDCA-1^+$), $CD4^+$ and $CD8^+$ T cells, whereas VSV induced infiltration of conventional $CD11c^+$ DCs (panels e-f), $CD4^+$ and $CD8^+$ T cells (panels g-h) but few NK cells, B cells (panels k-l) and pDCs (panels e-f). Staining with tetramers revealed a minor population of $CD8^+VSV-N$ T cells indicating that the majority of $CD8^+$ T cells did not recognize the immunodominant VSV nuclear protein determinant (panels i-j). Additional characterisation of the infiltrating leukocytes was performed in subsequent experiments including dendritic cell depletion and will be further discussed in Chapter V.

MOCK   VSV

a / b   CD11b / CD45

c 1 / d 70   MHCII / CD11b (microglia gate)

e 1 0 / f 11 2
0 / 4   CD11c / PDCA-1

g 1 0 / h 11 1
1 / 20   CD4 / CD8a

i 0 3 / j 0 8
91 / 89   Tetramer / CD11a (CD8 gate)

k 0 0 / l 0 0
6 / 8   CD49b / CD45R
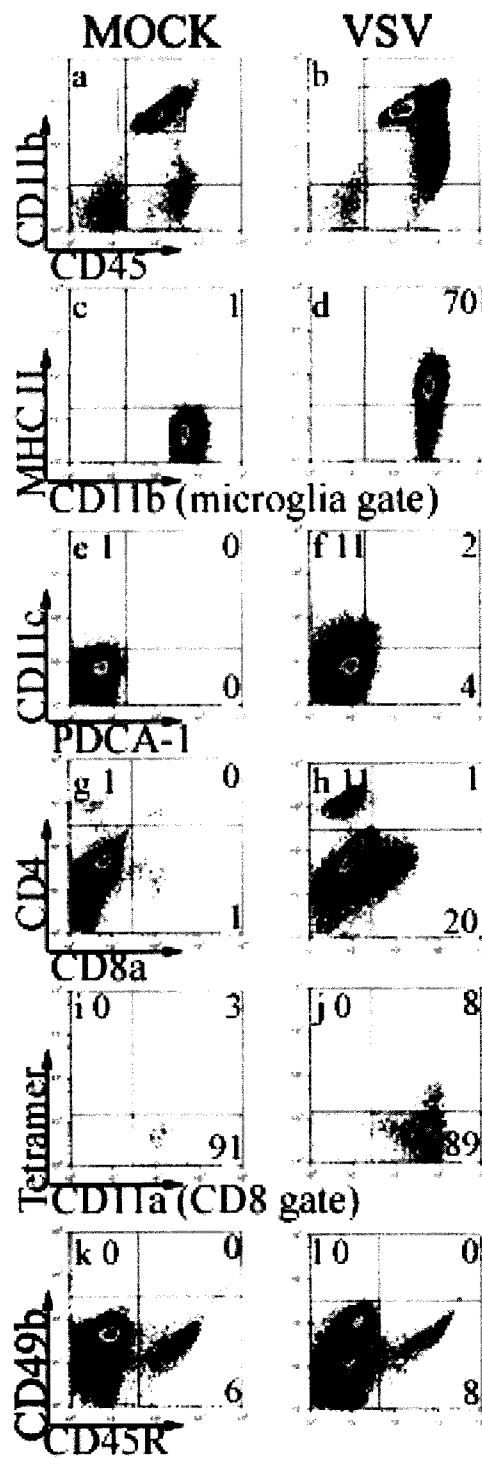
Fig. 2., Continued. *Intranasal application of VSV induces a vigorous mixed cellular infiltrate in the brain.*

Mice were given either PBS (Mock) or intranasal VSV at 2×10^5 PFU (VSV). Eight days post-infection, leukocytes were isolated from the brain and the infiltrate characterized by flow cytometry. Gates were defined for microglia based on expression of CD11b and CD45 (box in panels a-b) and expression of MHC class II evaluated (panels c-d). To characterize other infiltrating cell types, the presence of DC (panels e-f) and T cell subsets (panels g-h) was determined by flow cytometry. To identify VSV-N T cells, co-expression of CD11a and tetramers were assessed on gated $CD8^+$ cells (panels i-j). NK cells and B cells were identified as $CD45^{high}CD49b^+$ and $CD45^{high}$ $CD45R^+$, respectively (panels k-l). These data are derived from the pooled brains of 4 mice per group.

Kinetics of the Inflammatory Response in the CNS

The above study demonstrated that VSV recruited a variety of blood cells into the virus-infected brain corresponding to onset of morbidity in the animals. However, this study did not provide any insights into the kinetics of either the microglial response or the infiltrating leukocyte response. To address these questions, mice were inoculated with VSV for various periods of time and the number of microglia and the identity of infiltrating blood cells in the CNS determined by flow cytometry. It is apparent from Fig. 3A (panels a-c) that VSV induced an initial decrease in the number of microglia before a transient microgliosis became evident. This finding was reproducible in at least 3 experiments. It is possible that this decrease is due to altered expression of CD45 and CD11b; however, the forward scatter (FSC, size of cell) and side scatter (SSC, granularity of cell) profiles of brain-isolated leukocytes reveal a small (in terms of both quantity and size) but often distinct subpopulation of cells that is characteristically noted in the brain that was diminished in early VSV infection. Therefore, loss of CD45 and CD11b is unlikely to be the sole explanation for the reduced number of microglia noted. Although the infiltrate population in the naïve mice (panel a) appears to be smaller than that seen in Fig. 2 and Fig. 9, this is reflective of a smaller number of events acquired by flow cytometry. This infiltrate population is quantified later (Fig. 9) and is quite small in terms of both percentage and absolute number despite an apparently large population visible in the flow cytometry density plots. Microglia expanded rapidly beginning around 5 days post-infection. While these studies cannot rule out the possibility that peripheral leukocytes entered the CNS and differentiated to a microglial-like phenotype, a corresponding increase in the FSC x SSC profile is noted. Therefore, it is unlikely that differentiation alone would account for this growth in the microglial population. Similar kinetics were observed for $CD45^{high}$ blood cells (Fig. 3B, panel a), with an initial decrease of infiltrating leukocytes followed by rapid expansion beginning around 5 days post-infection. We also detected a gradual and sustained increase in the number of conventional $CD11c^{+}$ DCs although their numbers were small relative to other myeloid and lymphoid elements in the brain (Fig. 3B, panel b). VSV did not induce a significant infiltrate of pDCs, NK and NKT cells at any of the time points tested (Fig. 3B, panel e and data not shown).
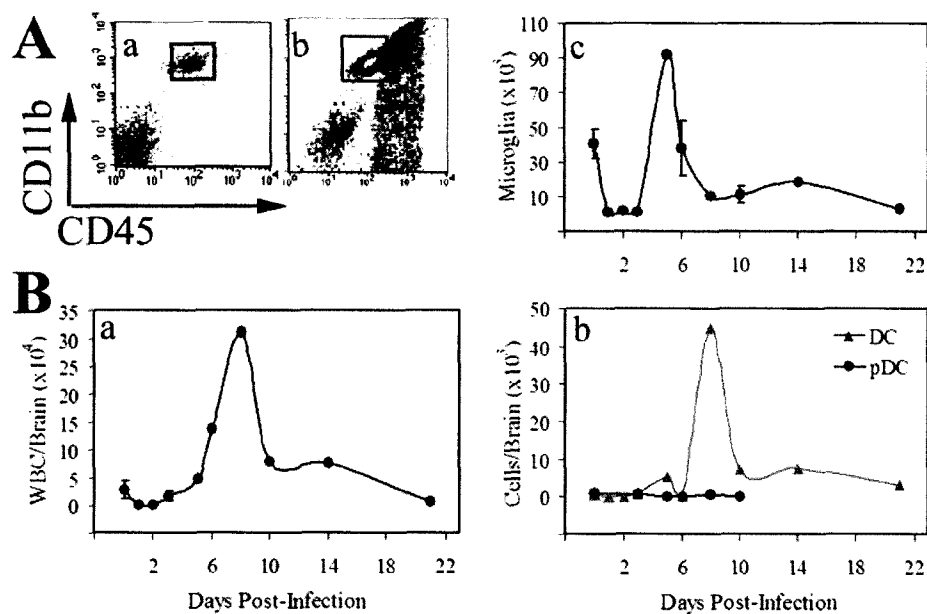
Fig. 3. *Kinetics of the inflammatory response following infection of the CNS.*

Mice were administered a single intranasal dose of VSV at the indicated times prior to euthanasia. Brains were excised, homogenized and the leukocyte fraction enriched by discontinuous Percoll gradient centrifugation. Cells were stained with the indicated mAbs and phenotyped by multiparameter flow cytometry. (A) Microglia isolated from mock (a) and VSV infected (b) brains were gated as $CD11b^+CD45^{low/int}$ (box) and the absolute number of microglia calculated at each of the indicated time points (c). (B) A similar calculation to determine absolute numbers/brain was performed for infiltrating blood-derived leukocytes identified as $CD45^{high}$ cells (d). The absolute numbers of conventional $(CD45^{high}CD11c^+PDCA-1^-)$ and pDCs $(CD45^{high}CD11c^+PDCA-1^+)$ per brain were similarly determined (e). The values presented represent the mean ± S.E.M. cell yields from the pooled brains of 3-5 mice and 2-9 experiments per time point. Absolute numbers were calculated based on cell recoveries in each organ and the percentage of microglia at each of the indicated time points. Note that the scales in Fig. 3B (panels d and e) are different.

The above results indicated that leukocytes, as a general class, reached peak infiltration around 7 days post-infection. Dendritic cells accounted for approximately 10% of the peak leukocyte infiltrate; however, the fraction of cells that included antigen-specific T cells was unclear. Therefore, we next defined the kinetics of T cell subset infiltration into the CNS following infection with VSV. In addition, we assessed the specificity of infiltrating $CD8^+$ cells using class I tetramers specific for the immunodominant epitope (VSV-N_{52-59}). Fig. 4 indicates that the brain contained a small basal population of T cells that did not expand for several days after virus infection (panel A). $CD8^+$ T cells began to infiltrate the brain on day 6, peaked on day 8 and gradually returned to basal levels on day 21-post infection. Similar kinetics were observed for $CD4^+$ cells with the exception that the infiltrate was smaller and the kinetics were slightly delayed. Virus-specific $CD8^+$ T cells (VSV-N) were detectable in the draining cervical lymph nodes (CLN) around day 3, reached maximal clonal expansion three days later and then their numbers rapidly diminished at a time when peak numbers appeared in the brain (panel B). Thus, VSV induces expansion of both $CD8^+$ and $CD4^+$ T cell populations including $CD8^+$ T cells specific for the nuclear protein of this virus. These kinetics, defined by flow cytometric analysis, are consistent with immunohistochemical studies reported by Reiss and her colleagues (Bi et al., 1995b; Forger et al., 1991). Although the peak tetramer response in the CNS occurs at 8 days post-infection, the peak of the tetramer response in the CLN occurs at 6 days post-infection, a time point which also shows clear leukocyte infiltration in the brain (see also Fig. 9). This allowed us to observe the immune response in both the CNS and the putative organ of antigen presentation (CLN) simultaneously, within the same animal. Thus, this time point was chosen for subsequent studies.

Phenotypic characterization of microglia isolated from encephalitic brains.

The presence of activated and an expanded population of VSV-N T cells in the brains of VSV-infected mice suggests that primary antiviral immune responses may be either initiated and/or propagated in the CNS. If this is true, it implies that the brain possesses a professional APC capable of driving clonal expansion and differentiation of naïve $CD8^+$ T cells.
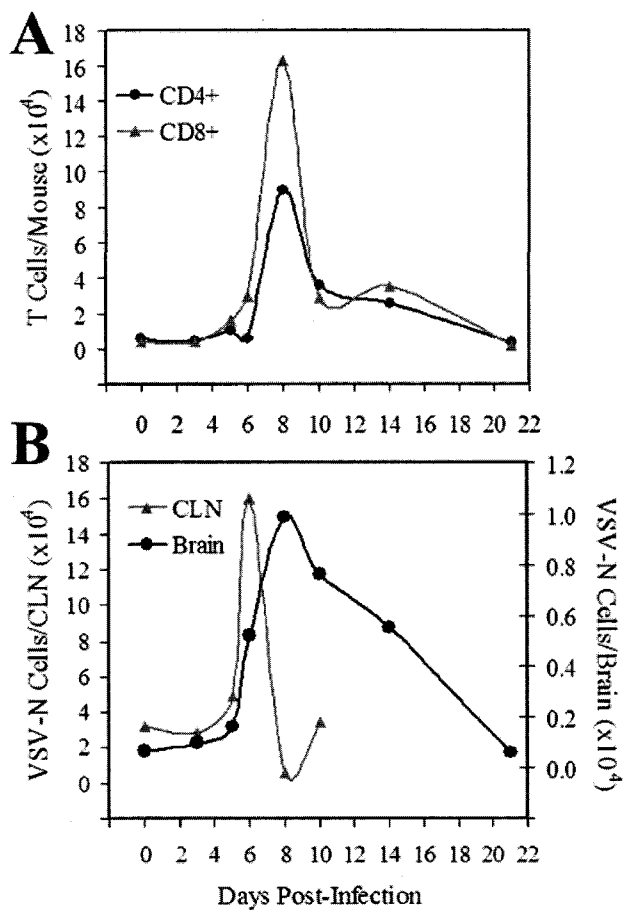
Fig. 4. *Kinetics of T cell subset infiltration in the encephalitic brain.*

Mice were infected with VSV and at the indicated times post infection, brains were excised, pooled and leukocytes isolated by Percoll gradient centrifugation. Single cell suspensions of pooled cervical lymph nodes (CLNs) were also prepared from the same animals. Cell populations were then phenotyped by flow cytometry. (A) Leukocytes infiltrating the brain were stained with mAbs to either CD8 or CD4 and the number of each T cell subset per brain calculated based on cell recoveries and percentage of each subset. (B) Cells were incubated with VSV-N- specific tetramers, washed and then stained with mAb to CD8. The absolute number of CD8^{+} VSV-N T cells present in the brain and CLN was then calculated based on the cell recoveries in each organ and percentage of CD8^{+}tetramer^{+} cells. These values represent the means ± SEM of 2-8 experiments with 3-5 mice per time point.

To examine the extent to which microglia may function as APCs, we evaluated microglial expression of several molecules essential for activation of naïve $CD8^+$ T cells during the early stages of the virus infection. As previously discussed, naïve microglia of mice expressed low to intermediate levels of CD45 and coexpressed CD11b, but were CD11c⁻. As previously reported, the vast majority of microglia from naïve mice expressed undetectable to low levels of MHC class I antigens, indicating that antigen presentation to $CD8^+$ T cells is not a constitutive function of these cells. However, virtually all microglia (96%) became class I^+ by day 3 with significant (~50%) class I expression being detected as early as 48 hours following infection (Fig. 5, panel A). Although the percentage of class I^+ microglia dramatically increased, reduced yields of microglia during these early time points prevented a corresponding increase in the absolute number of microglia in the VSV-infected brain (Fig. 5B, panel a). Class I expression was sustained for two weeks but eventually waned to achieve mock-infected levels, correlating with $CD8^+$ infiltrate (Fig. 4A). These results imply that microglia can acquire the capacity to present antigens to, and therefore activate, $CD8^+$ T cells under conditions of infection. Microglia slowly upregulated class II antigens (Fig. 5A, panel b) and as a result significant co-expression of these molecules was not seen until day 10 (Fig. 5B, panels b and c). Microglia also upregulated CD11c corresponding with onset of morbidity and increased inflammation in the brain (Fig. 5A and 4B, panel c). These results may imply improved T cell/microglial interactions during infection. Microglia did not upregulate CD80 or CD86 at early time points post-infection (data not shown), which are functionally required as costimulatory molecules to fully activate naïve T cells. Thus, microglia may serve to propagate rather than initiate adaptive immunity. We did not evaluate these molecules at later time points because antigen presentation was already occurring in the cervical lymph nodes. Interestingly, high constitutive levels of PD-1 were detected on microglia and virus infection induced further expression of this molecule so that essentially all microglia were PD-1$^+$ two days post-infection (Fig. 5A and B, panel d). The physiological significance of the negative regulator PD-1 during acute viral encephalitis is currently under investigation.

A

B

MHC I   MHC II   CD11c   PD-1
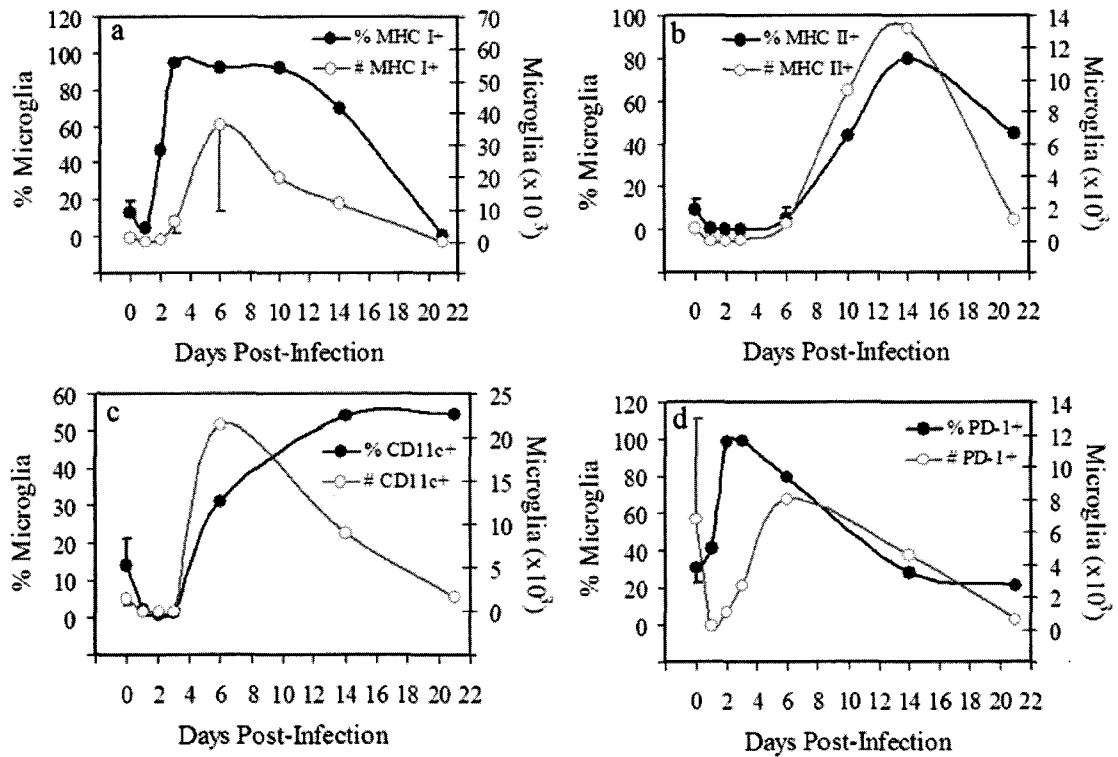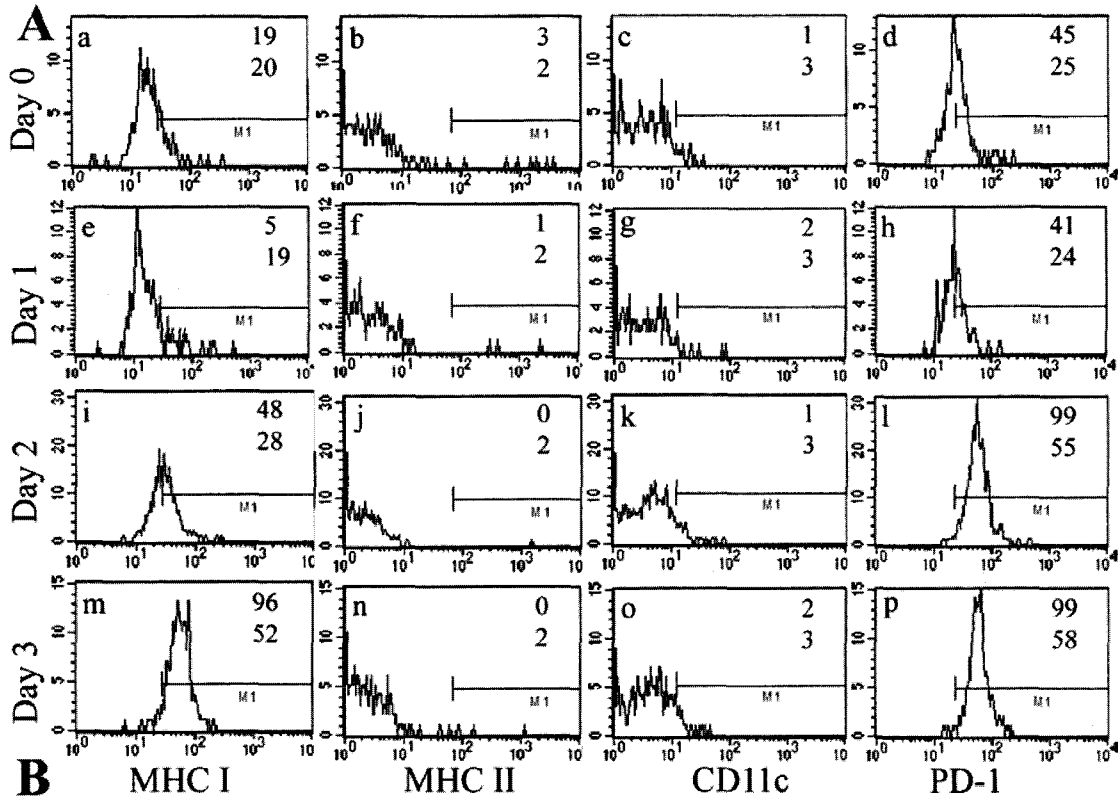
Fig. 5., Continued. *Vesicular stomatitis virus induces the rapid activation of microglia and a delayed*

microgliosis.

Mice were given a single intranasal instillation of VSV at the indicated times prior to euthanasia. Single cell suspensions of the brain were then prepared, subjected to Percoll gradient centrifugation and immunostained for flow cytometric analysis. (A) Microglia were defined as $CD45^{low/int}CD11b^{+}$ cells and expression of MHC I/II, CD11c, and PD-1 on gated microglia determined at early time points post-infection (4 mice per time point). The numbers in each panel refer to either % positive (upper) or MFI (bottom). (B) Kinetics of VSV-induced upregulation of MHC class I (panel a), class II (panel b), CD11c (panel c), or PD-1 (panel d) molecules expressed either as a percentage of total leukocytes per brain or absolute number of microglia per brain (calculated from cell recoveries in each organ). The values in panel B represent the mean ± SEM of 2-7 experiments using the pooled brains of 3-5 mice at each time point.

Cytokine Production in Response to Viral Infection

Cytokines and chemokines also play critical roles in immunity, particularly with regard to recruitment and activation of leukocyte subtypes. Therefore, to further characterise the immune response to VSV infection in the CNS, we assayed 96 cytokines using a membrane-based protein cytokine array (RayBiotech, Norcross, GA). Brain tissue was pooled from naïve or VSV-infected mice (25 mg/mouse, 5 mice/group) eight days post-infection and assayed with minor modifications to the manufacturer's protocols. Data was normalised to a group of cytokines with consistent ratios across all groups. Cytokines exhibiting a 50% change from uninfected levels were identified as up- or down-regulated in response to viral infection.

Fig. 6 presents the normalised intensities for cytokines with a 50% change in expression levels. At this time point, the primary immune response consisted of nonspecific leukocyte infiltration as well as peak $CD8^+$ T cell infiltration, small populations of dendritic cells, and proliferating microglia. Of these cytokines, only three (Dtk, SCF, and TECK) were significantly upregulated (GraphPad Prism 4, Two-Way ANOVA with Bonferroni Post-tests, $\alpha=0.05$). Dtk is a mouse growth factor receptor tyrosine kinase; it is highly expressed in the adult mouse brain, particularly by neurons (Gronowitz et al., 1984). SCF-1 (stem cell factor) belongs to the molecular class of inhibins and is involved in the growth and differentiation of myeloid leukocytes, and is synergistic with GM-CSF, G-CSF, and IL-7 in chemotaxis of leukocytes (Baghestanian et al., 1997) and is shown to be secreted by neurons in response to injury (Sun et al., 2004). TECK (thymus-expressed cytokine) was also significantly upregulated, which was surprising given that it is produced solely by thymic DCs (Vicari et al., 1997) and DCs are detected at low frequency by flow cytometry in the CNS at this time point. However, (Broxmeyer et al., 1999; Kim and Broxmeyer, 1999) some studies suggest that it may have chemotactic roles for macrophages and dendritic cells. Additional cytokines that were upregulated but did not achieve statistical significance included L-selectin, VEGF R2, and VEGF-D, which are likely involved in leukocyte adhesion and extravasation across the vascular endothelium into the CNS. FasL (apoptotic) was also upregulated by 50% but did not achieve statistical significance; this is likely due to expression on infiltrating lymphocytes and is involved in lysis of infected target cells. These results correspond well to the observed leukocyte infiltration into the CNS at this time.

A

Naive   VSV

Membrane 3

Membrane 4

B
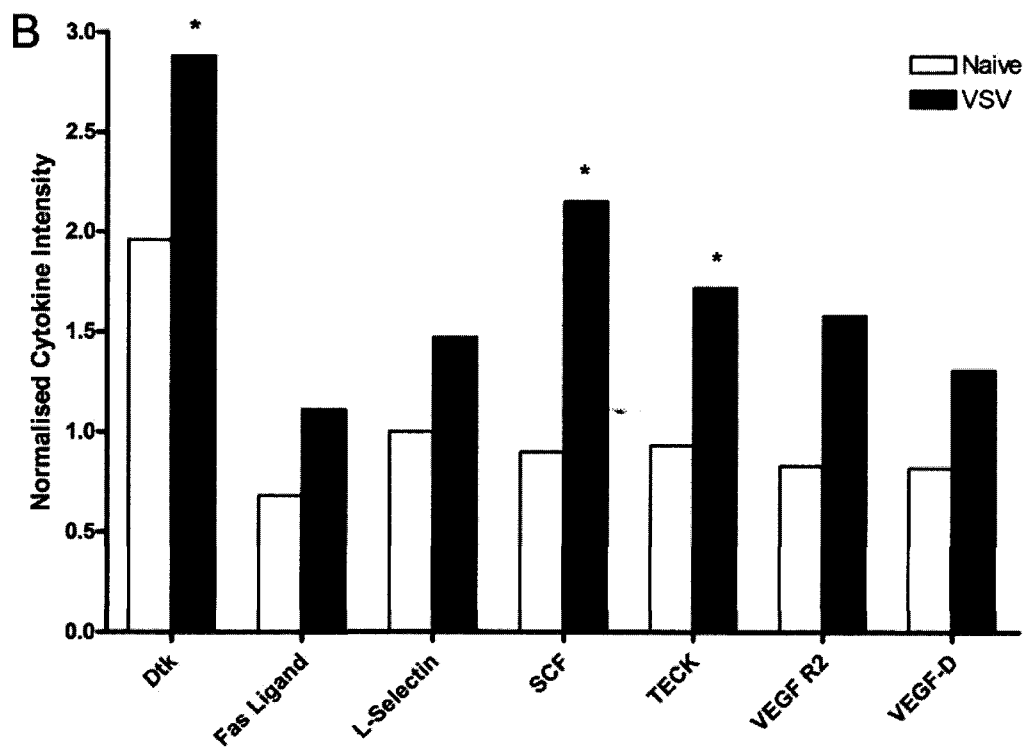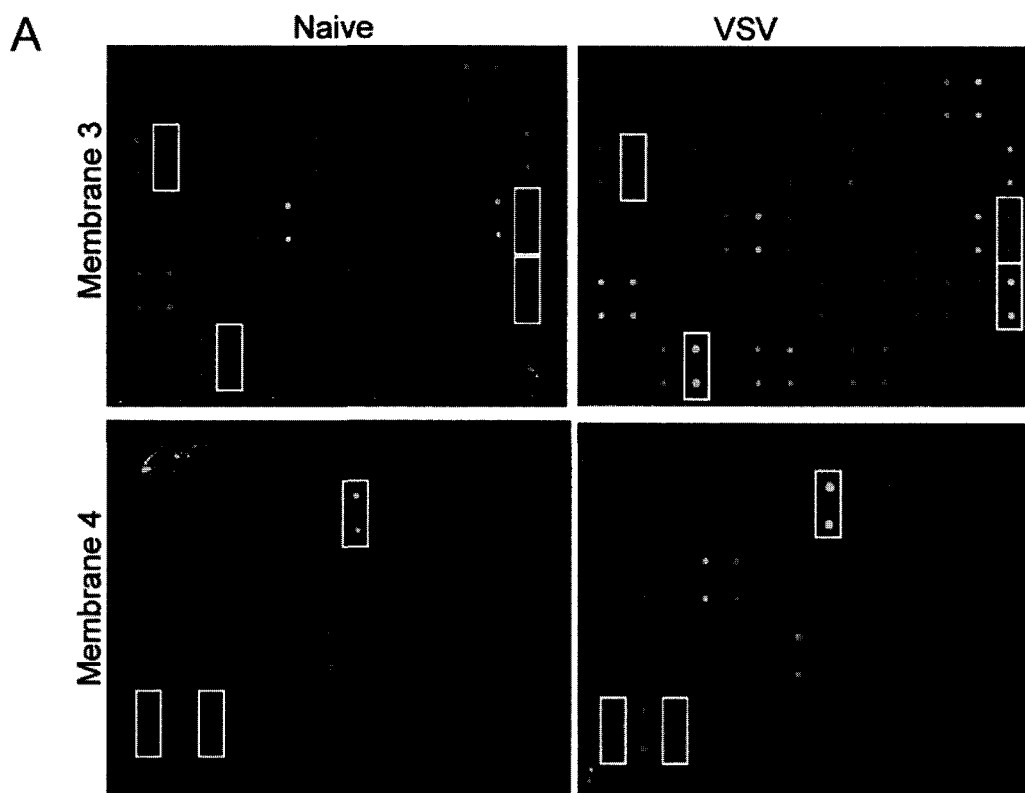
Fig. 6., Continued. *Protein Cytokine Array Results for Naïve and VSV-infected Animals*

Mice were intranasally infected with VSV or remained uninfected (naïve). Brain tissues were harvested 8 days post-infection and snap-frozen in liquid nitrogen before assays for cytokines were performed. Tissues from naïve and VSV groups were pooled (25 mg tissue/mouse, 5 mice/group). Protein extracts were prepared using a protease inhibitor cocktail (Calbiochem) and protein concentrations adjusted to 250 µg/mL prior to use with RayBiotech Cytokine Arrays. Protein spots were revealed with Streptavidin-IR 800CW (Li-Cor Odyssey) and scanned on the Odyssey Imaging system. (A) Protein Arrays are depicted with background correction (maximal fluorescence intensity is shown as white). Cytokines upregulated 50% above naïve levels are boxed. (B) Quantitation of fluorescence signals: a 3-pixel background was subtracted from the integrated fluorescence intensity of each spot and results were normalised. Cytokines demonstrating a 50% increase or decrease in expression relative to naïve control mice were identified. Asterisks indicate statistical significance ($\alpha=0.05$, GraphPad Prism 4).

Using a less stringent definition for upregulated cytokines of a 25-50% threshold change, 14 additional cytokines were identified as upregulated and 2 additional cytokines were downregulated. These cytokines are summarized in Table 2 and can be grouped by general function as chemotactic (6/14), adhesion molecules (5/14), or mitogenic (4/14). A more complete description of their functions and sources may be found in Appendix B.

Table 2: VSV-induced Cytokine Changes (25-50%)				
Cytokine	Naïve	VSV	% Change from Naïve	General Function(s)
Eotaxin	0.90	1.20	33%	chemotactic
Fcγ RIIB	0.83	1.04	25%	antigen clearance
Fractalkine	0.89	1.12	27%	chemotactic adhesion
HGF R	1.02	1.29	26%	mitogenic neurotrophic
IGFBP-6	0.76	0.98	30%	glucose regulation
IL-3	0.89	1.13	27%	mitogenic
IL-6	0.70	0.93	32%	mitogenic
IL-9	0.70	0.97	38%	mitogenic
MIP-1α	0.75	0.95	26%	proinflammatory chemotactic
RANTES	1.06	1.42	33%	chemotactic adhesion
sTNF RII	0.79	0.99	26%	antiinflammatory
VEGF R1	0.78	1.04	34%	adhesion
VEGF R3	1.27	1.59	26%	adhesion
Eotaxin-2	1.75	1.26	-28%	chemotactic
Thymus CK-1	1.60	1.14	-29%	chemotactic

Discussion

The present understanding of the CNS as an immune privileged site is rapidly changing in response to closer scrutiny. It is no longer held that the BBB is impenetrable because several studies have demonstrated that some areas of the brain are unprotected by a BBB. These areas (meninges, choroid plexus, circumventricular organs and ventricles (Farina et al., 2007; Galea et al., 2007a) and the perivascular spaces were initially termed lymphatic clefts by Goldman (Bechmann et al., 2007). Our results demonstrate low numbers of activated T cells in the draining cervical lymph nodes despite their presence in the brain, and provides indirect evidence for more direct, site-specific activation of antigen-specific T cells.

The work of Huneycutt et al. demonstrated that VSV antigen is detectable in the olfactory bulb as early as 12 hours post-infection and spreads caudally through the forebrain by 7 days post-infection, with only a few areas of the midbrain demonstrating antigen reactivity (Huneycutt et al., 1994). Previous studies by Reiss and colleagues demonstrated a high rate of morbidity/mortality in this model that correlated with high titres of VSV at 7 days post-infection and loss of the BBB function late in the infection. Surviving mice efficiently cleared VSV from the CNS, suggesting that the host can mount an efficient antiviral immune response in the CNS (Barna et al., 1996; Huneycutt et al., 1994; Plakhov et al., 1995). This view is further supported by immunohistochemical studies that demonstrated a VSV-induced CNS infiltrate composed primarily of macrophages and lymphocytes (Bi et al., 1995a). The kinetics we demonstrated in the CB6F1/DTRTg mouse are similar to those previously reported (Bi et al., 1995b). Starting as early as 3 days post-infection, we observed a mixed infiltrate of leukocytes in the CNS. Consistent with the findings of Bi et al. (Bi et al., 1995b), the infiltrate contained primarily $CD45^{high}CD11b^{+}$ macrophages/neutrophils, DCs, and T cells, but did not include B cells, NK or NKT cells. Macrophage and lymphocyte infiltration of the CNS increased sharply between days 6-8, corresponding with the peak of viral infection and onset of hindlimb paralysis, morbidity, and mortality. By 8 days post-infection, a significant number of both $CD4^{+}$ and $CD8^{+}$ T cells (both antigen-specific and nonspecific) had entered the brain. Our data demonstrate that CD8 infiltration coincides with CD4 entry into the brains of infected mice, consistent with previous studies (Ireland and Reiss, 2006). Peak numbers of antigen specific (VSV-N) T cells appeared initially in the CLN and then in the brain, suggesting that they were derived initially from the CLN. In this model, activation of

lymphocytes in the CLN correlated temporally with VSV replication in the CNS; this indicates that viral

antigen is CNS-derived rather than originating from the nasal mucosa. These data imply that antigen

presentation and T cell clonal expansion occurs initially in the CLN rather than in the brain. However,

these data do not exclude the possibility that activated microglia induce further antigen-driven proliferation

and effector cell development in the brain.

Microglia become phenotypically similar to DC when activated (Ponomarev et al., 2005a;

Ponomarev et al., 2005b; Shortman and Liu, 2002) and can upregulate several cell surface antigens,

including MHC I and II, CD80, and CD40 (Ponomarev et al., 2005a; Ponomarev et al., 2005b) which are

critical for full activation of naïve T cells. Activated microglia can present antigen to $CD4^+$ T cells and

secrete various chemokines (Persidsky et al., 1999) that help recruit activated lymphocytes. Additionally,

exposure to GM-CSF has been reported to direct the phenotypic and morphologic maturation of naïve

microglia into DC-like cells (Fischer and Reichmann, 2001). Juedes and Ruddle showed that CNS derived

microglia can stimulate IFN-γ production in T-MOG (myelin oligodendrocyte glycoprotein)-specific

lymphocytes (Juedes and Ruddle, 2001). Following these studies, Mack et al. demonstrated that microglia

from the inflamed CNS in the presence of antigen can serve as antigen-presenting cells (APC) for myelin

proteolipid protein ($PLP_{139-151}$)-specific T cells, resulting in the production of IFN-γ and cellular

proliferation (Mack et al., 2003). Our results demonstrated that microglia upregulated MHC I and II in

response to infection, with MHC I appearing as early as 2 days post-infection and MHC II increasing much

later during the course of infection (days 6-10). The prompt expression of class I antigens on microglia is

consistent with their putative role as APCs in the CNS. Together, these data suggest that microglia express

peptide/MHC class I molecules essential for antigen recognition by naïve $CD8^+$ T cells. However, the

infiltration of DCs into the virus-infected brain complicates evaluation of microglia functional APCs. Thus,

their role as functional APCs for a primary antiviral immune response in the CNS remains to be confirmed.

It is interesting to note that $\leq 25\%$ of $CD8^+$ T cells bound class I tetramers at the peak of the

proliferative response. This suggests that most brain infiltrating CD8 T cells are either not specific for

VSV or recognize a novel VSV cryptic determinant displayed in the CNS but not in the periphery. Recent

studies demonstrated an antigen-specific pathway for $CD8^+$ T cells across the BBB (Bechmann et al.,

2007). It is perhaps not surprising that non-specific CD8$^+$ T cells infiltrate the brain. VSV upregulates

both early (CD25/IL-2 receptor, CD69) and late (CD11a/integrin α, CD49d/integrin α4) activation antigens

on essentially all CD8$^+$ and CD4$^+$ T cells by a DC-independent mechanism. CD69 has been shown to play

a role in the very early activation of T cells independently of macrophage/dendritic cell stimulation

(Nakamura et al., 1989). Interleukin 2 (IL-2) also promotes proliferation of T cells. Expression of some

the later activation antigens (CD11a, CD49d) may be required for penetration of the BBB, given their roles

in leukocyte adhesion and extravasation. VSV also disrupts the BBB and this may contribute to T cells

penetration of the brain parenchyma (Bi et al., 1995b). Thus, all of these factors may contribute to the

predominance of CD8$^+$ T cells in the CNS that lack obvious specificity for the inducing virus. It is unclear

why activated CD8$^+$ T cells remain in the brain in the absence of cognate antigen.

The cascade of cytokines, critical for leukocyte attraction and activation, that occurs in response to

viral infection remains poorly studied in CNS infections. The study presented here represents one of the

first to apply protein array detection methods to investigating cytokine production in the central nervous

system. Previous detection of cytokines in the CNS in response to viral infection relied on RNase

protection assays, which semiquantitatively determine steady-state mRNA levels, but may not accurately

reflect protein levels. The work of Carol Reiss et al. determined that CCL1 and CXCL10 mRNA levels

were upregulated early during infection and persisted at high levels throughout the infection (Ireland and

Reiss, 2006). CCL1 is primarily responsible for neutrophil and macrophage chemotaxis (Devi et al., 1995;

Doyle and Murphy, 1999). Based on the protein array data acquired, we found that CCL1 was detectable at

above-average levels but was not upregulated in response to viral infection. Production of CXCL10 is

induced by IFN-γ and TNF-α in many cell lineages including monocytes. It has direct

antibacterial/microbicidal activity. In experimental autoimmune encephalitis (EAE), CXCL10 was shown

to be chemotactic for inflammatory monocytes and inhibition was correlated with improvement in clinical

and histological symptoms (Fife et al., 2001). Our data for CXCL10 revealed only low levels of this

cytokine that were also unresponsive to viral infection. RNase protection assays also demonstrated

upregulation of mRNA for MIP-2, IL-1β, and IL-10. MIP-2 is primarily known for chemotaxis of

neutrophils, which is consistent with reports of those cells being the first to enter the CNS in response to

infection (Ireland and Reiss, 2006). IL-1β has been shown to be constitutively expressed in the brain (Rothwell, 1991) and is proinflammatory, serving as both a chemoattractant and mitogen for leukocytes (Beck et al., 1986; Hestdal et al., 1992; Rothwell, 1991). IL-10 is generally anti-inflammatory: it reduces proliferation of activated T cells and indirectly inhibits production of pro-inflammatory cytokines (Howard and O'Garra, 1992). We found that these cytokines were also expressed at low levels but were not upregulated during VSV infection. The lack of MIP-2 is particularly concerning, given the high granulocytic infiltrate (likely to remain high in neutrophils, although this cell type was not directly phenotyped; neutrophils may comprise up to 40% of leukocytes) observed during VSV infection, including eight days post-infection (the time point studied). We found high levels of other cytokines in mice (MCP-1, IL-12) that did not increase during infection and were not detectable by RNase protection assays. It is interesting to note here that IL-12 was previously demonstrated to have a protective effect in VSV infections of the CNS (Bi et al., 1995b; Chesler and Reiss, 2002; Komatsu et al., 1997) despite the lack of mRNA upregulation (Ireland and Reiss, 2006). These differences may reflect differential regulation at the mRNA and protein levels, rapid reuptake and degradation of the cytokine (low levels of free/detectable cytokine), or may be due to differences in sensitivity and detection method. RANTES, MIP-1α, and eotaxin were common to both the RNAse protection assays performed by Reiss et al. and our protein cytokine array and demonstrated consistent upregulation at both the mRNA and protein levels. All three of these cytokines are involved in leukocyte recruitment to sites of infection (Janeway et al., 2001).

Our data shows that a number of cytokines are responsive to viral infection, although very few reach statistical significance. Of these, Dtk is constitutively expressed in the adult mouse brain and has defined roles in neuronal survival. Its role in immunity in the CNS, if any, is unclear. However, two recent studies imply that the marked upregulation of this cytokine may have implications for immunomodulation: it has been shown to inhibit toll-like receptors and the resultant chemokine cascades *in vitro*, which would lead to an anti-inflammatory condition in the brain (Rothlin et al., 2007). Dtk has also been shown to play a pivotal role in NK cell differentiation (Caraux et al., 2006). Although NK cells were not observed by flow cytometric analysis at this time point, it is possible that the cytokine may have a novel impact on the development of the immune response of the CNS. This cytokine may also work in concert with SCF-1,

which was also upregulated, and has defined roles differentiation of leukocytes. Together, these two cytokines could play a role in directing microglial differentiation/development in response to viral challenge in the CNS. SCF-1 has also been demonstrated to be chemotactic for leukocytes. In this regard, SCF-1 would likely augment leukocyte extravasation in concert with L-selectin, VEGF R2, and VEGF-D, all three of which belong to the integrin class of cell surface molecules and promote leukocyte adhesion. Further studies, including tandem RNA/protein studies, need to be performed in order to fully determine whether these cytokines are truly affected by viral infections and the physiological relevance of such regulation.

These experiments demonstrate a complex, mixed cellular infiltrate into the CNS of virally infected animals that corresponds well with previously reported studies. Microglia respond early and with prolonged duration to viral challenge, upregulating several key surface molecules that imply APC function. Our data indicate that viral antigen is presented in the CLN rather than directly in the CNS, leading to activation of lymphocytes. Cytokine and chemokine production is highly varied and indicative of recruitment of broad leukocyte subtypes into the CNS. Infiltration of various leukocyte and lymphocyte populations corresponds well to viral clearance and mouse survival. These studies provide several attractive targets for APC capacity (DCs, macrophages, microglia) and antiviral clearance (CD8^{+} T cells, macrophages, microglia) that will be further evaluated in the next chapters.

CHAPTER V

IMPACT OF PERIPHERAL DENDRITIC CELL ABLATION ON THE INFLAMMATORY RESPONSE IN THE CENTRAL NERVOUS SYSTEM

Introduction

The primary focus of this chapter is to determine whether peripheral DCs serve as primary APCs for CNS infections. Our secondary goal was to determine the mechanistic basis for the failure of viral clearance from the CNS following peripheral viral infection when dendritic cells were selectively ablated via diphtheria toxin administration in transgenic mice. Those early studies indicated a crucial role for peripheral dendritic cells in modulating the antiviral immune response in the CNS, which had not been previously reported. However, the unpredictable infection rate of CNS infections (33%) observed with the intraperitoneal infection model necessitated the change to an intranasal mode of infection. **This chapter focuses on testing the hypothesis that peripheral DCs serve as the primary APC in viral infections of the CNS.** We used diphtheria toxin (DT) to selectively deplete peripheral dendritic cells (DCs) in a transgenic mouse line (CB6F1/DTRTg). Based on the current model for antiviral immunity in the CNS, we predicted that loss of DCs would impair T cell activation within the cervical lymph nodes (CLN) and result in loss of proliferation and infiltration into the CNS of infected animals. Concurrent with the loss of infiltrating lymphocytes, we anticipated poor viral clearance and increased morbidity/mortality of mice.

We first characterised the impact of DT treatment on brain-resident populations to ensure that microglial populations were not susceptible to DT-mediated depletion. We next confirmed that a loss of peripheral DCs impaired viral clearance as noted with the intraperitoneal model of infection. As with the initial characterisation of the primary antiviral immune response, we investigated changes in the frequency and phenotype of leukocytes infiltrating the CNS during viral infection resulting from loss of peripheral DCs. We also evaluated changes in the cytokine response during primary viral infection associated with

depletion of peripheral DCs. These studies demonstrate a global suppression of leukocyte infiltrate into the CNS that correlates with increased morbidity and impaired viral clearance in the absence of DCs

Diphtheria Toxin depletes peripheral, but not brain-resident, dendritic cells.

The diphtheria toxin transgenic (DTRTg) mouse line allows for the selective depletion of dendritic cells *in vivo*. Expression of the high-affinity simian diphtheria toxin receptor gene is driven by the ITGAX (integrin α-x) promoter, resulting in selective expression of the receptor on CD11c$^+$ cells. We previously reported that administration of diphtheria toxin (DT) intraperitoneally resulted in depletion of splenic dendritic cells (Ciavarra et al., 2006). However, it was not known whether dendritic cells in the brain would be depleted by this technique as well. Therefore, we treated DTRTg mice with either PBS or 4ng/g DT i.p. 48 hours apart. This schedule corresponds to the dosing and infection schedule that we typically used to induce acute infection in the brain, with virus given on the intervening day. Mice were euthanized 24 hours following the last DT treatment, transcardially perfused with PBS and ice-cold 10% buffered formalin, and brains were snap-frozen in OCT using liquid nitrogen. Tissues were sectioned by the histology core facility at EVMS and immunohistochemistry was performed by Ms. Debbie Sullivan (laboratory of Dr. Woong-Ki Kim) for CD11c (N418 clone). Sections of naïve spleen were used for positive controls. Dendritic cells were readily identifiable in the choroid plexus (Fig. 7) of untreated animals, but not in DT-treated animals. Arrows indicate comparable regions of the choroid plexus that stained positive for CD11c in naïve animals, but were unstained in DT-treated mice. This indicates successful depletion of dendritic cells resulting from DT treatment in regions of the brain unprotected by the blood-brain barrier. Dendritic cells were not detectable by immunohistochemistry in the brain parenchyma, which is consistent with flow cytometric analysis. Note that due to the quality of the histological sections, perivascular regions could not be identified with confidence, and thus their status with regard to DT-mediated depletion is unknown.

We also evaluated potential depletion of microglia and/or perivascular macrophages resulting from administration of DT. Brain sections were stained with antibodies directed against the macrophage marker F4/80, which is expressed at differential levels on microglia (low expression) and macrophages

(high expression). The biological role of this marker is currently unknown. Microglia were readily identifiable as lighter-colored dendriform cells in the brain parenchyma, while perivascular macrophages clustered around blood vessels and stained more intensely for F4/80. Fig. 8 shows that treatment of mice with DT does not deplete either CNS-resident parenchymal microglia or perivascular macrophages.

These initial studies indicate that DT treatment successfully depletes DCs of the periphery (and locations of the CNS unprotected by the BBB), while leaving brain-resident microglia and perivascular macrophage populations intact. Therefore, we can specifically address the role of peripheral DCs in the immune response of the CNS during acute viral challenge.
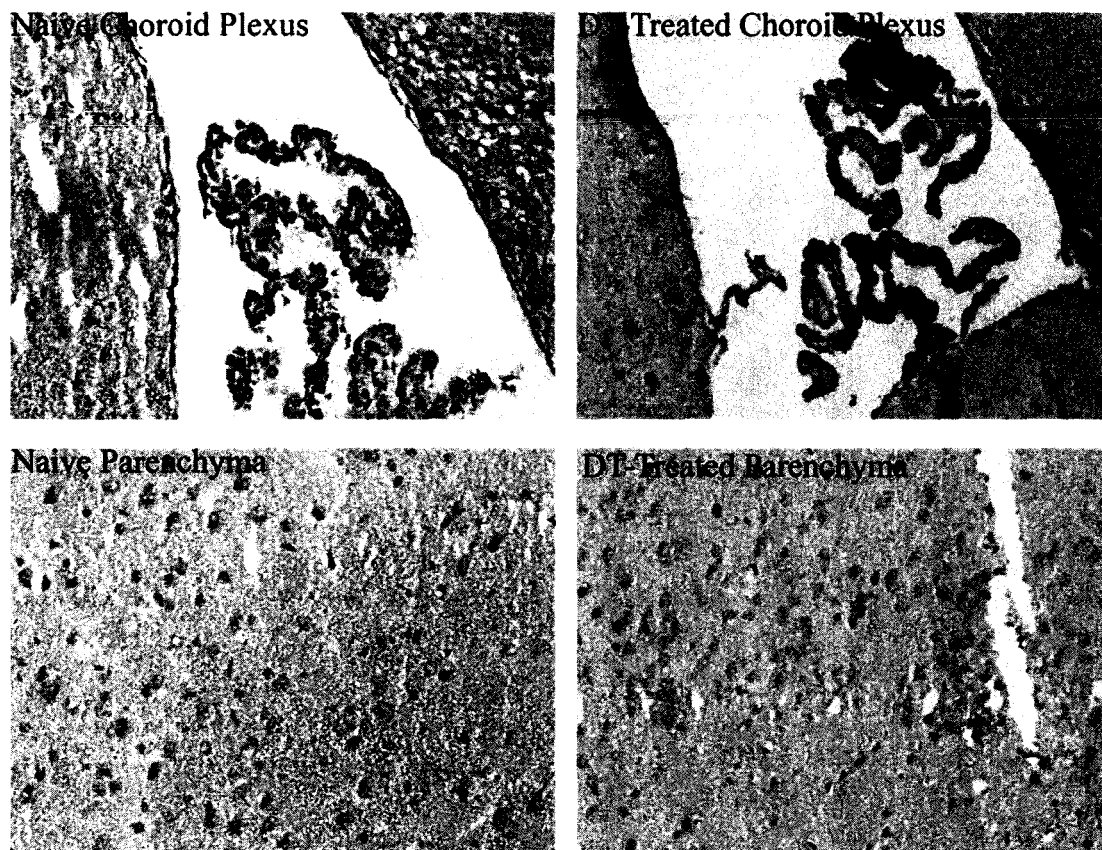
Fig. 7. *Immunohistochemistry of diphtheria toxin mediated depletion of dendritic cells.*

DTRTg mice were treated with PBS or 4ng/g diphtheria toxin (DT) i.p. 48 hours apart, corresponding to the treatment schedule used in future experiments (viral infection would be performed on the intervening day). Mice were euthanized 24 hours following the second DT treatment and transcardially perfused with PBS followed by ice-cold 10% buffered formalin. Brains were excised and snap-frozen in OCT for sectioning and immunohistochemistry with CD11c. Images were acquired for regions of the brain not protected by a blood-brain barrier (choroid plexus) and parenchyma for peripheral and brain-resident dendritic cells. Dendritic cells (CD11c$^+$ appear as dark, sharply defined cells in these images. Note that dendritic cells are absent in the parenchyma of both normal and DT-treated mice, but are markedly depleted in the choroid plexus of DT-treated animals. Arrows indicate DCs in a region of naïve choroid plexus that are absent in the DT-treated mouse. These results are representative of 3-4 mice. Magnification 20X.

NAIVE   DT
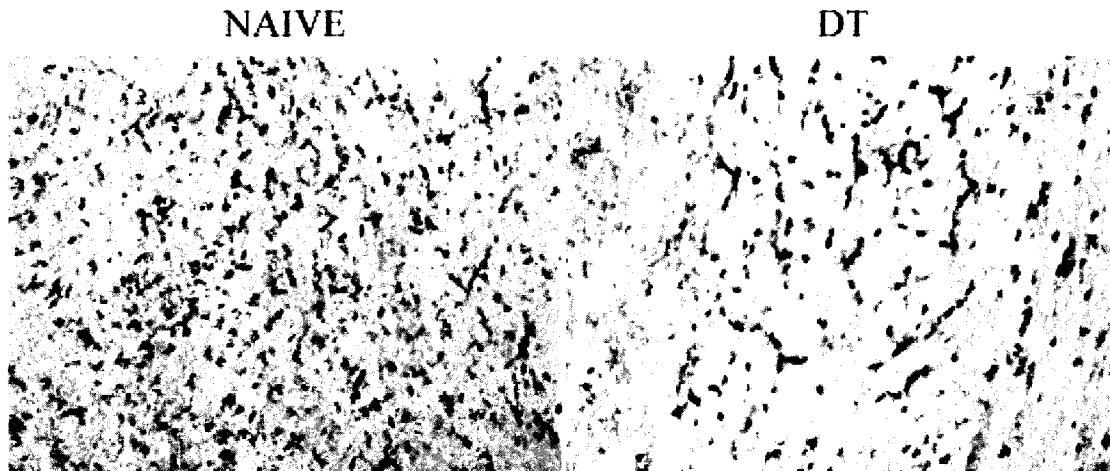
Fig. 8. *Treatment with diphtheria toxin does not deplete microglia or perivascular macrophages.*

DTRTg mice were treated with PBS or 4ng/g diphtheria toxin (DT) i.p. 48 hours apart, corresponding to the treatment schedule used in future experiments (viral infection would be performed on the intervening day). Mice were euthanized 24 hours following the second DT treatment and transcardially perfused with PBS followed by ice-cold 10% buffered formalin. Brains were excised and snap-frozen in OCT for sectioning and immunohistochemistry with F4/80. This antibody stains both perivascular macrophages with differential intensity. Arrows indicate likely perivascular macrophages identified by more intense expression of F4/80 and their proximity to blood vessels, while lighter-stained, dendriform cells are parenchymal microglia. These results are representative of 3-4 mice. Magnification 20X.

Depletion of peripheral dendritic cells impairs viral clearance, survival, and inflammation.

Our previous results demonstrated that microglia became activated in response to viral infection of the CNS and expressed surface molecules appropriate for antigen presentation. This virally-induced phenotypic change implied that microglia may serve as functional APCs. However, DCs also infiltrated the encephalitic CNS, complicating the identification of the true APC. To address this concern, we depleted DCs from DTRTg mice with either PBS (mock) or DT and infected with VSV via the intranasal route. Mice were monitored for survival, euthanized when moribund, and virus titres determined on the brain and peripheral organs. It is apparent from Fig. 9 (panel A) that the majority (63%) of mice depleted of peripheral DCs did not survive this dose of virus, whereas only 15% of control mice became moribund and had to be euthanized. Decreased survival was associated with delayed viral clearance in the brain in mice depleted of DCs (panel B). As previously reported, VSV was rapidly cleared from peripheral organs even in moribund mice depleted of DCs (Ciavarra et al., 2006). Thus, ablation of peripheral DCs specifically inhibits viral clearance from the CNS and as a result likely contributes to the observed increase in morbidity/mortality.

The inability of mice to efficiently clear VSV from the CNS suggests that the antiviral immune response was impaired in mice depleted of DCs. To assess this possibility DTRTg mice were treated with either PBS or DT and then infected intranasally with VSV. Six days post-infection, the number of myeloid (CD11b$^+$CD45^{high}) and lymphoid (CD11b$^-$CD45^{high}) cells in the brain was examined by flow cytometry. This time point was used due to extreme morbidity and mortality noted in DC-depleted mice. At six days post-infection, a robust microglial and infiltrating response was underway despite varying kinetics of individual subsets of leukocytes (demonstrated in Figs. 3-4). Furthermore, we were able to simultaneously evaluate the draining cervical lymph nodes for activation and proliferation of lymphocytes prior to their migration to the CNS; by 8 days post-infection, this response was significantly less noticeable (Fig. 4). As expected, microglia were readily detectable as a CD45$^{low/int}$ CD11b$^+$ population (Region 1, R1) in mock-infected mice (Fig. 9B, panel a). No significant changes in the number of microglia were observed in mice treated with DT alone, a result consistent with low endogenous CD11c expression on resting microglia (panel b) and immunohistochemistry (Fig. 7). However, VSV infection was associated with a microgliosis

that was not inhibited by prior DC depletion (compare R1, panels c and d). These data also imply a marked proliferation of microglia in DT+VSV treated mice by percentage (Fig. 9C, bottom). However, the absolute number of microglia per brain is very similar to VSV-infected mice that were not depleted (Fig. 9C, upper). This discrepancy between percentage and absolute number is reflective of smaller cellular recoveries in general from brains of DT+VSV treated mice.

As expected, infection of the brain induced a potent inflammatory response revealed by the accumulation of a prominent population of $CD45^{high}$ $CD11b^+$ cells (R2) in the brains of VSV infected mice. Surprisingly, prior DT treatment profoundly inhibited this infiltrate (panel d). This was evident whether data were expressed as a percentage or absolute number of infiltrating myeloid cells (panel C). Clonal expansion and/or infiltration of VSV-N T cells into the encephalitic brain were also profoundly suppressed by prior DC ablation (panel D). Thus, DT treatment of transgenic mice ablates DCs but preserves resident microglia. In the absence of peripheral DCs, the inflammatory response as well as the accumulation of clonally expanded $CD8^+$ VSV-specific T cells is markedly suppressed in the CNS. This likely contributes to poor viral clearance and increased morbidity and mortality of mice.

As demonstrated in Fig. 9 (panel D), a well-defined $CD8^+$ $tetramer^+$ population was present in the encephalitic brain despite the absence of $CD45^{high}CD11b^-$ cells (panel C). This apparent contradiction may reflect VSV-induced upregulation of CD11b on activated T cells at this time point. Thus, most of the infiltrating $CD8^+$ T cells would be found in the $CD45^{high}CD11b^+$ gate. This finding is consistent with reports from other models of inflammation (Andersson et al., 1994; Bullard et al., 2005; Christensen et al., 2001; Soilu-Hanninen et al., 1997).

A

a
Percent survival vs Days Post-Infection
VSV
DT+VSV

b
PFU (x10³)/gram vs Days Post Infection

B

CD11b vs CD45

a R1
b
c R2
d R3

C

a
% Cells per Brain
Normal
DT
VSV
DT+VSV
Microglia (R1)   CD11b+ (R2)   CD11b- (R3)

b
Abs # Cells per Brain (x10³)
Microglia (R1)   CD11b+ (R2)   CD11b- (R3)

D CD8 gate

Tetramer vs CD49d

a 1
b 22
c 4
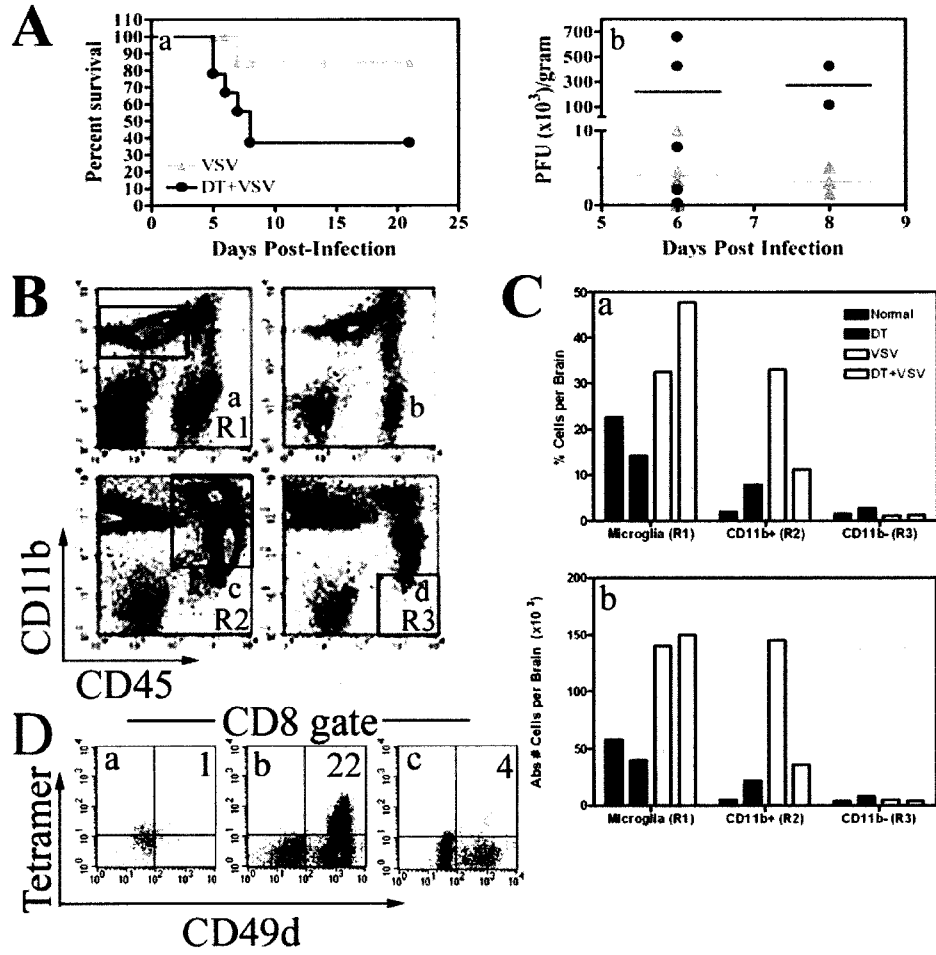
Fig. 9., Continued. *Ablation of peripheral dendritic cells in vivo markedly suppresses the CNS innate and*

adaptive antiviral immune response.

(A) DTRTg mice were given either PBS or DT one day before and after intranasal instillation of VSV

(2×10^5 PFU). Mice were then monitored for morbidity (panel a). Grey triangles represent VSV-infected

mice, while black circles represent DT+VSV-treated mice. Mice were euthanized when moribund and

brains and peripheral organs evaluated for VSV titres by plaque assay (panel b). Again, grey triangles

represent VSV-infected mice and black circles represent DT+VSV-treated mice. These data are derived

from 17 VSV-infected mice and 18 DT-treated, VSV-infected mice. (B) Mice were treated with either PBS

(panels a, c) or DT (panels b, d). Cohorts either remained uninfected (panels a, b) or were given an

intranasal inoculation of VSV at 2×10^5 PFU/mouse (panels c, d). Six days post-infection, brains were

homogenized and then subjected to Percoll gradient centrifugation to enrich for leukocytes. Cells were then

phenotyped by flow cytometry and a microglia gate defined as CD11b$^+$CD45$^{low/int}$ cells (panel a, R1 gate).

A second gate was established for peripheral macrophages/monocytes defined as CD11b$^+$CD45^{high} (panel c,

R2). A final CD11b$^-$CD45^{high} gate was used to evaluate lymphocytes (panel d, R3). (C) The percent

positive and absolute number of cells was then calculated within each of these gates and is summarized in

the bar graphs. (D) To identify CD8$^+$VSV-specific T cells, cells were first incubated with H-2Kb/VSV-

N52-59 tetramers and then stained with mAbs to CD45, CD8, and the activation antigen CD49d. CD8$^+$

cells were gated and the percentage of VSV-specific T cells within this gate determined by tetramer

staining and co-expression of CD49d. Brains from 3-5 mice were pooled within each group. This

experiment has been repeated two additional times and yielded similar results.

Phenotypic characterization of infiltrating leukocytes in encephalitic brains.

We demonstrated in Fig. 2 that VSV induced a large mixed infiltrate of leukocytes into the brains of mice infected intranasally. Fig. 2, panels a-b show that the infiltrating leukocyte population is primarily $CD11b^+$, a phenotype typically associated with macrophages. However, we also observed a large infiltrate of $CD11c^+$ cells that are found in the $CD11b^+CD45^{high}$ population (Fig. 2), which clearly demonstrated the heterogeneity of this population. Dendritic cells are typically identified by flow cytometry due to high expression of CD11c. The expression of other surface molecules may be used to differentiate among the various subpopulations of DCs: PDCA-1 for plasmacytoid DCs, CD11b or 33D1 for myeloid DCs, and CD8 for lymphoid DCs provide a general characterisation of the heterogeneous population. Although the $CD11c^+$ cells identified in this previous study coexpressed CD11b, it was unclear whether these cells truly represented myeloid DCs, or whether CD11b was a more general characteristic of infiltrating leukocytes. Plasmacytoid DCs were not found during our initial experiments (Fig. 2) and were not further explored. This experiment provided a more in-depth characterisation of DC subtypes that infiltrate the VSV-infected CNS and may be sensitive to DT-mediated depletion, which could potentially aid in identification of a crucial DC subtype involved in antigen presentation.

We performed five-colour flow cytometric analysis (Fig. 10), to more clearly differentiate myeloid or lymphoid DCs based on additional surface antigens. Within the standard infiltrating leukocyte populations (defined in panels a-c), myeloid DCs were distinguished by coexpression of 33D1 (Lu et al., 1995; Lu et al., 1994; Masurier et al., 1999; Pulendran et al., 1997) and CD11c (panels d-f), which has previously been used to identify DCs in the brains of mice with chronic CNS infections of *Toxoplasmosis gondii* (Fischer et al., 2000; Nussenzweig et al., 1982). Both the antigen recognised by and the physiological role of the 33D1 monoclonal antibody are currently unknown. Lymphoid DCs were defined as $CD8a^+$ (panels g-i). It is interesting to note that the infiltrating $CD11c^+$ cells did not express either canonical marker for myeloid or lymphoid DCs; thus, their nature remains unclear. However, the upregulation of the CD11b integrin is likely reflective of adhesion to the vascular endothelium, required for migration across the BBB. Since these cell types were not detectable in VSV-infected animals, we were

unable to determine whether one particular subclass of DCs was more sensitive to DT-mediated depletion than another.

The CD11b$^+$CD45^{high} population defined in Fig. 2 included a large, apparently macrophage-based infiltrate. Therefore, we attempted to further define this population based on expression of granulocytic markers (Gr-1) and a recently reported marker for inflammatory macrophages, CD49b. It should be noted that CD49b, clone DX5, is also used to identify natural killer cells, which are not seen in Fig. 2. Despite the lack of a large population, it remained possible that more selective gating might reveal expression of this marker on a subset of macrophages and shed light on their role during CNS inflammation. Within this population, we showed approximately a 50% F4/80$^+$ macrophage-lineage cells and 50% granulocytic cells (panels j-l). The F4/80$^+$ infiltrating macrophages did not coexpress CD49b (Fig. 10, panels m-o), which indicates that they are not phenotypically inflammatory macrophages (Getts et al., 2008). Influx of these cells into the CNS of infected mice was markedly inhibited following DC depletion, but is not likely to be directly related due to lack of coexpression of CD11c.

Finally, the CD11b$^+$CD45^{high} gate (infiltrate) was previously demonstrated to include both CD4 and CD8$^+$ lymphocytes. Here again, lymphocyte infiltration into the CNS was significantly impaired following DT-mediated depletion of DCs. The results presented in panels p-r are consistent with previously described lymphocyte infiltrates for both T cell subsets.

Taken together, administration of DT to deplete peripheral DCs greatly suppressed but did not completely abolish influx of all infiltrating leukocyte subsets. In light of the poor survival of DC-deficient mice, it is apparent that resident CNS cells (such as microglia, which maintained a robust response) are insufficient to mediate viral clearance alone. This strongly suggests that one or more infiltrating leukocyte populations are responsible for or contribute to antigen presentation and subsequent viral clearance. These results also exclude microglia as likely candidates for APC function, since they were not depleted by DT and were insufficient to drive lymphocyte activation and proliferation. However, the global loss of infiltrating leukocytes does not allow us to distinguish between DCs and macrophages as potential APCs at this point.

NAIVE   VSV   DT+VSV

	NAIVE	VSV	DT+VSV
CD11b / CD45	a 35 7	b 9 43	c 13 50
33D1 / CD11c	d 1 0 14	e 0 0 13	f 0 0 13
CD8a / CD11c	g 12 2 12	h 40 3 10	i 18 2 11
F4/80 / Gr-1	j 16 14 15	k 5 17 39	l 4 37 23
CD49b / Gr-1	m 3 1 29	n 3 1 55	o 3 3 57
CD4 / CD8a	p 12 1 13	q 14 1 46	r 12 1 19
CD8a / Tet	s 15 0 2	t 48 2 4	u 20 1 3
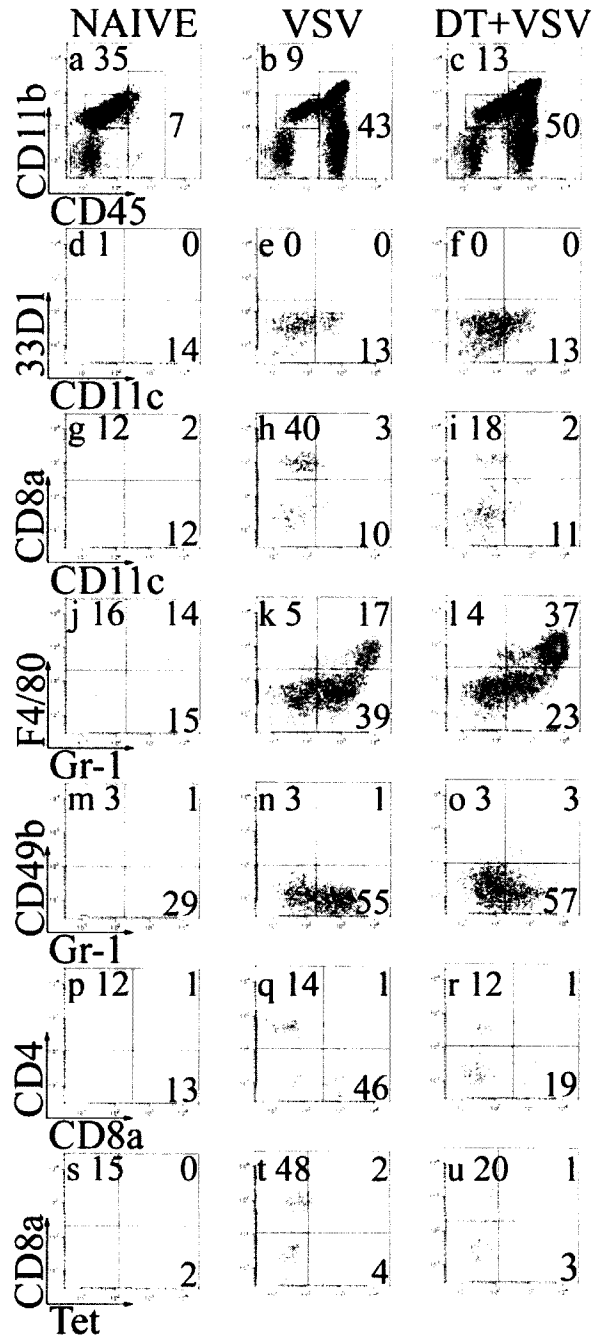
Fig. 10., Continued. *Depletion of DCs alters frequency, but not phenotype, of infiltrating leukocytes.*

DTRTg mice were treated with 4ng/g DT i.p. one day before and after intranasal infection with 2×10^5 PFU

VSV. Mice were euthanized six days post-infection, and brains were harvested and pooled for multicolour

flow cytometry. Microglia were defined as $CD45^{low/int}CD11b^+$ (panels a-c, left box). Infiltrating leukocytes

were gated on forward and back scatter, followed by a $CD45^{high}$ expression profile (panels a-c, right-hand

box). The cellular composition of the infiltrate gate was assessed for myeloid and lymphoid DC subsets

(panels d-f and g-i, respectively). Granulocytes and macrophages within the infiltrate gate were readily

distinguished by F4/80 expression (j-l), but were not inflammatory macrophages ($CD49b^-$, panels m-o).

Lymphocytes within the infiltrate gate were defined as $CD4^+$ or $CD8^+$ (panels p-r), with few or no antigen-

specific cells detected in this experiment. This experiment has been repeated twice with similar results

except for the lack of VSV-N tetramer staining noted in this experiment.

We further investigated the phenotypic characteristics of CD11b+CD45high infiltrating leukocytes

by observing costimulatory markers within this population. These cellular antigens provide indications

about the activation status of lymphocytes (particularly $CD8^+$ T cells) that are entering the CNS, and may

further help define which cells are driving the antigen-specific response. Leukocytes were harvested from

brains of VSV-encephalitic mice at 6 days post-infection and phenotyped by multicolour flow cytometry in

Fig. 11. Gates in all panels were set with appropriate isotype controls; based on this definition, the majority

of infiltrating ($CD45^{high}$) leukocytes expressed intermediate levels of CD11b (Fig. 11A, panels a-b). Thus,

the infiltrating leukocyte population was divided into a $CD11b^+CD45^{high}$ group and a $CD11b^-CD45^{high}$

group. Given that the majority of the infiltrating leukocytes (~74%) expressed CD11b at intermediate

levels, we focused on the phenotype of these cells. Note that infected mice demonstrated a fairly typical

$CD8^+$ influx (panels c-d) and that a subset of the $CD8^+$ cells were antigen-specific (e-f); however, due to

limitations in cell recoveries and staining combinations, the CD11b x CD45 profile could not be

determined for these cells in this experiment. As previously observed in Fig. 9, depletion of DCs

profoundly inhibited the $CD45^{high}$ infiltrate. These data expands on the observed loss of infiltrate to

demonstrate that $CD4^+$ and $CD8^+$ T cell populations are both inhibited by the loss of peripheral DCs (panels

d-f) as well as antigen-specific CTLs (panels g-i). These populations were quantified in Fig. 11B.

With regard to the $CD11b^+CD45^{high}$ infiltrate , the majority of cells in both naïve and virally

infected animals expressed chemokine receptor 7 (CCR7; panels g-h; 86-98%, respectively). A slight loss

in CCR7 expression was observed for DC-depleted animals, as only 66% of infiltrating leukocytes were

positive. CCR7 is primarily noted on lymphocytes and macrophages, but not granulocytes (Kim et al.,

1998; Reape et al., 1999). This receptor enables expressing lymphocytes to respond to the chemotactic

ligand macrophage inflammatory protein 3β (MIP-3β). As in Fig. 9, a marked increase in $CD11b^+CD11c^+$

infiltrate was observed in response to viral infection (44% above naïve control animals). Infiltrating

leukocytes continued to express CD11c in the absence of peripheral DCs. Infiltrating $CD11b^+$ cells also

expressed the costimulatory marker CD40 and macrophage colony stimulating factor (M-CSF receptor,

CD115) at high levels, as well as the T-cell activation antigen CD80. These costimulatory antigens on

lymphocytes must be engaged by their corresponding ligands on DCs to fully activate naïve T cells. Of these antigens, all were significantly diminished in DC-depleted mice. Therefore, it is likely that those few lymphocytes that do enter the CNS in DT+VSV treated mice are functionally inactive or naïve, and may not be capable of mediating cytotoxic effect/viral clearance. Since peripheral DCs are not present to drive lymphocyte activation, this idea is consistent with a model of lymphocyte activation occurring at a site outside the CNS (such as the cervical lymph nodes). Notably, expression of these costimulatory markers in VSV-only mice greatly exceeds the relative frequencies of any particular leukocyte subset, implying that they are broadly upregulated on multiple cell types in response to viral encephalitis. Thus, it is plausible that additional costimulatory signals may be required in the CNS for a fully productive immune response resulting in viral clearance and survival. Furthermore, these data indicates that microglia alone (despite upregulation of primary antigen-presenting MHC complexes) are insufficient to activate T cells in the CNS. The absolute number of infiltrating leukocytes expressing activation/costimulatory antigens is quantified in Fig. 11C.
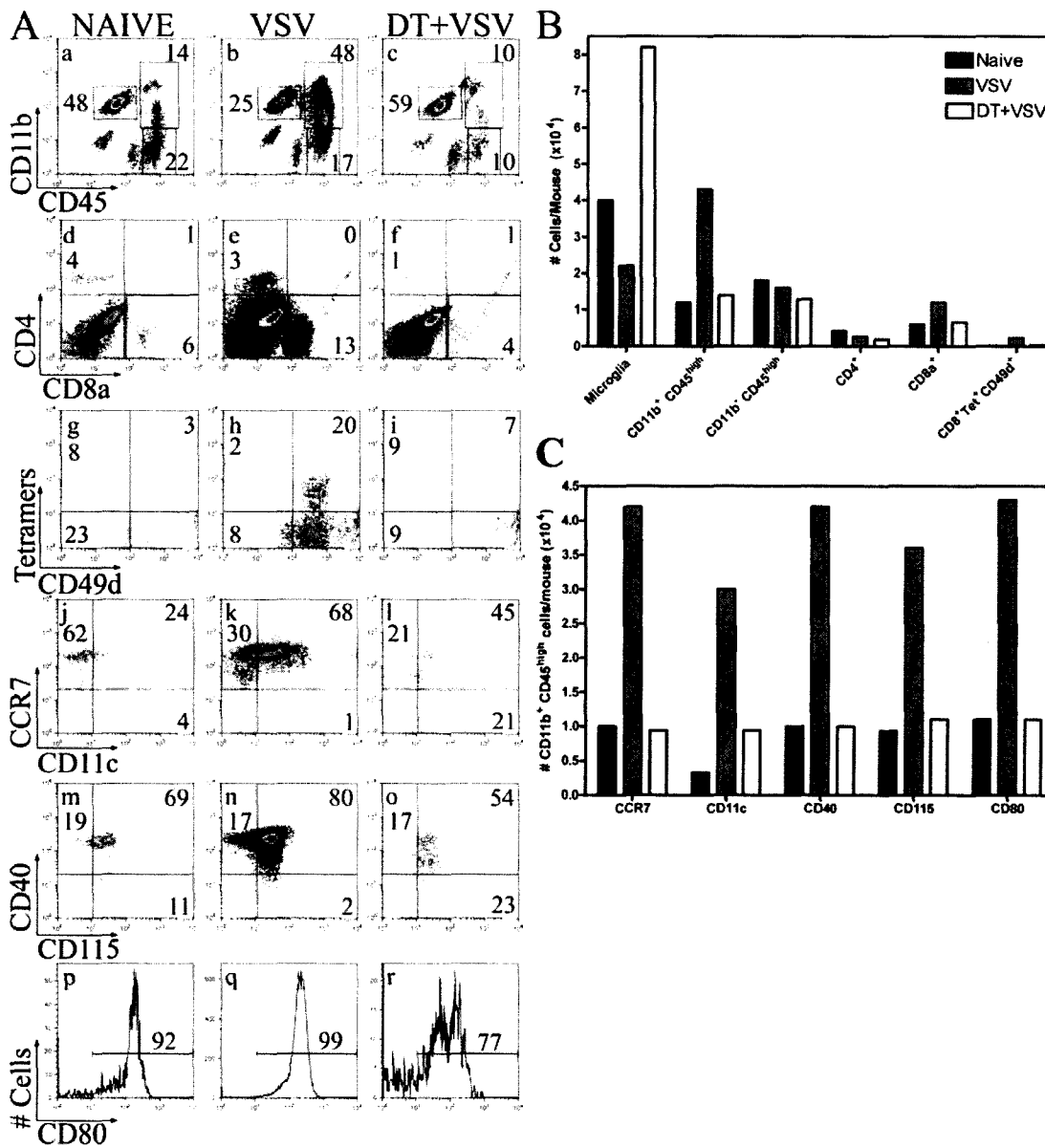
Fig. 11., Continued. *Phenotypic characterisation of infiltrating leukocytes in VSV-encephalitic*

brains of normal and DC-depleted mice.

(A) DTRTg mice were given either PBS or DT one day before and after intranasal instillation of VSV

(2×10^5 PFU). Six days post-infection, brains were homogenized and then subjected to Percoll gradient

centrifugation to enrich for leukocytes. Cells were then phenotyped by flow cytometry and a microglia gate

defined as $CD11b^+CD45^{low/int}$ cells (panels a-c, left regions). A second gate was established for peripheral

mΦ/monocytes defined as $CD11b^+CD45^{high}$ (panels a-c, upper right regions). A final $CD11b^-CD45^{high}$ gate

was used to evaluate lymphocytes (panels a-c, lower right regions). Infiltrating leukocytes were evaluated

for $CD4^+$ and $CD8^+$ T cell frequency (panels d-f), and a $CD8^+$ gate established. The frequency of $CD49d^+$

tetramer$^+$ T cells was determined based on the $CD8^+$ gate (panels g-i). Note that panels a-i not gated on

CD11b/CD45 expression. Subsequent analysis was performed on the $CD11b^+CD45^{high}$ infiltrating

leukocytes to examine costimulatory and activation markers (panels j-r). (B) The absolute numbers of

infiltrating leukocytes and (C) $CD11b^+CD45^{high}$ cells expressing various antigens (lower) was calculated

based on frequency and cell recoveries. These results were obtained based on 3-4 mice per group. These

staining protocols are unique to this experiment; however, results at this time point are reproducible with

other experiments presented herein.

Resting lymphocytes do not express CD11b. However, the number of CD4$^+$ and CD8$^+$ cells exceeded the number of CD11b$^-$ leukocytes in the brain. This did not make sense if in fact lymphocytes were CD11b$^-$. We therefore hypothesised that lymphocytes may upregulate CD11b in response to viral infection of the CNS. To address this discrepancy, we specifically stained for antigen-specific T cells (as a true lymphocyte) and CD11b in the same sample for flow cytometry.

Cells from naïve animals, VSV-infected animals, and DT+VSV animals were harvested seven days post-infection and stained for multicolour flow cytometry. Gates were established on forward (FSC) and side scatter (SSC) characteristics of leukocytes, followed by infiltrating cells (CD45^{high}). The expression of CD8a and antigen-specific tetramers was used to identify lymphocytes, and backgating analysis was then performed using FlowJo to show the CD8$^+$ populations in the previous gates (Fig. 12). This analysis shows that lymphocytes are distributed primarily in the CD11b$^{low/int}$CD45^{high} populations described in Fig. 9 and Fig. 11, which verifies that lymphocytes in this infection model do express CD11b. Furthermore, depletion of DCs with DT does not have a marked impact on the distribution of lymphocytes in the CD11b/CD45 or FSC/SSC gates, although the frequency of these T cells is markedly suppressed in treated mice. Although the functional significance of CD11b upregulation on T cells remains unclear, it is likely that it aids in leukocyte extravasation across the BBB and penetrance into the CNS (Christensen et al., 2001; Persidsky, 1999; Prieto et al., 1988).

These studies reveal an infiltrating leukocyte population of predominantly CD11b$^+$ cells, which includes the T cells and cells that express CD11c, but are not clearly definable as any particular subset of DCs (myeloid, lymphoid, or plasmacytoid). Further studies will be required to clarify the roles of both CD11c and CD11b in CNS immunity. Administration of diphtheria toxin, and the resulting suppression of leukocyte infiltration into the CNS, strongly supports a novel role for peripheral DCs in directing the immune response of the CNS. Furthermore, these results indicate that resident CNS cells, despite phenotypic APC capacity, are insufficient to initiate lymphocyte activation in response to viral challenge.
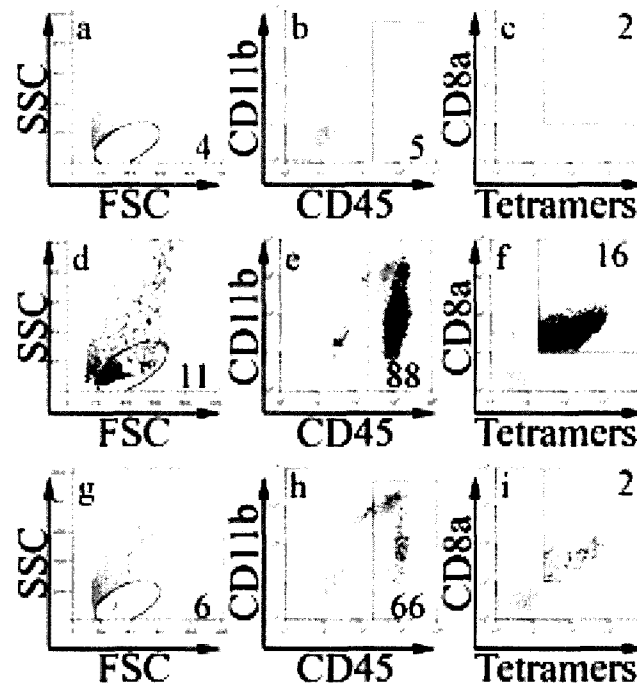
Fig. 12. *CNS-infiltrating lymphocytes express CD11b.*

Mice were treated with DT one day before and after intranasal infection with VSV. Seven days post-infection, mice were euthanized and perfused with PBS, and brains were harvested. Leukocytes were purified by Percoll centrifugation and analysed by flow cytometry. Panels a-c are derived from naïve animals; d-f are from VSV-infected animals, and g-i are from DT+VSV animals. These data were obtained from the pooled brains of 4 mice/group. Backgating analysis performed by FlowJo shows CD8^{+}Tetramer^{+} cells (heavy black dots) in each of the gating profiles.

Blood-brain barrier integrity is maintained in the absence of dendritic cells.

We previously demonstrated a lack of cellular infiltrate in the CNS of DC-depleted mice. However, the mechanistic basis for the failure of leukocyte infiltration was unclear. Furthermore, while a suppression of T cell activation and infiltration was anticipated, we were surprised that other, nonspecific peripheral leukocytes (CD8⁻ CD45^{high}) cells such as neutrophils and macrophages would also fail to enter the CNS. These results conflicted with our prediction that only lymphocyte and DC migration into the CNS would be impaired. The work of Reiss et al. has demonstrated that intranasal application of VSV results in a loss of blood-brain barrier integrity beginning around six days post-infection in Balb/c mice (Bi et al., 1995a). Therefore, we hypothesised that dendritic cells may play a key role in regulation of blood-brain barrier integrity. If dendritic cells contributed to breakdown of the BBB, we anticipated that in DT-treated (DC deficient) mice, the BBB would be maintained. This would prevent VSV-induced penetration of nonspecific leukocytes into the CNS. Thus, we injected VSV-infected and DT+VSV mice intravenously with 2% Evans blue 15 minutes prior to euthanasia. Mice were euthanized and transcardially perfused with PBS to remove Evans blue from the brain vasculature to improve visualisation of dye leakage into the parenchyma.

Fig 13. shows that Evans blue penetration of the virally infected parenchyma was pronounced at seven days post-infection. These results are consistent with the observations of Reiss et al., and closely correspond with the reported kinetics of the spread of VSV through the CNS, which indicate that viral antigen is detectable in the ventral striatum and caudate putamen at seven days post-infection (arrow in Fig. 13). However, mice acutely depleted of DCs prior to infection showed no leakage of dye into the CNS parenchyma even at eight days post-infection despite extreme morbidity, which demonstrates that the BBB remained intact. These data supports the hypothesis that the failure of leukocyte infiltration is the result of dysregulation of blood-brain barrier permeability caused by loss of peripheral DCs.

VSV Day 7   DT+VSV Day 8
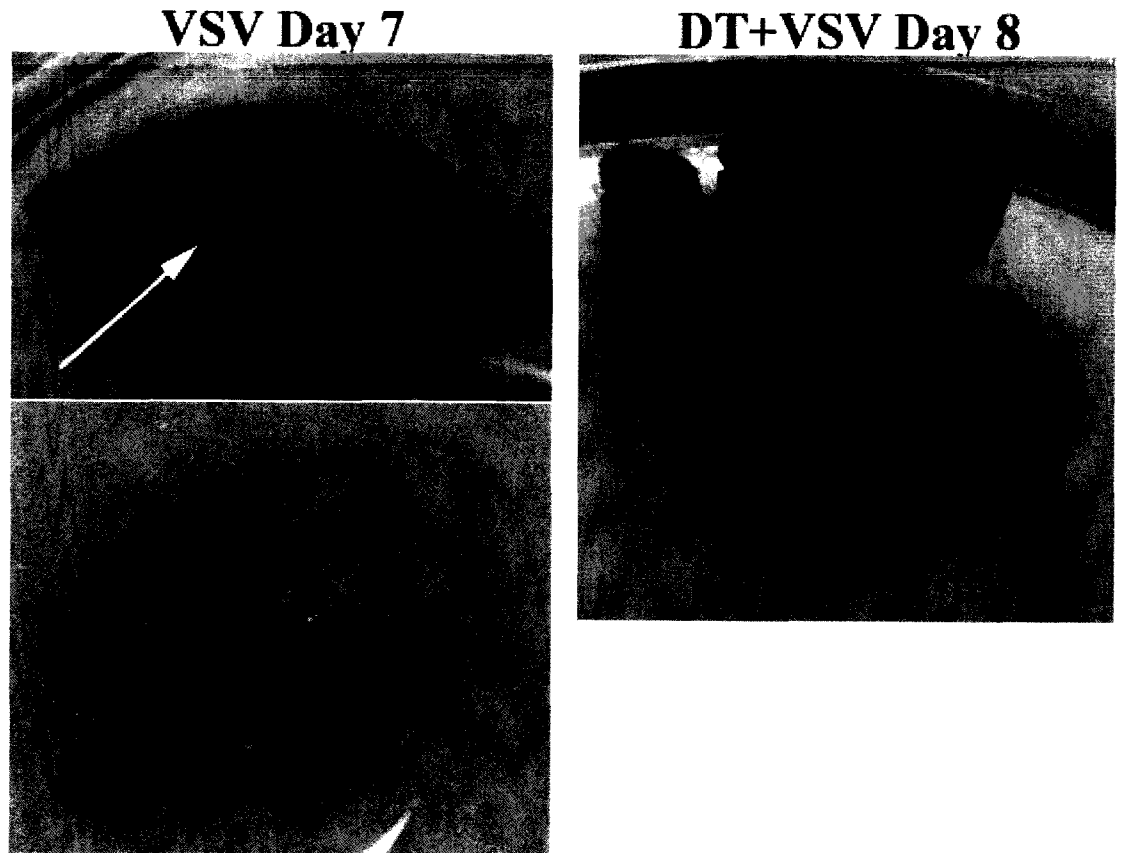
Fig. 13. *Blood-brain barrier integrity is maintained in mice acutely depleted of dendritic cells prior to viral infection.*

DTRTgF1 mice were treated with 4ng/g DT i.p. one day before and after VSV infection with 2×10^6 PFU VSV i.n (n=8). CB6F1 mice were infected on the same schedule (n=9). DT+VSV mice became ill starting 5 days post-infection (1 found dead; 3 morbid). At 6 days p.i., 1 additional DT+VSV mouse was ill. 7 days p.i., 2 VSV-only mice were sick (one with hindlimb paralysis, one morbid). All surviving mice were euthanized at 8 days p.i. Mice were injected with ~200 µL Evans Blue (2% in 0.9% NaCl, filter sterile) one hour prior to euthanasia with CO_2 at all time points. Mice were then perfused with ~30 mL PBS until the lungs were white and the livers blanched to remove Evans Blue from the vasculature. Brains were excised and examined under a dissecting microscope, then photographed. The arrow indicates a region of dark Evan's blue staining in a VSV-only brain. No DT+VSV brains exhibited significant dye penetration in the parenchyma of the CNS at any time points.

Antigen presentation in the cervical lymph nodes is impaired in the absence of dendritic cells.

This model indicates a failure of leukocyte infiltration into the CNS of mice depleted of peripheral

DCs. However, it was not clear whether this failure was due to the aberrantly regulated BBB (Fig. 13), or

whether it was due to a failure of antigen presentation. Therefore, we evaluated clonal expansion of

activated antigen-specific T cells in the draining cervical lymph nodes (CLN).

Fig. 14 shows that activated, antigen-specific $CD8^+$ T cells were detectable in the CLN of VSV-

infected mice at low frequency (panels b). Although the cell frequency is lower than we might expect, this

is likely due to the fact that activated T cells rapidly (within hours) migrate from the draining lymph nodes

(here, the CLN) to the site of infection and do not accumulate significantly within the lymph nodes. Data

from the VSV-infected animals was included as part of the study on kinetics in the CLN documented in

Fig. 4.

In the CLN of DC-depleted mice, antigen-specific T cells failed to proliferate normally (panel c).

These results indicate that a critical APC population was depleted by DT treatment, and supports the

hypothesis that peripheral DCs are the primary APCs for viral infections of the CNS. Furthermore, these

results indicate a novel role for DCs in driving the antiviral immune response of the CNS as modulators of

BBB integrity (Fig. 13).
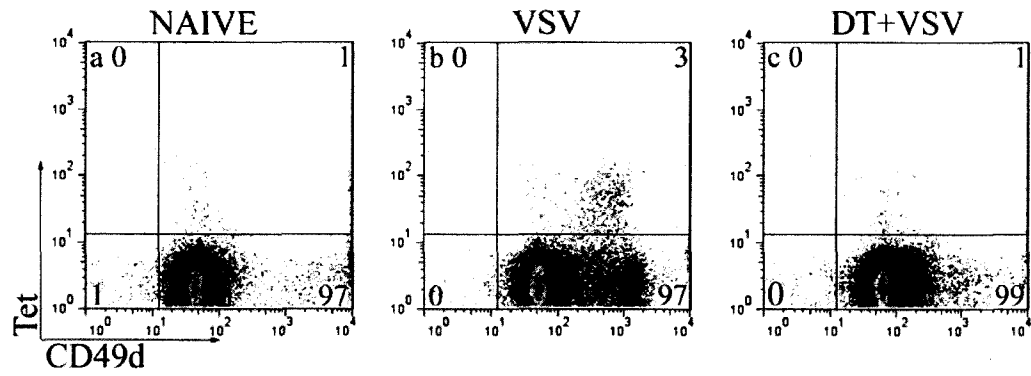
Fig. 14. *Antigen presentation is impaired in the cervical lymph nodes of DC-depleted mice.*

DTRTg mice were given either PBS or DT one day before and after intranasal instillation of VSV (2×10^5 PFU). Six days post-infection, cervical lymph nodes (CLN) were harvested from mice and subjected to flow cytometry. The frequency of $CD49d^+$ $tetramer^+$ T cells was determined based on the $CD8^+$ gate (panels a-c). These results were obtained from the pooled CLN of 3-4 mice per group.

Virus-induced IFN-γ response in the CNS is not dependent on peripheral dendritic cells.

Although we have addressed potential cellular mechanisms of viral clearance, cytokines also have direct antiviral roles. In the CNS, interferon γ (IFN-γ) has been shown to inhibit viral replication and in some models is required for viral clearance (Komatsu et al., 1996; Parra et al., 1999). Furthermore, *in vitro* studies have shown that IFN-γ can inhibit VSV replication (Binder and Griffin, 2001; Chesler and Reiss, 2002; Komatsu et al., 1996; Komatsu et al., 1999). Because IFN-γ is largely considered a T cell product (Kundig et al., 1993) and these cells are not present in the CNS of DC-depleted mice, it is plausible that lack of IFN-γ represents a mechanism for the failure of viral clearance. Although IFN-γ is not the sole cytokine that may be directly involved in mediating viral clearance in the CNS, it appeared to be the most likely candidate. Therefore, we assayed the number of IFN-γ producing cells in the CNS by ELISPOT assay. It should be noted that cells were cultured overnight in ELISPOT plates in the absence of exogenous virus or viral peptide to more accurately estimate the number of actual cytokine-producing cells *in vivo*.

IFN-γ-producing cells were detected at very low frequencies in the brains of uninfected mice. However, IFN-γ-producing cells were readily detected in the brains of mice infected with VSV (Fig. 15). These results are consistent with previous reports of high levels of IFN-γ in the CNS of infected mice (Chesler and Reiss, 2002; Komatsu et al., 1997). In striking contrast to the proliferative response of class I-restricted VSV-N (antigen-specific) T cells, mice depleted of DCs mounted a normal VSV-induced IFN-γ cytokine response in the CNS. This was consistently observed whether the data was expressed as frequency (upper panel) or total number of IFN-γ-producing cells per brain (lower panel). Indeed, in some experiments DC ablation actually enhanced this response (data not shown). Although an IFN-γ response could be detected in the CLNs, this response was modest at this time point relative to the CNS (data not presented). Thus, the VSV-induced IFN-γ cytokine response in the CNS is not inhibited by systemic depletion of conventional and pDCs and implicates that T cells are not essential for IFN-γ production; therefore, microglia or other resident CNS cells may be the source of this cytokine. Furthermore, our data indicate that IFN-γ alone is not responsible for viral clearance in the CNS. Additional cytokines were evaluated in the following studies using protein cytokine array detection methods.
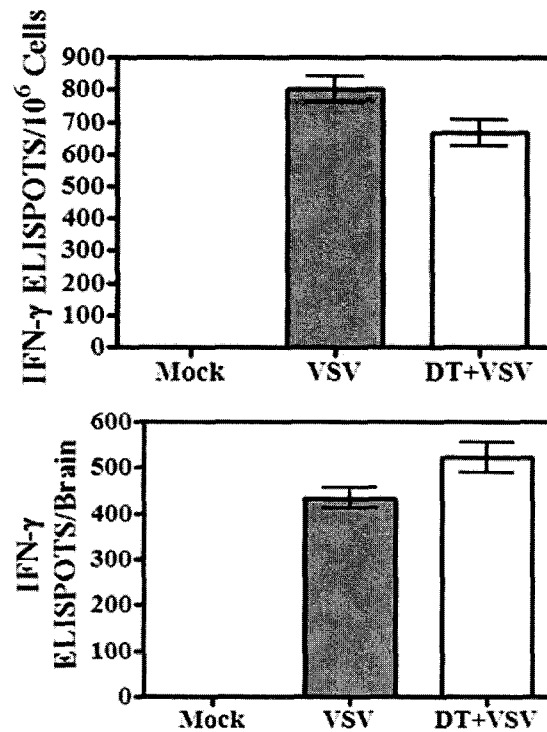
Fig. 15. *Systemic ablation of peripheral dendritic cells does not suppress the virus-induced IFN-γ response*

in the CNS.

Mice were given a single intranasal instillation of VSV after being treated with either PBS (VSV) or DT (DT + VSV). Control mice were not infected (mock). Six days post-infection, brains were removed, pooled and leukocytes isolated by Percoll gradient centrifugation. Cells were seeded into ELISPOT plates in triplicate at up to 2×10^6 cells/well and incubated overnight. No exogenous virus or viral peptide was added to these cultures. The following day plates were developed and the number of ELISPOTs/input cell number determined under a dissecting microscope. The number of ELISPOTs/10^6 cells determined for each triplicate input cell number was averaged and expressed as the mean ± S.E.M. (top panel). The total number of IFN-γ-producing cells/brain was then calculated based on this value and cell recoveries (bottom panel) per organ. Brains from 4-5 mice were pooled within each group. This experiment is representative of two additional experiments.

Protein Cytokine Array in DC-depleted mice

Our previous results indicated that the BBB was maintained in DC-deficient mice. This represented one possible explanation for the failure of leukocyte penetrance into the CNS. The integrity of the BBB and leukocyte recruitment (chemotaxis) are primarily cytokine/chemokine-mediated events. Chemokines may be derived from either CNS-resident cells (such as microglia) or from periperhal leukocytes (such as activated DCs and lymphocytes). This leads to two possible causes for the lack of BBB disruption in DC-deficient mice: chemokine/cytokine dysregulation from either the periphery or from within the CNS. If cytokines/chemokines were dysregulated in the CNS, this could imply either a failure to recruit leukocytes to the brain or a failure to mediate BBB disruption directly. However, if the cytokine/chemokine profile in the brain were normal, this would implicate peripheral dysfunction. We therefore analysed the cytokine profile in DC-depleted mice using a membrane-based cytokine array. This array included a wide variety of chemokines involved in chemotaxis, BBB integrity, viral clearance, and cellular activation.

For this experiment, mice were harvested and analysed concurrently with the groups from Fig. 6. Statistical analysis of the normalised integrated fluorescence intensities revealed that only one cytokine (Dtk, Fig. 16) was significantly inhibited (69% reduction in protein levels) in DT+VSV mice relative to VSV-only mice. The loss of Dtk may reflect neuropathogenicity of VSV and cell death. Several other cytokines showed lesser, non-significant dysregulation (Table 3). Under conditions of DC ablation, all upregulated cytokines corresponded directly to chemotaxis of granulocytes/monocytes with the exception of CTACK (cutaneous T-cell attracting chemokine, CCL27), which has no known function in the CNS. Despite the upregulation of these chemotactic cytokines, leukocyte infiltration into the CNS of virally infected, DC-depleted mice remained strikingly poor. This implies that attempts to recruit leukocytes to the CNS are relatively intact and points toward peripheral dysfunction. Furthermore, it indicates that there may be a CNS-localized source of these cytokines such as microglia, since these cells are not directly affected by DT-mediated depletion. However, there was a reduction in protein levels for HGF R (haematopoietic growth factor receptor), TARC (thymus and activation regulated cytokine) and SCF (stem cell factor). SCF

belongs to the molecular class of inhibins, involved in growth and differentiation of CD34$^+$

(undifferentiated myeloid leukocytes), and synergistic with GM-CSF, G-CSF, and IL-7 in chemotaxis of

leukocytes. SCF, along with TECK, were significantly upregulated in response to VSV infection.

Following depletion with DT, levels of both cytokines declined somewhat (25-35% of VSV-infected levels,

Table 3). The loss of these cytokines tends to indicate that they may be peripherally derived, particularly

since they are implicated in haematopoeisis (HGF R), leukocyte maturation (SCF), and T cell maturation

(which occurs in the thymus; TARC and TECK). IGF-1 (insulin-like growth factor 1) was also impaired,

which indicates dysregulation of circulating glucose, but is also reported to be neuroprotective. This may

reflect the aggravated morbidity and weight loss observed in DC-depleted mice. Perhaps most notable was

a loss in MMP-3 (matrix metalloproteinase 3), which is directly involved in degradation of the blood-brain

barrier (Gurney et al., 2006) and is expressed during inflammation of the CNS (Rosenberg, 2002). Loss of

this protein corresponds well with observations that Evans blue does not penetrate the parenchyma of DC-

depleted mice supporting VSV infections of the CNS. Microglia are the only CNS cell type currently

reported to play a role in secretion of MMP-3 under inflammatory conditions (Candelario-Jalil et al., 2009;

Rosenberg, 2002). Loss of MMP-3 tends to indicate that this cytokine may in fact be peripherally derived,

since resident CNS populations of microglia are intact and other cytokines (such as IFN-γ, Eotaxin,

CXCL16, CTACK, and CXCL10) continue to be expressed at or above levels noted for VSV infection in

DC-intact mice.

With regard to antiviral cytokines, IL-12 and TNF-α have been shown to play key roles in

mediating viral clearance in both *in vitro* and *in vivo* models (Chesler and Reiss, 2002; Komatsu et al.,

1997; Komatsu et al., 1996; Komatsu et al., 1999; Lauterbach et al., 2006; Parra et al., 1999; Patterson et

al., 2002). These two cytokines were also assayed using the protein array, but failed to show significant

increases in response to VSV using this technique despite sensitivities of 100 pg/mL for both IL-12 and

TNF-α. Both IL-12 and TNF-α were unaffected by DT treatment. These results, combined with the

information from IFN-γ ELISPOT assays, indicate that the primary mechanism of viral clearance from the

CNS is not cytokine-mediated, but rather cellular. This is in keeping with current models that hold that

CD8$^+$ CTL are primarily responsible for control of viral infection, and the inability of DC-deficient mice

(with corresponding defect in CD8$^+$ lymphocyte activation and recruitment) to clear virus.

Table 3: DC-dependent Cytokine Changes (25-50%)				
Cytokine	VSV	DT+VSV	% Change from VSV	General Function(s)
Eotaxin	1.20	1.71	43%	chemotactic
CXCL16	1.43	1.87	31%	chemotactic
CTACK	1.22	1.57	28%	chemotactic
CRG-2 (CXCL10)	0.94	1.19	26%	chemotactic
IGF-I	1.30	0.97	-25%	glucose regulation
HGF R	1.29	0.96	-25%	haematopoietic
TECK	1.72	1.29	-25%	chemotactic
TARC	1.37	1.00	-26%	chemotactic
MMP-3	1.45	1.05	-28%	BBB integrity
SCF	2.15	1.39	-35%	chemotactic mitogenic
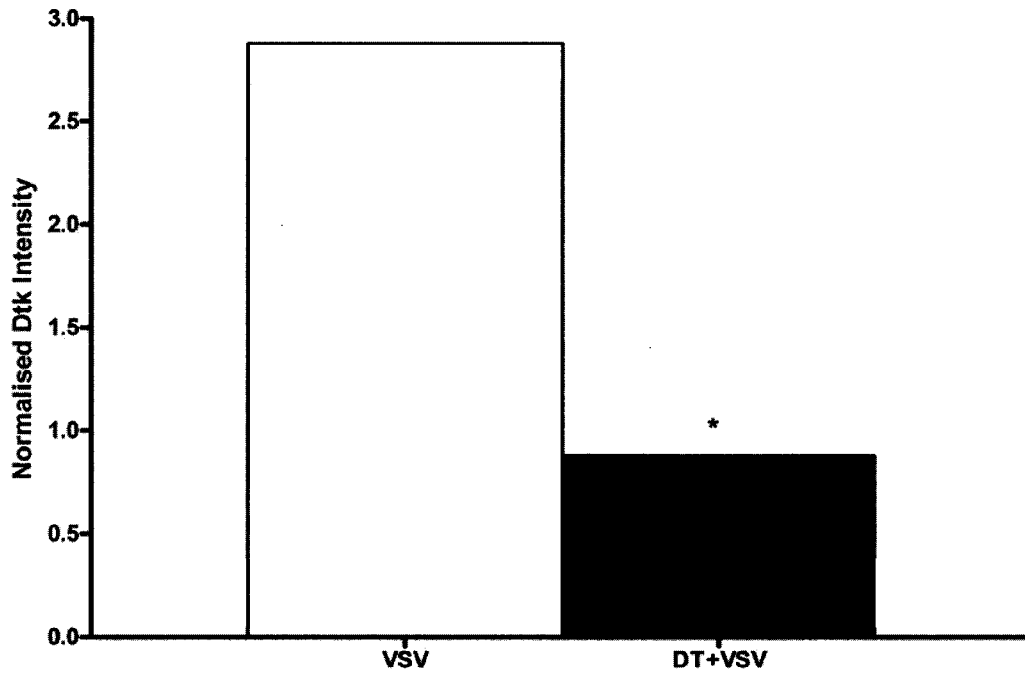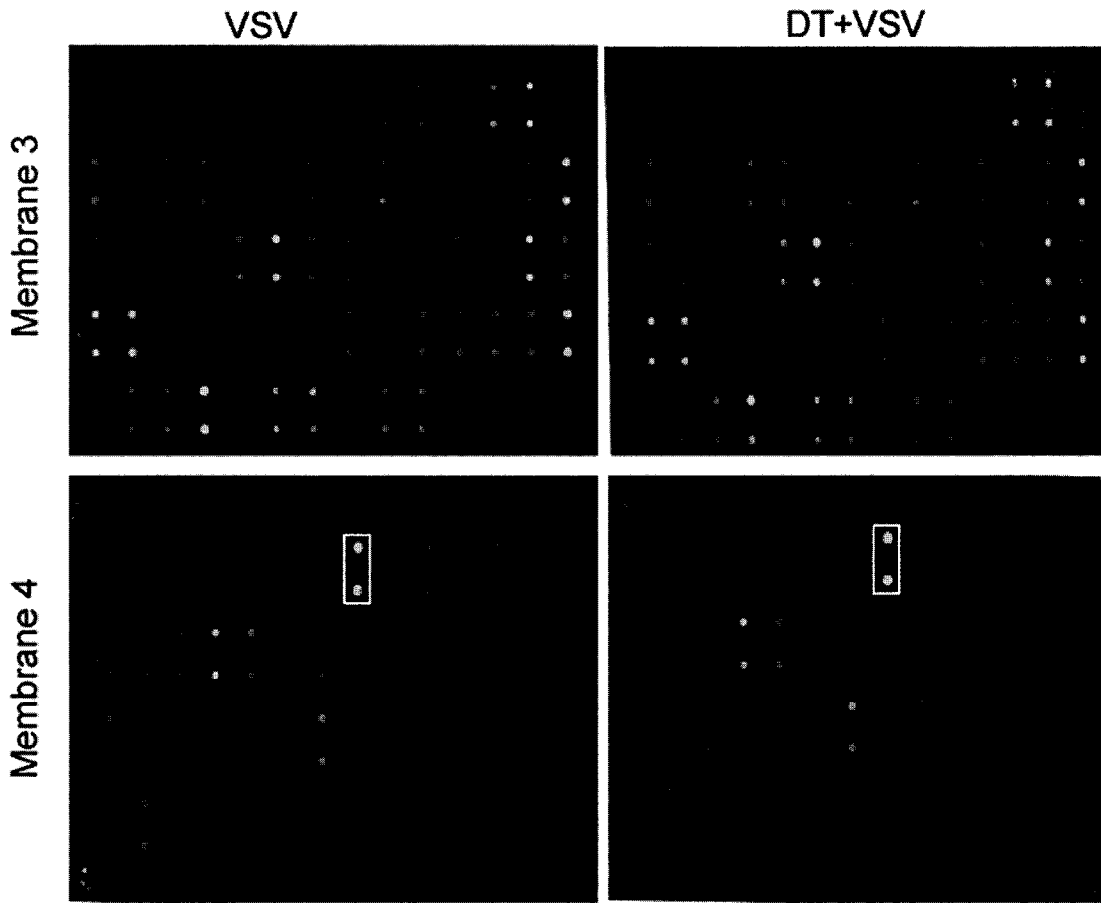
Fig. 16., Continued. *Protein Cytokine Array Results for DC-deficient, VSV-infected mice.*

Mice were treated with 4ng/g DT IP one day before and after intranasal VSV infection. Brain tissues were harvested 8 days post-infection and snap-frozen in liquid nitrogen before assays for cytokines were performed. Tissues from VSV and DT+VSV groups were pooled (25 mg tissue/mouse, 5 mice/group). Protein extracts were prepared using a protease inhibitor cocktail (Calbiochem) and protein concentrations adjusted to 250 μg/mL prior to use with RayBiotech Cytokine Arrays. Protein spots were revealed with Streptavidin-IR 800CW (Li-Cor Odyssey) and scanned on the Odyssey Imaging system. (A) Protein Arrays are depicted with background correction (maximal fluorescence intensity is shown as white). Significantly altered cytokines are boxed. (B) Quantitation of fluorescence signals: a 3-pixel background was subtracted from the integrated fluorescence intensity of each spot and results were normalised. Cytokines demonstrating a 50% increase or decrease in expression relative to naïve control mice were identified. Asterisks indicate statistical significance ($\alpha=0.05$, GraphPad Prism 4).

Discussion

We previously reported that depletion of conventional and pDCs with DT treatment markedly inhibited clonal expansion of naïve CD8^{+} VSV-N T cells in non-neuronal sites (Ciavarra et al., 2006). However, recent studies by Probst and colleagues (Probst et al., 2005) questioned the specificity of this ablation model because they reported that DCs and macrophages were depleted by DT treatment of DTRTg mice. In our experience, the dose of DT used by these investigators was toxic and killed a significant percentage of mice prior to virus infection. Furthermore, we titrated the dose of DT administered to deplete DCs and found efficient and systemic depletion of DCs was achieved with as little as 0.5 ng/g DT (data not shown) without any detectable morbidity. We also observed that different commercial preparations of DT vary in toxicity and potency. The lowest dose (per preparation of DT) that efficiently and specifically depleted DCs *in vivo* was used in the studies presented in this report. We previously reported that this treatment does not ablate T cells or macrophages, despite upregulation of CD11c on these cells following peripheral infection (Ciavarra et al., 2006).

Our current studies expand the observed inhibition of peripheral CD8^{+} VSV-N T cells resulting from DT treatment to include the CNS. Thus, in both the periphery and the CNS, clonal expansion of naïve VSV-specific T cells is DC-dependent, an observation consistent with studies demonstrating that CNS DCs are crucial for antigen presentation to CD4^{+} T cells (Bailey et al., 2007; Miller et al., 2007). Ablation of DCs also profoundly inhibited VSV-induced infiltration of peripheral leukocytes, including nonspecific macrophages, granulocytes, and neutrophils. These results were somewhat surprising, given that the traditional role for DCs is primarily as an activator of naïve T cells. Although DT can penetrate the blood-brain barrier and has been used to selectively kill oligodendrocytes in a similar DTR depletion model (Buch et al., 2005; Gropp et al., 2005), this required a high dose of DT (100ng/injection) and 3 injections/day for one week. Diphtheria toxin has a very short serum $T_{1/2}$ life (90% cleared in 6 hours) with poor CNS penetrance (low blood/CNS transfer constant (Wrobel et al., 1990), and this may explain why multiple high dose injections were required to deplete oligodendrocytes. Thus, it is very unlikely that we depleted DCs in the brain because such treatment conditions were not employed in our studies ($\leq$20ng/injection, two injections). This view is further supported by the observation that microgliosis was not diminished by DT

treatment despite upregulation of CD11c during virus infection (data not shown). These studies imply that activated microglia are not sufficient for a normal inflammatory response to VSV indicating that peripheral DCs provide a unique and essential function in the CNS. This function could be early chemokine production by these cells or, alternatively, reflect a DC-glial cell interaction essential for chemokine production and blood cell infiltration into the CNS. However, our results indicate few cytokines were dysregulated in the CNS following DC depletion, which indicates that DCs are not critical for glial activation or chemokine production. Although the lack of T cell infiltration is in keeping with the paradigm of lymphocyte activation in the CLN, the infiltration of monocytic cells was also profoundly inhibited by depletion of DCs. Previous characterization of the DTRTg model and our titration of DT demonstrated that our dosage did not deplete macrophages (Ciavarra et al., 2006); therefore, peripheral DC apparently play a role above and beyond that of T cell activation in regulation of the CNS immune response.

Although DC ablation profoundly inhibited CNS inflammation and proliferation of VSV-N T cells, it reduced neither microgliosis nor the secretion of IFN-γ in response to viral infection. While IFN-γ is primarily considered a product of T cells, the levels observed in the brains of mice do not correspond with T cell infiltration and are not sensitive to DT-mediated loss of T cell infiltration. Thus, it is apparent that a cellular source of IFN-γ is present in the native CNS and studies in other models suggest that microglia may represent one source of non-lymphoid derived IFN-γ (Kawanokuchi et al., 2006; Suzuki et al., 2005; Wang and Suzuki, 2007). This view is further supported by the observation that IFN-γ production in response to EAE was not significantly reduced in CD11b$^{-/-}$ mice (Bullard et al., 2005). Microglia can also produce significant amounts of IFN-γ in response to antigenic stimulation (Bi et al., 1995b; Fischer and Reichmann, 2001; Mack et al., 2003; Speth et al., 2007). Perhaps importantly, IFN-γ does not appear to have a significant protective effect in peripheral VSV infections (Muller et al., 1994), however, it does appear to promote VSV clearance in the CNS (Bergmann et al., 2003; Kundig et al., 1993; Parra et al., 1999). Our results contrast sharply with these studies and indicate that IFN-γ is insufficient to promote viral clearance or survival in the absence of infiltrating leukocytes.

Given the lack of leukocyte infiltrate seen by flow cytometry, it was surprising that so few cytokines were suppressed in the DT+VSV treated animals compared to the VSV-only controls. Loss of T cell infiltrate was anticipated in diphtheria-treated animals, and consistent with this finding, the T cell-specific chemotactic TARC cytokine was depressed in DC-ablated mice. Of the 96 cytokines assayed, only four that were directly involved in the immune response appeared to be DC-dependent: HGF-R, SCF, MMP-3, and TARC. The role of TECK is still disputed, but it may play a noncanonical role in chemotaxis in the CNS. Dtk, which is highly expressed in the neurons of adult mouse brain (Lai et al., 1994), was markedly decreased in DC-depleted animals, which may simply reflect neuronal pathogenesis and morbidity in this group of mice. However, a few reports indicate that Dtk may also play a role in immunomodulation, particularly with regard to cellular adhesion (Lai et al., 1994; Lu and Lemke, 2001; Schulz et al., 1995). One study found that Dtk may also be expressed on peripheral macrophages and dendritic cells (but not lymphocytes), and may serve to dampen the immune system following antigen clearance (Lu and Lemke, 2001). Our results showing loss of Dtk and increased morbidity/mortality may indicate that macrophages and/or DCs infiltrating the CNS contribute to overall Dtk levels. A loss in Dtk could potentially be correlated with increased CNS inflammation, morbidity, and mortality. IGF-1 was also dysregulated, and may also reflect the morbidity noted in these animals. Several chemotactic cytokines were upregulated relative to VSV-infected mice with intact DC populations. The upregulation of these cytokines (Eotaxin, CXCL16, CTACK, and CXCL10) despite the lack of apparent leukocyte infiltrate indicates that a CNS-resident cell type is the source of these cytokines. The ELISPOT assay indicated a relative frequency of around 740 ELISPOTs/10^6 cells (0.07% of cells), which was not responsive to DT-mediated loss of DCs or other infiltrating leukocytes. We also evaluated IFN-γ production by the protein array and found that it was not highly expressed (normalised intensities of 0.92 and 1.01 for VSV and DT+VSV mice, respectively), although the protein array assay has a reported sensitivity of 500 pg/mL for IFN-γ. This corresponds well with the low frequencies of IFN-γ-producing cells found by ELISPOT assay. Unfortunately, IFN-γ was not noticeably increased in VSV-infected mice relative to naïve controls (a 12% increase), which may be due to assay sensitivity. An ELISA assay using the same antibodies as those used for the ELISPOT assays (at the same capture and detection

concentrations) is reported by eBioscience to have a linear detection range of 1.6-200 pg/mL, which is significantly more sensitive than the protein array. IL-2 and IL-4 were not detected in ELISPOT assays (sensitivity 4-500 pg/mL for each), but were detected in the protein array (sensitivity 10 pg/mL each). IL-2 showed a 24% increase in VSV-infected animals relative to naïve controls and a subsequent 11% increase in DT+VSV mice, whereas IL-4 was decreased in VSV infected mice relative to naïve controls but increased by 14% in DT+VSV animals. These differences may reflect different harvest techniques (*in vitro* culture compared to snap-frozen and protease inhibited) or assay techniques. Cumulatively, these results provide early evidence that cytokine dysregulation is not the primary cause of the failure of leukocytes to infiltrate the virally infected CNS.

The mechanistic basis for the failure of peripheral blood cells to infiltrate the brain in mice depleted of peripheral DCs remains to be clarified. However, our results indicate that the primary defect is in the failure of BBB breakdown, rather than failure to activate brain-resident microglia or lack of chemoattractant cytokines. This points to a peripheral dysfunction resulting from loss of DCs, although the specific cell type or cytokine(s) responsible for BBB breakdown in this model was not identified. Based on our data, the most likely candidate for a cytokine-mediated failure to open the BBB would be MMP-3, which was downregulated following DT-mediated depletion of DCs. However, DCs have not been shown to directly secrete MMP-3. Therefore, it is possible that DCs play a role in activating a currently unidentified cell type responsible for MMP-3 secretion and modulation of BBB integrity. Loss of DCs causes also failure of CD8$^+$ T cells to infiltrate the CNS, a likely reason underlying the failure of viral clearance, morbidity, and mortality in DT-treated mice.

In summary, VSV applied to the nasal mucosa caused reproducible encephalitis in mice characterized initially by microglia activation and microgliosis followed by a massive infiltrate of myeloid and lymphoid blood cells. CD8$^+$ T cell infiltration into the brain correlated temporally with the rapid upregulation of MHC class I on microglia. Kinetic analysis of the development of VSV-N T cells supported a model wherein VSV-N T cells became initially sensitized to VSV in the CLN, underwent clonal expansion and then emigrated from the CLN into the brain. This view is consistent with studies by Mendez-Fernandez and colleagues who demonstrated that sensitization of naïve CD8$^+$ TMEV T cells

requires the presence of peripheral lymph nodes (Mendez-Fernandez et al., 2005). We were able to demonstrate that microglia are not primary APCs in CNS infections. It is possible that once in the CNS, sensitized VSV-N T cells underwent further clonal expansion and effector cell differentiation driven by peptide/MHC class I complexes displayed on activated microglia. In contrast, the lack of T cell clonal activation and proliferation in the CLN confirms that the primary APC for CNS infections is a DC. However, VSV-induced production of IFN-γ was completely independent of conventional and pDCs suggesting that this response was driven by cells resident in the CNS. IFN-γ was unable to rescue DC-depleted mice from morbidity and mortality, which demonstrates that it is insufficient to mediate viral clearance alone or in combination with microglia. Thus, our data supported T cells as critical mediators of viral clearance; however, we were unable to rule out a contribution of macrophages to viral clearance. This possibility will be further explored in the next chapter. Our data also supported a novel role for peripheral DCs in regulating BBB integrity, possibly through direct or indirect production of MMP-3. The cellular interactions and underlying mechanism(s) that render both the innate and adaptive antiviral immune response dependent on peripheral DCs is currently being investigated.

CHAPTER VI

IMPACT OF MACROPHAGE DEPLETION ON THE

INFLAMMATORY RESPONSE IN THE CENTRAL NERVOUS

SYSTEM

Introduction

Early characterisation of the cellular immune response to viral encephalitis revealed a pronounced infiltrate of $CD11b^+$ cells. These cells are typically identified as macrophages. However, our previous results indicated that the $CD11b^+$ population of infiltrating leukocytes also included $CD8^+$ T cells, granulocytes, and DCs. Of particular note, loss of peripheral dendritic cells profoundly inhibited all $CD11b^+$ infiltrate into the CNS. Although this population was heterogeneous, the loss of macrophage infiltrate was concerning because these cells are not DC-reliant. Macrophages are phagocytic, and in many models they mediate viral clearance. Our previous studies in the peripheral immune system indicated that they play a key role in clearance of VSV in immunocompetent mice (Ciavarra et al., 2006). Therefore, these cells, rather than $CD8^+$ lymphocytes, may be responsible for viral clearance in the CNS of normal mice. The increased morbidity and mortality of DTRTg mice depleted of DCs, and concurrent loss of macrophage infiltrate to the CNS, supported this hypothesis. Whether or not peripheral macrophages contributed to CNS immunity either as mediators of viral clearance in our model of CNS infection remained unclear. **This chapter focuses on testing the hypothesis that peripheral macrophages mediate viral clearance in the CNS of virally infected mice.** In addition, we continued to monitor macrophages as ancillary APCs, although we had clearly demonstrated DCs as the primary APC for CNS infections. To more closely evaluate the contribution of macrophages to viral immunity of the CNS, several macrophage depletion strategies were employed.

Depletion of macrophages in MAFIA mice

In the MAFIA (macrophage fas-induced apoptosis) transgenic mouse line, depletion of macrophages was achieved with injection of AP20187, which induces apoptosis in cells expressing high

levels of *c-fms* (receptor for macrophage colony-stimulating factor-1). A more thorough description of the mechanism of depletion may be found in Chapter II) endogenously express enhanced green fluorescence protein (EGFP), which provides easy identification of the target cell population by flow cytometry. Furthermore, this mouse strain has the C57BL/6 genetic background (H-2^b) and is thus appropriate for tetramer studies, but demonstrated slightly different kinetics from Balb/c and CB6F1 mouse strains. Therefore, our first studies in this mouse strain required calibration of viral dose to result in similar morbidity to that seen in the CB6F1 mouse strain. Despite similar severity in symptoms, the onset of morbidity was still delayed relative to CB6F1 mice.

After establishing an appropriate dosing and infection regimen, we treated mice with AP20187 via intravenous injection daily for 5 days, followed by intranasal application of VSV. Mice were euthanized six days post-infection to evaluate successful macrophage depletion, a time point sufficiently early to note infiltrating leukocytes, but not at peak morbidity/mortality. We then characterised the phenotype of brain-resident and infiltrating leukocytes in the CNS of AP20187-depleted, virally infected animals.

We anticipated that treatment with AP20187 and subsequent VSV infection would result in the loss of macrophage infiltrate (CD11b$^+$CD45^{high}) to the CNS, while leaving the CD8$^+$ T cell and DC infiltrating populations intact. The presence of a pronounced infiltrate of CD11b$^+$CD45^{high} cells in the brains of VSV infected mice treated with dimeriser (Fig. 17A, panels a-c and data not shown) made us question the efficacy of our dimeriser (AP20187) treatment. To insure that we achieved peripheral depletion of macrophages, we repeated the experiment and also evaluated the extent to which CD11b$^+$ cells remained depleted in the peritoneum and bone marrow. AP20187 treatment of MAFIA mice did not impair the infiltrating leukocyte response in the brain induced by VSV (Fig. 17A). The microglial population (CD45$^{low/int}$EGFP$^+$) did not appear to expand in response to VSV infection in this mouse strain, and was unaffected by dimeriser treatment in conjunction with VSV infection.

Analysis of the peritoneum of MAFIA mice indicated that naïve mice contained a prominent population of CD45^{high}CD11b$^+$ cells that diminished modestly in mice given VSV and then expanded in mice treated with VSV plus dimeriser (Fig. 17A, panels d-f). This population of CD45^{high}CD11b$^+$ cells contained both EGFP$^{low/int}$ and EGFP^{high} subsets (note that EGFP is endogenous), with the EGFP^{high} subset

markedly diminished by VSV infection. The loss of these cells may reflect either sensitivity to VSV in the periphery, or migration from the peritoneum to another site in response to CNS infection. These EGFP^{high} cells were no longer detectable in mice given dimeriser and VSV (Fig. 17A, panels g-i). This indicates that EGFP^{high} cells (macrophages) were in fact depleted by dimeriser treatment. These results were consistent with previously reported findings (Steel et al., 2008). The EGFP$^{low/int}$ population was more stable in VSV infected mice and expanded slightly in mice given both dimeriser and VSV. CD45^{high}CD11b^{+}EGFP$^{low/int}$ cells were predominantly Gr-1^{-}, indicating that these cells were likely immature macrophages (monocytes) and not granulocytes (panels g-i). This corresponds with observed increases in band cells following dimeriser treatment (Sandra Burnett, unpublished observations/personal communication). The peritoneum of peripherally VSV infected mice given dimeriser remained essentially devoid of mature macrophages (CD45^{high}CD11b^{+}Gr-1^{-}EGFP^{high}) even 8 days post-dimeriser treatment (unpublished observations). During peripheral infection studies, there appeared to be a compensatory increase in immature macrophages (CD45^{high}CD11b^{+}Gr-1^{-}EGFP$^{low/int}$) in the peritoneum (Steel et al., 2008).

In the haematopoietic bone marrow, the number of CD45^{high}CD11b^{+} cells remained fairly stable regardless of the experimental manipulation (Fig. 17A, panels j-l and Fig. 17B). In naïve mice, this CD45^{high}CD11b^{+} population contained only an EGFP$^{low/int}$ subset that was markedly reduced in virus infected animals but expanded in the dimeriser treated group (panel m-o). In contrast to the peritoneum, virtually all CD11b^{+} cells in the bone marrow expressed Gr-1. When cells recoveries were calculated for these different populations, similar conclusions were reached (Fig. 17B). Perhaps not surprisingly, the bone marrow appears to have compensated for the loss of macrophages targeted by the dimeriser by production of cells with a phenotype characteristic of immature macrophages (CD45^{high}CD11b^{+}Gr-1^{+}EGFP$^{low/int}$).

NAIVE   VSV   AP20187+VSV

B   Peritoneum

C   Bone Marrow
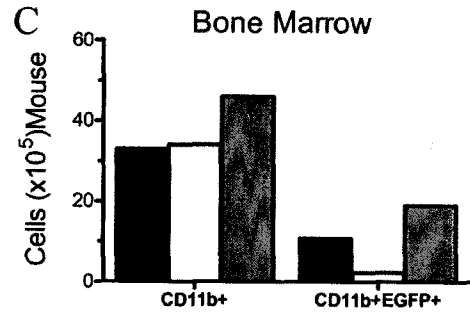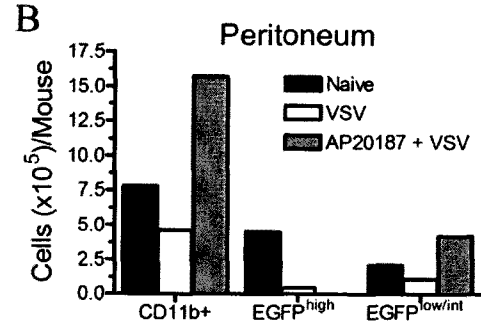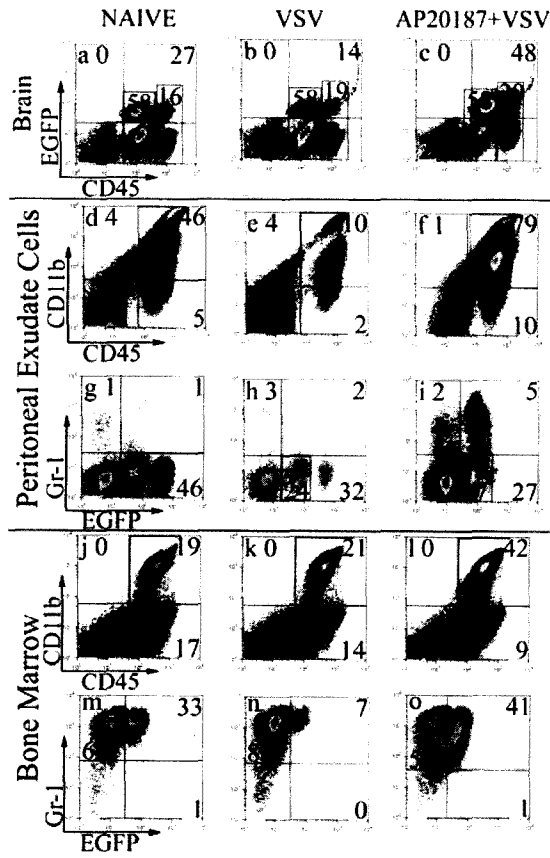
Fig. 17., Continued. *Sustained depletion of EGFP⁺ macrophages following AP20187 treatment of MAFIA*

mice.

MAFIA mice were treated with AP20187 intravenously for 5 consecutive days and on the following day given an intranasal application of VSV (2×10^5 PFU). Six days post infection, brain leukocytes were isolated as described above along with bone marrow and peritoneal exudates cells. Cells were incubated with the indicated mAbs and then phenotyped by flow cytometry. (A) Cells were stained with mAbs to CD45 and endogenous EGFP to characterize the inflammatory infiltrate in the brain (panels a-c) and to evaluate the consequences of dimeriser treatment on macrophages derived from the peritoneum (panels d-f) and bone marrow (panels j-l). Coexpression of Gr-1 and endogenous EGFP on gated CD45^{high}CD11b$^+$ cells was then evaluated on cells derived from the peritoneum (panels g-i) and bone marrow (m-o). (B) The absolute number of cells of the indicated phenotype was calculated by multiplying total leukocyte recoveries x percentage of cells with the selected phenotype.

Characterisation of antiviral response in macrophage-depleted MAFIA mice

Next, transgenic MAFIA mice were treated with AP20187 and given an intranasal application of VSV one day after the last dimeriser injection. Control mice were either uninfected (naïve) or just given VSV. It should be noted that uninfected control mice are CB6F1 mice, which do not endogenously express EGFP on microglia and therefore appear as $CD45^{low/int}EGFP^-$ in Fig. 18, panel e. Treatment of MAFIA mice with AP20187 alone did not diminish resident microglia ($CD45^{low/int}CD11b^+$, box in panels a-b) because dimeriser treated MAFIA mice had approximately the same number of cells in the microglia gate as did untreated control mice (Fig. 18A, panels a, b and Fig. 18B). However, virus infection was associated with loss of microglia and this was exacerbated by prior treatment with dimeriser (panels a-d). Strikingly, microglia loss was selective in that only $EGFP^+$ microglia disappeared from the encephalitic brain (panels e-h, quantified in Fig.18 B). This loss could not be explained by upregulation of CD45 because $EGFP^+$ cells were not detected in the $CD45^{high}$ population. Thus, VSV infected mice (both control and macrophage depleted) contained only $CD45^{low/int}CD11b^+EGFP^-$ microglia. These results were somewhat surprising, although they correspond well to the observed loss of $EGFP^{high}$ cells in the peritoneum. Microglial EGFP intensity is tenfold lower than EGFP intensity noted in the peritoneum; however, it is possible that cells expressing the transgenic Fas construct are more sensitive to VSV infection. The dramatic loss of microglia in VSV-infected MAFIA mice is likely due to the loss of the $EGFP^+$ population; the remaining microglia appear to have been activated normally. This activation occurred independent of peripheral macrophages because MHC class II antigens were upregulated on microglia isolated from dimeriser treated mice (panels i-l). Surprisingly, systemic depletion of monocytes/macrophages did not diminish the VSV-induced infiltrate of $CD45^{high}CD11b^+$ cells (compare panels a-d).

Further characterization revealed a trace population of resident DCs ($CD11c^+$) in mock infected mice that expanded modestly in control and dimeriser treated mice following virus infection. However, plasmacytoid DCs ($CD11c^+PCDA-1^+$) were not detected in either mock or VSV infected mice (panels m-p). A trace population of $CD8^+$ T cells was also identified in brains of mock infected mice that were not activated ($CD49d^-$) and did not recognize VSV (tetramer$^-$). In contrast, encephalitic brains from both control and dimeriser treated mice contained two expanded $CD8^+CD49d^+$ populations, one specific for

VSV (tetramer[+]) and a second with unknown specificity (panels q-t). These results do not support a role for macrophages as crucial APCs in initiating the primary antiviral response in the CNS.

Mice depleted of macrophages remained healthy during the course of this experiment indicating efficient viral clearance from the CNS, whereas two VSV infected mice developed hind limb paralysis 6 days post infection. Thus, these data are in striking contrast with the DTRTg model where ablation of DCs profoundly suppressed both innate and adaptive antiviral immune response in the CNS. Therefore, macrophages also do not appear to mediate viral clearance in the CNS, and even appear to exacerbate encephalitis. Given that macrophages are generally associated with inflammation and tend to produce proinflammatory cytokines which mediate cellular damage, these results are not entirely surprising. This experiment lends additional support to the model wherein CD8^{+} T cells are responsible for viral clearance.

The presence of antigen-specific CD8^{+} T cells in the CNS implied that DCs were not affected by treatment with AP20187 and were thus available to present antigen in the CLN. To verify that antigen presentation was not impaired, we evaluated the CLN for tetramer^{+} CD8^{+} T cells. Fig. 19 (panels a-c) show a low frequency of cells in the CLN that show some slight impairment in AP20187-treated mice relative to VSV-only controls. However, this loss of T cells is most likely due to the extremely large influx seen in the CNS at the same time (Fig. 18).

This model did not provide evidence for macrophages as either APCs or key mediators of viral clearance. These results confirm DCs as primary APCs for CNS infections as well as CD8^{+} T cells as the primary means of viral clearance. Thus, macrophages appear to play no critical role in antigen presentation or viral clearance and may be considered superfluous to antiviral immunity. However, the improved survival and health of mice suggests that macrophages may contribute to the pathogenesis noted in the CNS during acute viral infection.

B
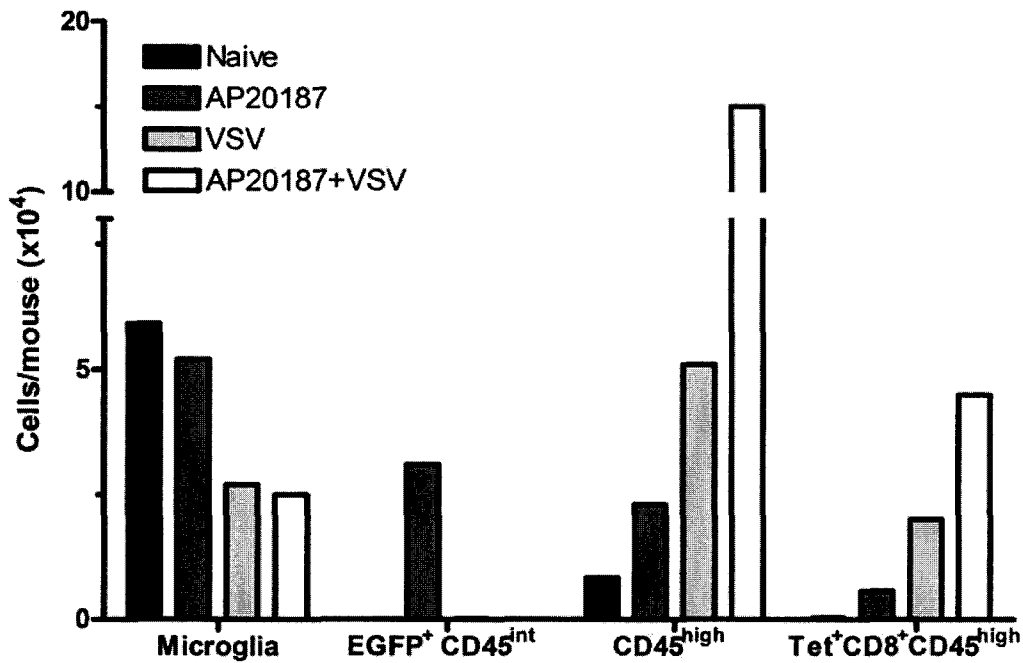
Fig. 18. *Systemic elimination of macrophages with AP20187 does not inhibit cellular immunity.*

MAFIA mice were treated with 20 mg/kg AP20187 via intravenous injection in the retro-orbital venous sinus for 5 consecutive days prior to virus infection with 2×10^6 PFU VSV. **A.** Naïve mice (left column, panels a, e, i, m) were left untreated. Additional mice were treated with AP20187 but uninfected (panels b, f, j, n), or were only infected with VSV (c, g, k, o). The fourth group of mice were treated with AP20187 and infected with VSV (panels d, h, l, p). Mice were euthanized 8 days post-infection. Gates were defined for microglia (panels a-d, box) and infiltrating leukocytes based on CD45 and CD11b expression. Note that treatment of mice with AP20187 did not reduce the microglial population relative to untreated controls. Activation of microglia was evaluated based on expression of MHC II (panels e-h). The presence of DCs/pDCs (panels i-l) and antigen-specific CD8^{+} T cells (tetramer^{+}, panels m-p) was also monitored during infection and were not diminished by AP20187 treatment. These data are derived from the pooled brains of 3-5 mice per group. **B.** The absolute numbers of microglia and infiltrating leukocytes was calculated from the cell recoveries per brain.
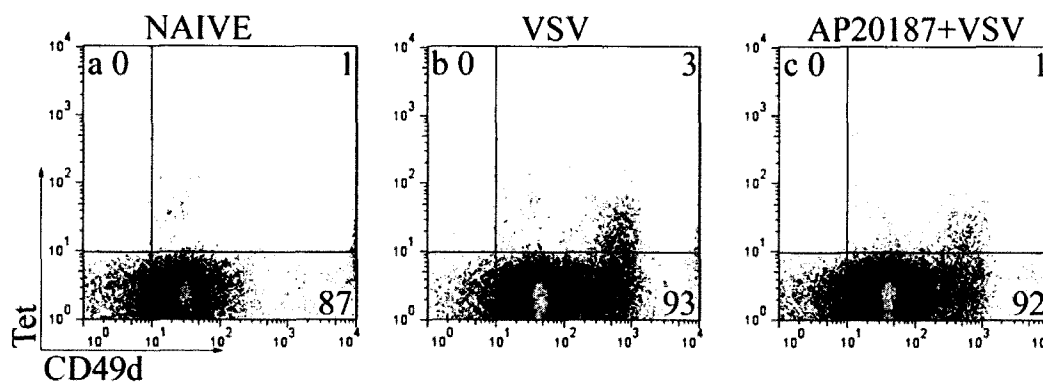
Fig. 19. *Antigen presentation in the cervical lymph nodes is not impaired by AP20187.*

MAFIA mice were treated with AP20187 intravenously for 5 consecutive days and on the following day given an intranasal application of VSV (2×10^5 PFU). Six days post infection, brain leukocytes were isolated as described above along with bone marrow and peritoneal exudates cells. Cells were stained for antigen-specific (Tet+) CD8+ T cells expressing CD49d. Panels a-c above were gated on the CD8+ subset of lymphocytes.

Inhibition of monocyte-macrophage maturation with MGBG

Dr. Michael McGrath (University of California, San Francisco) reported that methylglyoxal bis(guanylhydrazone) (MGBG) inhibited the maturation of monocytic-lineage cells into mature macrophages with subsequent loss of macrophage infiltrate in a model of simian immunodeficiency virus encephalitis (McGrath and Hadlock, 2007). Therefore, it was possible that MGBG could act similarly in our model of VSV encephalitis. Furthermore, it provided an attractive alternative to the MAFIA model (which required daily intravenous injections of AP20187 to achieve depletion) because it could be administered intraperitoneally fewer doses. We also hoped to avoid some of the complications that arose in the MAFIA model, such as loss of microglia and a bone-marrow initiated expansion of immature peripheral macrophages. In this model of macrophage depletion, MGBG was administered intraperitoneally to CB6F1 mice, followed by intranasal infection. Again, we characterised the resident and infiltrating leukocyte responses to the viral infection. We treated CB6F1 (non-DTRTg) mice with 15 mg/kg MGBG i.p. starting one day before intranasal VSV infection and continuing every other day until euthanasia at 7 days post-infection. Mice treated with MGBG alone had no observable reaction to the drug alone. However, virally-infected mice that had been treated with MGBG showed increased morbidity and mortality (50%) at 7 days post-infection relative to untreated virally infected control mice. One MGBG+VSV mouse died at 6 days post-infection and was not included in this analysis; the three remaining mice became ill and required euthanasia at 7 days post-infection. At the time of necropsy, no gross abnormalities were apparent in MGBG-treated mice. However, one mouse was excluded from the VSV-only group due to gross systemic abnormalities at autopsy. The brains and CLNs of mice were harvested for PFU assay and multicolour flow cytometry as previously described.

Administration of MGBG alone did not deplete microglia (Fig. 20A, panels a-b, left box). However, in virally infected animals, microglia not only failed to proliferate (panels c-d), but they also demonstrated inhibition of MHC I and II upregulation relative to VSV-only mice (panels e-h), as well as inhibition of the costimulatory markers PD-1 and CD80 (panels i-l, compare to Fig. 5). The lack of these activation-dependent markers on migroglia implies that MGBG not only crossed the BBB, but also had a direct inhibitory effect on microglial response to VSV.

The percentage of infiltrate in infected animals was not reduced with MGBG treatment (panels c-d, right box), including the granulocyte (Gr-1$^+$) and tetramer$^+$ CD8$^+$ subsets of the infiltrate (panels m-p and q-t). Notably, the percentage of DC infiltrate nearly doubled in MGBG-treated virally infected animals. However, when the absolute numbers of infiltrating leukocytes were calculated, a loss of granulocyte and T cell infiltrate was apparent (Fig. 20B), although the increase in DCs was maintained. Together, these three populations account for all of the infiltrating leukocytes; a purely macrophage population was not seen.

The slight loss of antigen-specific CD8$^+$ T cells in this model was surprising, given that macrophages are not demonstrated to be the primary cell type responsible for initiating adaptive immunity. To verify that this was due to loss of activation rather than failure to penetrate the CNS, we also evaluated the CLNs of uninfected, VSV-infected, and MGBG+VSV treated mice. Fig. 21 reveals low levels of antigen-specific T cells in the CLN of VSV infected mice, consistent with expectations and infiltration of activated T cells into the CNS. However, mice treated with MGBG showed impaired T cell activation relative to VSV-only mice. Despite the almost total loss of T cells in the CLN, inhibition was not complete, as levels in the CNS declined by only about 50% in MGBG mice (Fig. 20).

In these studies, administration of MGBG inhibited microglial activation and proliferation. This may provide a novel model for assessing the role of microglia in antiviral immunity. However, since inhibition was incomplete and corresponded with inhibition of infiltrate, we were unable to directly relate CNS immune dysfunction to microglia. Mice typically clear VSV from peripheral organs within 24-48 hours, and immunocompetent mice appear to clear virus from the CNS rapidly. Viral clearance was diminished by treatment with MGBG at 7 days post-infection (Fig. 20C), which is consistent with the loss of T cells and observed morbidity of mice. Given that the APC population (DCs) should not be inhibited by this drug, it is possible that some of the loss of T cell activation and infiltration may reflect restimulation requirements in the CNS (perivascular spaces or microglial). However, the loss of CLN T cell activation complicated interpretation of these results. Microglia were again demonstrated to be irrelevant as primary APCs. These results generally support T cells as the primary mediators of viral clearance in the CNS; additional studies are needed to determine whether a possible suppression of IFN-γ also contributed to poor viral clearance.

A

Fig. 20, Continued

B

C
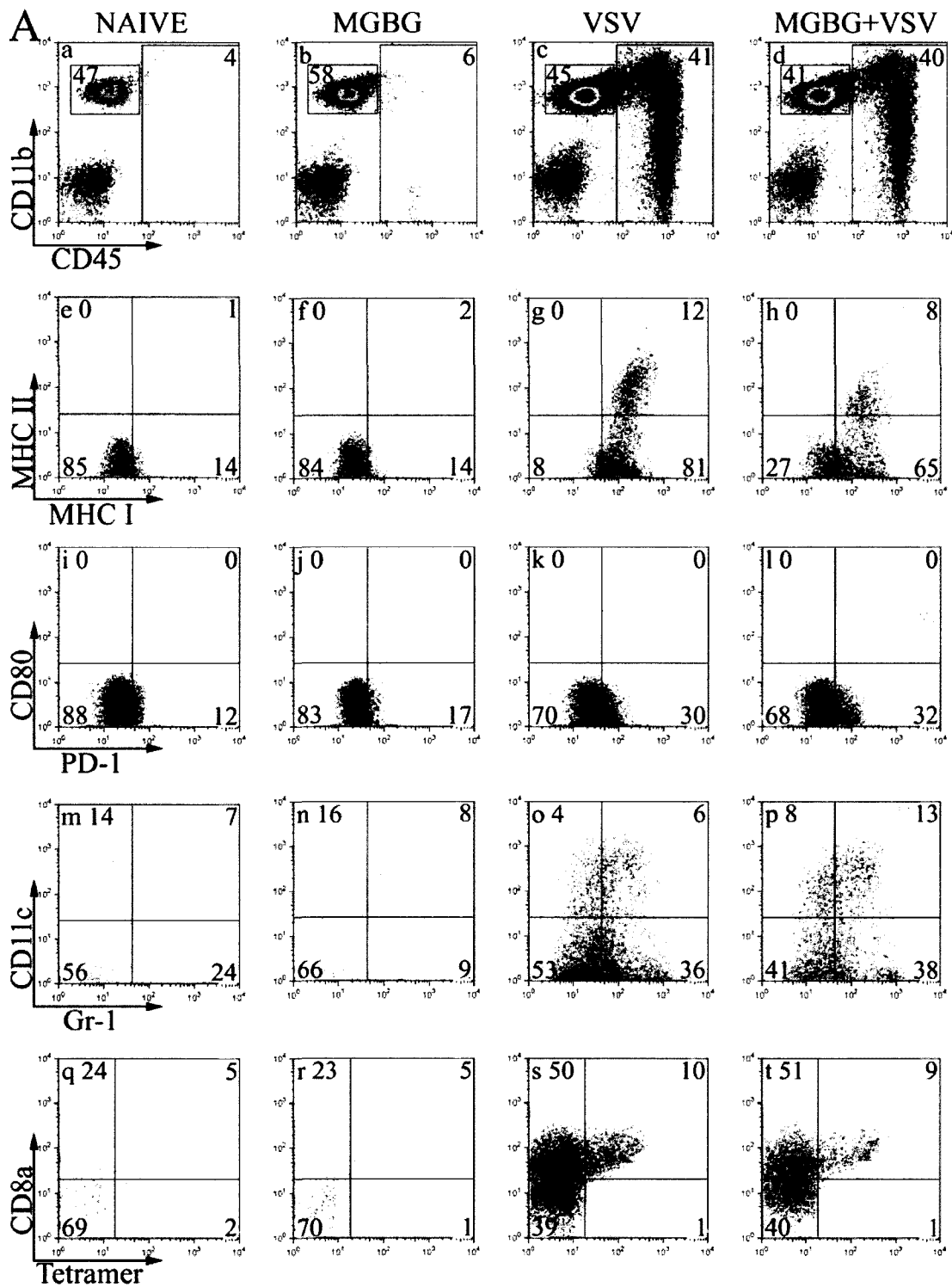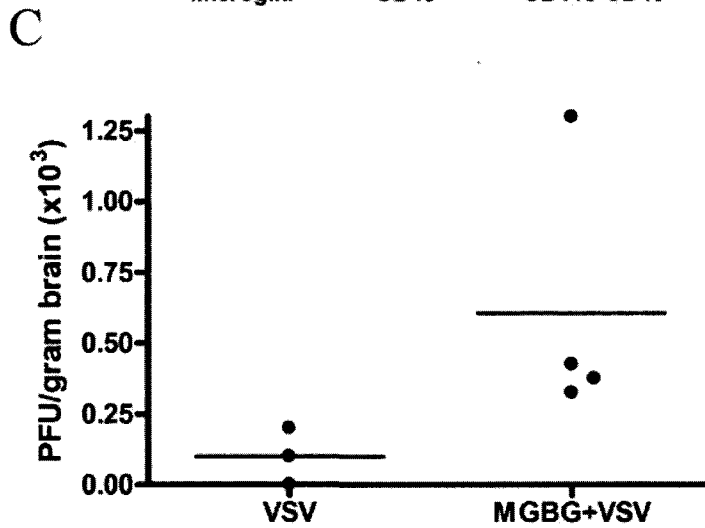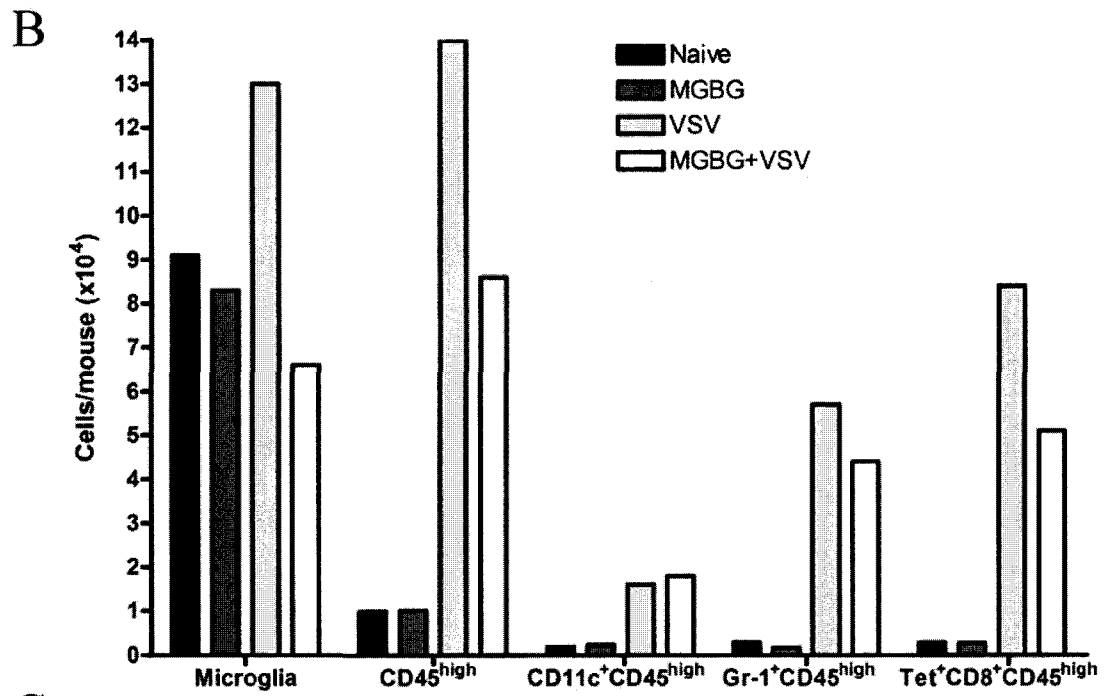
Fig. 20., Continued. *Treatment of mice with MGBG alters microglial response, but not CNS-infiltrating*

leukocytes.

CB6F1 mice were treated with 15 mg/kg MGBG via intraperitoneal injection every other day, beginning one day prior to virus infection with $2x10^5$ PFU VSV and continuing to 7 days post-infection (4 treatments). **A.** Naïve mice (left column, panels a, e, i, m, q) were left untreated. Additional mice were treated with MGBG but uninfected (panels b, f, j, n, r), or were only infected with VSV (c, g, k, o, s). The fourth group of mice were treated with MGBG and infected with VSV (panels d, h, l, p, t). Mice were euthanized 7 days post-infection. Gates were defined for microglia (panels a-d, left box) and infiltrating leukocytes based on CD45 and CD11b expression (right box). Note that treatment of mice with MGBG did not reduce the microglial population relative to untreated controls. Activation of microglia was evaluated based on expression of MHC I and II (panels e-h), PD-1, and CD80 (panels i-l). The presence of infiltrating ($CD45^{high}$) DCs, granulocytes (panels m-p), and antigen-specific $CD8^+$ T cells (tetramer$^+$, panels q-t) was also monitored during infection and were not diminished by MGBG treatment. These data are derived from the pooled brains of 5 mice per group. **B.** The absolute numbers of microglia and infiltrating leukocytes was calculated from the cell recoveries per brain. **C.** Treatment with MGBG reduces viral clearance.
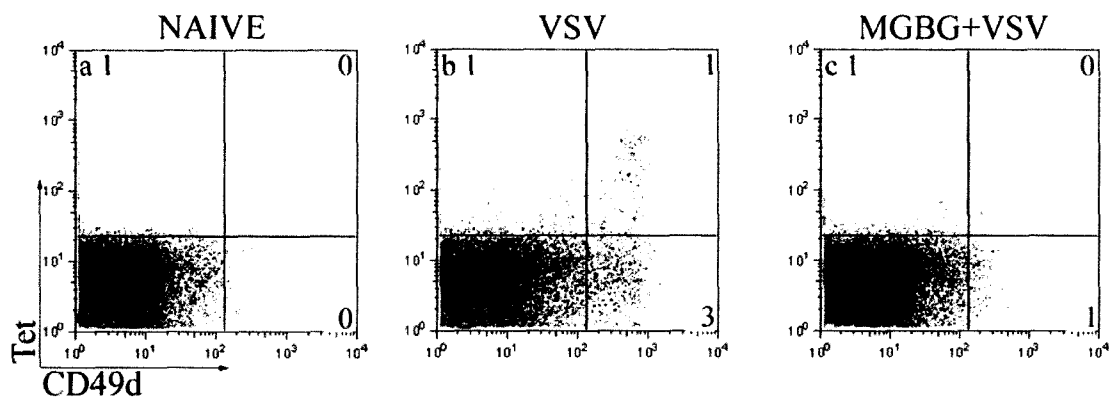
Fig. 21. *Antigen presentation is reduced in virally-infected mice treated with MGBG.*

CB6F1 mice were treated with 15 mg/kg MGBG via intraperitoneal injection every other day, beginning one day prior to virus infection with $2x10^5$ PFU VSV and continuing to 7 days post-infection (4 treatments). Cervical lymph nodes (CLN) were harvested and stained for antigen-specific (Tet^+) $CD8^+$ T cells as evidence of antigen presentation (panels a-c, gated on CD8). These data are derived from the pooled brains of 3-5 mice per group.

Depletion of mature circulating macrophages with clodronate liposomes

Thus far, we have attempted to globally deplete or inactivate peripheral macrophages. To compare these results to an established model of macrophage depletion, we utilised liposome-encapsulated clodronate (CL2MDP), which has previously been shown to target circulating monocytes/macrophages in the bone marrow, spleen and liver while leaving lymph nodes (including the draining cervical lymph nodes) intact (van Rooijen, 2006). We reasoned that if lymphocyte activation occurred in the cervical lymph nodes according to the current model, the VSV-specific adaptive T cell response should remain intact. This technique targets mature, circulating phagocytic macrophages for depletion. In our previous peripheral studies with clodronate liposomes, we did not observe the expansion of immature monocyte/macrophage lineage cells noted in the MAFIA model (Ciavarra et al., 2005). Therefore, we should be able to assess the contribution of infiltrating macrophages into the CNS during acute viral infection.

MAFIA mice were treated with a single intravenous injection of 200 μL clodronate liposomes via the retro-orbital venous sinus while in a surgical plane of isoflurane-induced anaesthesia. Following depletion of circulating mature macrophages (24 hours), mice were infected with 2×10^5 PFU VSV intranasally and monitored for signs of illness; control mice were infected with VSV only. Seven days post-infection, mice were euthanized and perfused with ~30 mL PBS. Tissue was homogenized and subjected to Percoll fractionation for flow cytometry. In these studies, we replaced CD11b with F4/80 in order to differentiate granulocytes (which may be CD11b$^+$, but are F4/80$^-$) from macrophages (which are F4/80$^+$).

Recall that in this mouse strain, EGFP is endogenously expressed on macrophage lineage cells including macrophages. Consistent with previous results in the MAFIA mouse strain, we observed a loss of CD45$^{low/int}$EGFP^{high} microglia in VSV-infected mice. However, this loss of EGFP^{high} cells was not seen in CL2MDP+VSV infected brains (Fig. 22A, panels a-c), although this population did not exceed baseline levels observed in naïve mice. These EGFP^{high} microglia may represent expanded cells from the small remaining population in VSV-infected animals. Alternatively, it is possible that treatment with CL2MDP conferred a protective effect on microglia.

The intent of this mode of depletion was to reduce or eliminate infiltration of peripheral macrophages into the CNS following VSV infection while leaving other cell populations intact. Granulocytes (Gr-1$^+$) have low phagocytic activity and therefore should not be depleted by CL2MDP. These cells should thus comprise a large fraction of the CD45^{high} infiltrate during VSV infection. In the MAFIA mouse model, granulocytes should have a low endogenous expression of EGFP (Burnett et al., 2004). VSV induced a pronounced infiltrate of granulocytes (Fig. 22A, panels d-f), a subset of which were EGFP$^+$ granulocytes (panels g-i). The lack of F4/80 coexpression with Gr-1 (panels j-l) indicated that these cells were not macrophages. However, a population of EGFP^{high}Gr-1$^+$ cells was observed in VSV infected mice. Tissue-variable EGFP expression on MAFIA macrophages has been reported and a cell type that was EGFP^{high}Gr-1$^+$ was noted in the lungs of MAFIA mice (Burnett et al., 2004 26). The presence of cells coexpressing high levels of endogenous EGFP and Gr-1 was not reported by Burnett et al. in the peritoneum, but their presence in the lung implies that populations of these cells may exist in other tissues. Because these cells do not coexpress F4/80, they are not considered to be mature macrophages, but may represent either an immature subpopulation that has not upregulated F4/80, or a subpopulation of granulocytes that express high levels of the EGFP transgenic construct. Treatment of mice with CL2MDP significantly depleted EGFP^{high} cells entering the CNS (panels c and i). This did not deplete or inhibit EGFP$^-$ granulocytic infiltration (panels h-i) relative to VSV-only mice, but did markedly reduce the fraction of EGFP^{high} granulocytes observed. Thus, the EGFP^{high}Gr-1$^+$ cells appear to have phagocytic capability, and are eliminated by intravenous administration of CL2MDP. These cell types are quantified in Fig. 22C.

In this experiment, infiltrating macrophages would be defined as CD45^{high}Gr-1$^-$F4/80$^+$ (Fig. 22A, panels j-l). A population of these cells was noticeable in the brains of naïve mice, which may represent perivascular macrophages. These cells were virtually eliminated by VSV infection (panel k), which is consistent with the loss of macrophages noted previously in most MAFIA mice tissues (refer to Fig. 18). In CL2MDP-treated, VSV infected animals, macrophage infiltrate was increased relative to VSV-only control mice, but did not reach levels seen even in naïve animals. Furthermore, the expression level of F4/80 on these cells was decreased relative to VSV-only controls. Therefore, these cells may represent some relatively immature, non-phagocytic monocyte precursors. Again, these cells are quantified in Fig. 22C.

Myeloid dendritic cells (CD8⁻) have phagocytic capacity and have been demonstrated to be sensitive to CL2MDP-mediated depletion in the periphery. However, lymphoid (CD8⁺) DCs were unaffected by peripheral depletion, implying lower phagocytic activity (Ciavarra et al., 2005). In these mice, serum titres of IFN-α remained high, which implies that plasmacytoid DC (CD11c⁺PDCA-1⁺) were also unaffected by CL2MDP-mediated depletion (unpublished observations). Because our results from the DTRTg model imply a crucial role for DCs in BBB regulation and activation of adaptive immunity, we phenotyped DCs infiltrating the VSV-infected CNS. As previously noted, CD11c⁺ cells were not detectable in the naïve brains of mice (panels m and p). Plasmacytoid DCs were also not observed infiltrating the CNS (panels m-o). Encephalitic brains contained a CD11c⁻PDCA-1⁺ population whose lineage and function are unknown. However, these cells were also observed in peripheral studies of DC depletion using the DTRTg model (Ciavarra et al., 2006), and were not depleted byDT treatment. Both myeloid and lymphoid DCs did penetrate the CNS following viral infection (panels p-r), which is consistent with other mouse strains (Fig. 10). In addition, the absolute number of both myeloid and lymphoid populations of infiltrating DCs was reduced by approximately 50% (Fig. 22D).

A prominent influx of CD8⁺ cells was also noted in encephalitic brains (panels s-u) containing a subset that bound class I tetramers indicating that this subset recognized the immunodominant epitope present in the nuclear protein of VSV (panels s-u). Mice rendered deficient of peripheral macrophages also displayed impaired adaptive immunity because clonal expansion of CD8⁺VSV-N T cells was also suppressed in these mice (panels s-u and Fig. 22D). The inhibition of T cell response is reasonable given the depletion of antigen-presenting DCs noted above.

Unlike the MAFIA+AP20187 model, clodronate-treated mice showed dramatically increased morbidity and mortality relative to VSV-only controls. Half of the mice (3/6) died at 6 days post-infection (two days earlier than typical onset of morbidity for this strain) and by 7 days post-infection the remaining mice were moribund, while VSV-only controls showed only early signs of pathogenesis. Despite the morbidity and mortality of mice, viral clearance was apparently unimpaired (Fig. 22B), which is surprising given the reduction in infiltrating T cells. These results may indicate that although suppressed, the small population of CD8⁺ T cells that still infiltrated the CNS were able to mediate viral clearance. However, it

is more likely that the PFU assay results were abnormally low due to experimental error. For this experiment, supernatants from brain homogenate were used; we typically noted poor viral recoveries from such samples (data not shown). It should also be noted that the viral titres were obtained from a duplicate experiment with similar instances of morbidity/mortality and do not correspond exactly to the flow cytometry data shown.

The lack of T cells and other leukocytes infiltrating the CNS implied a loss of antigen presentation in the CLN, which has been documented in both the DTRTg model (Fig. 14) and the MGBG model Fig. 21). To verify that antigen presentation was inhibited, we evaluated the CLNs for the presence of antigen-specific (tetramer$^+$) CD8$^+$ T cells. Fig. 23 demonstrates effective antigen presentation in the CLNs of VSV-only mice (panel b). Surprisingly, antigen presentation and clonal expansion of antigen-specific CD8$^+$ T cells was preserved in mice treated with intravenous clodronate (panel c). This indicates that the functional APC for the CNS was not depleted by this technique. In Fig. 22, we note that PDCA-1$^+$ cells (a phenotype typically associated with plasmacytoid DCs) were not depleted. These data corresponds with previous observations in the DTRTg model of peripheral DC depletion (Ciavarra et al., 2006). Although these cells have not been reported in the literature, it is possible that they represent either immature pDCs or a novel pool of circulating pDCs. If the latter explanation were true, they may represent the APC for CNS infections. Differences in both route of administration and depletion mechanism might account for the discrepancies between the DTRTg model (where APC function is lost) and the IV-LIPO model (where APC function is retained). Further characterisation of these CD11c$^-$PDCA-1$^+$ cells is required.

Our previous studies did not support a role for IFN-γ as the sole mediator for viral clearance in the CNS of VSV-infected mice. However, it did not rule out a supporting role. Given that viral clearance was not significantly inhibited in LIPO+VSV mice, we anticipated a robust IFN-γ response. Therefore, we determined the frequency of IFN-γ producing cells in the CNS of VSV infected and mice treated intravenously with CL2MDP prior to viral infection. Fig. 24 demonstrates that only trace numbers of IFN-γ-secreting cells were detected in the brain of naïve mice. However, this population expanded in the brains of VSV infected mice, whereas clodronate treatment prior to virus infection markedly suppressed this response. This was true when data was expressed either as the number of ELISPOTS/10^6 cells or total

number of ELISPOTs per brain (top and bottom panels, respectively). Thus, the VSV-induced IFN-γ response in the CNS was markedly impaired in mice rendered deficient of peripheral macrophages and DCs. In the DTRTg model, we suggested that microglia may represent a source of IFN-γ in the CNS. If these cells are in fact the major producers of this cytokine, CL2MDP treatment may have functionally impaired microglia despite their ability to proliferate somewhat. The lack of IFN-γ in this experiment agrees with the findings from the DTRTg model wherein the presence of IFN-γ alone was insufficient to mediate viral clearance.

In summary, this experiment revealed a marked loss of infiltrating leukocytes following depletion of peripheral macrophages and DCs. This depletion technique impaired both innate and adaptive antiviral immune responses, but did not impact viral clearance for unknown reasons. The loss of both aspects of the immune response in this model of depletion is likely due to the concurrent depletion of DC populations in the periphery, and is more similar to results seen in the DTRTg mouse model than in the MAFIA mouse models. This comparison is further supported by the loss of IFN-γ, which did not correlate with viral clearance in the CL2MDP model. Despite successful viral clearance, mice exhibited significant morbidity and mortality, which implies that viral infection contributes to, but is not solely responsible for, CNS pathogenesis in infected animals. We were also able to demonstrate that the crucial DC responsible for antigen presentation in the CNS does not fit the classical definition of either lymphoid or myeloid, but is of an undetermined type that is not sensitive to clodronate-mediated depletion. However, the integrity of the BBB suggests that either or both of these DC subpopulations is crucial to the modulation of the BBB.

A

NAIVE   VSV   LIPO +VSV

B
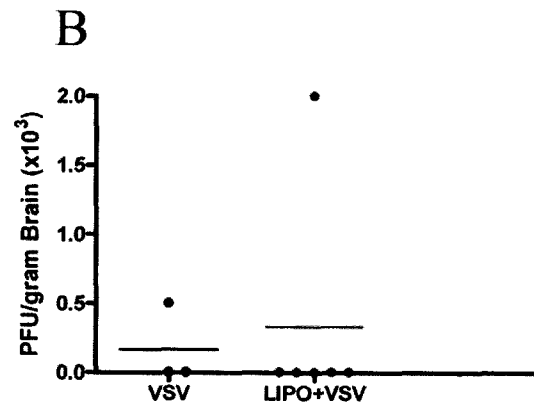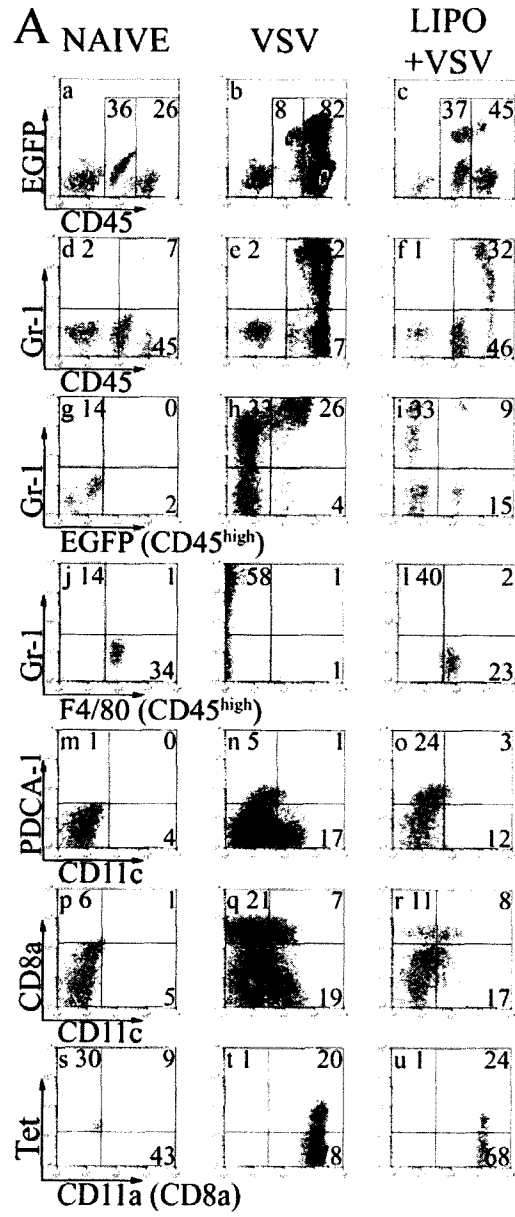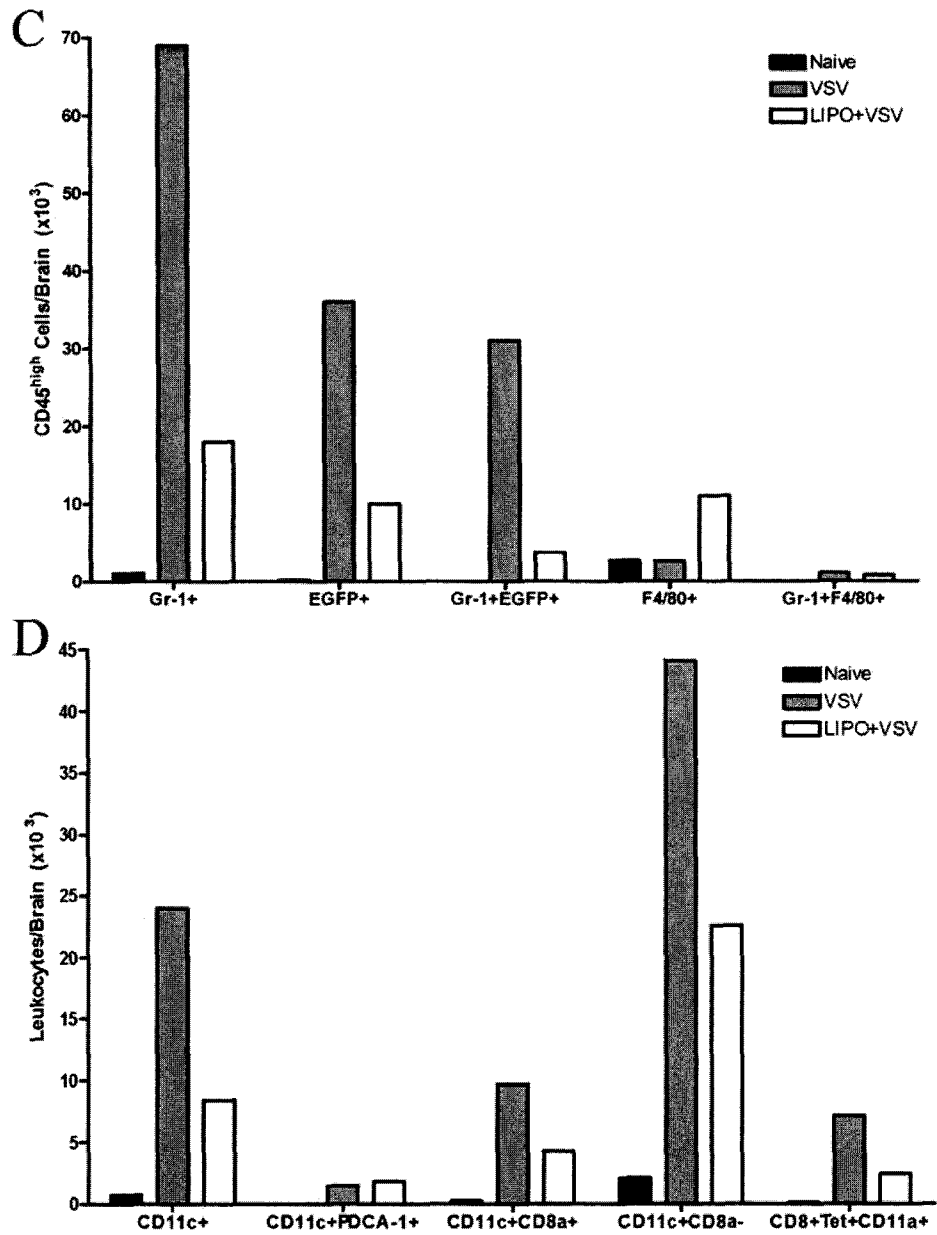
Fig. 22, Continued

Fig. 22., Continued. *Intravenous administration of clodronate liposomes inhibits antiviral*

immunity.

MAFIA mice were treated with 200μL clodronate-bearing liposomes i.v. via the retro-orbital venous sinus while in a surgical plane of anaesthesia using isoflurane (2%). Mice were allowed to recover for 24 hours prior to i.n. infection with 2×10^6 PFU VSV. **A.** Multicolour flow cytometry was performed on brains from naïve (left column, panels a, d, g, j, m, p, s), VSV-infected (centre column, panels b, e, h, k, n, q, t) and LIPO+VSV mice (right column, panels c, l, i, f, o, r, u). **B.** Viral titres from standard PFU assay for VSV-infected and LIPO+VSV mice. **C.** Quantitation of data presented for ungated (m-r) cell populations. These data are representative of three to six mice per group and was repeated three times. **D.** Quantitation of data presented for infiltrating leukocytes (g-l) and CD8 (s-u) gated leukocytes. Note that these results are from a duplicate experiment and do not correspond exactly to the flow data shown in parts A-C.
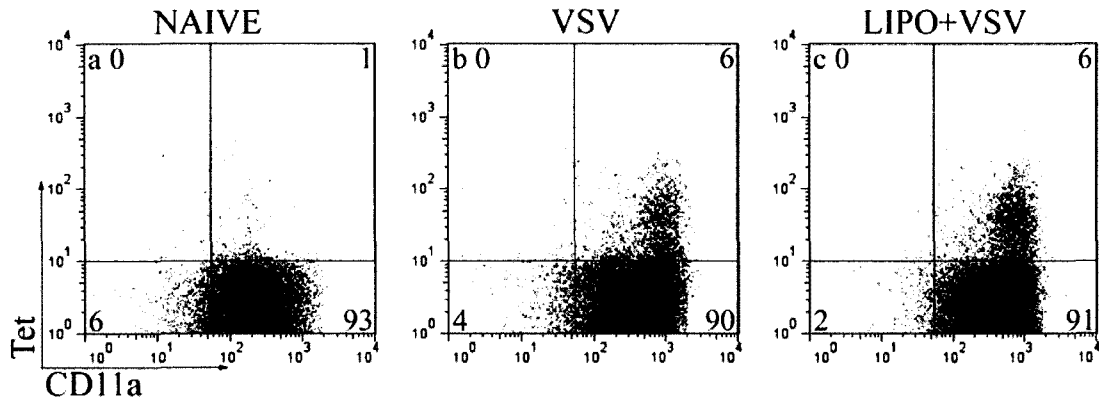
Fig. 23. *Antigen presentation is not impaired in the cervical lymph nodes of mice treated with intravenous clodronate.*

MAFIA mice were treated with 200μL clodronate-bearing liposomes i.v. via the retro-orbital venous sinus while in a surgical plane of anaesthesia using isoflurane (2%). Mice were allowed to recover for 24 hours prior to i.n. infection with $2x10^6$ PFU VSV. Cervical lymph nodes were harvested and subjected to multicolour flow cytometry for antigen specific (Tet$^+$) CD8$^+$ T cells (panels a-c, gated on CD8).
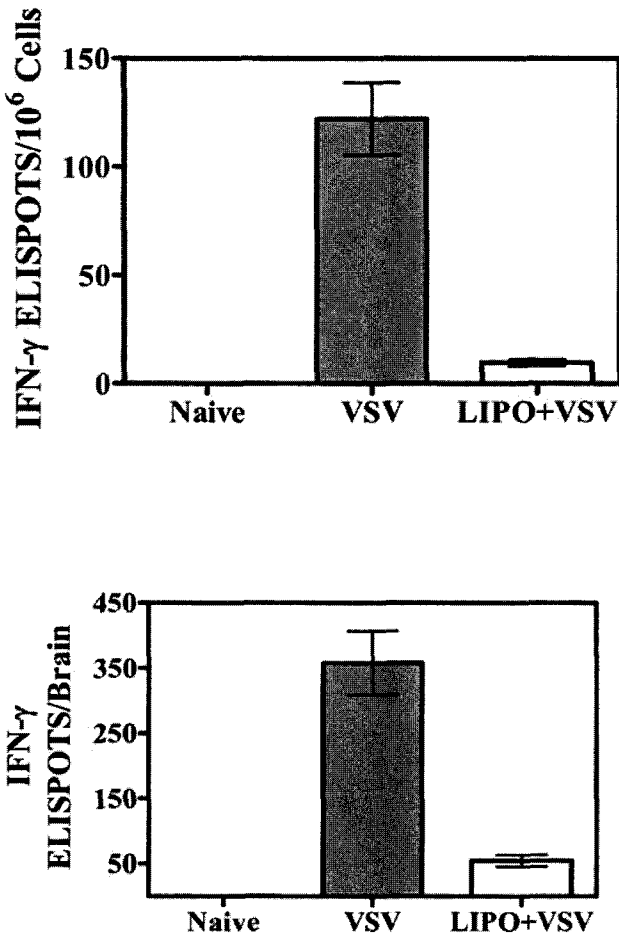
Fig. 24. *Ablation of peripheral macrophages suppresses the VSV-induced interferon gamma*

response in the CNS.

MAFIA mice (3-6 per group) were either untreated or given intravenous clodronate. The following day

mice were infected with VSV via the intranasal route and brain leukocytes isolated seven days post

infection. An IFN-γ ELISPOT assay was then performed as previously described using three replicates per

input cell number. Cells were not re-stimulated with VSV *in vitro* to more accurately estimate the number

of cytokine-producing cells *in vivo*. Data are expressed as either the number of cytokine-producing

cells/10^6 cells (upper panel) or total number of cytokine-producing cells per brain (bottom panel).

Depletion of perivascular macrophages with clodronate

Several recent studies have demonstrated that macrophages residing in the perivascular spaces in the CNS play a key role in mediating the antiviral immune response and may be more important than microglia for antiviral immunity in our model. Perivascular macrophages have been shown to express MHC II and present antigen (Fabriek et al., 2005; Fischer and Reichmann, 2001; Griffin, 2003; Perry, 1998; Polfliet et al., 2001b; Stoll and Jander, 1999; Williams et al., 2001). Their unique location at entry points to the CNS (vascular spaces) made them attractive targets as an *in situ* APC. We reasoned that this brain-resident pool of macrophages may be insensitive to AP20187-mediated depletion in MAFIA mice, as the drug does not cross the BBB. Because these cells have differentiated from monocyte precursors upon entry into the CNS, it was also unlikely that they were affected by MGBG. Therefore, we hypothesized that perivascular macrophages may play a role in initiation and/or propagation of the adaptive immune response of the CNS and/or in viral clearance. Intracerebroventricular administration of clodronate liposomes was shown to deplete perivascular macrophages, but not microglia, in the rat CNS (Polfliet et al., 2001a). This technique therefore allowed us to assess the contribution of perivascular macrophages to antiviral immunity in the CNS.

To assess the contribution of perivascular macrophages to CNS antiviral immunity, CB6F1 (non-DTRTg male) mice were surgically administered 8 μL Cl2MDP in the left lateral ventricle of the brain (intracerebroventricular injection, ICV). Surgical procedures were performed by Laurie Wellman of Dr. Sanford's lab. Because this was a difficult and time-consuming procedure, ICV-LIPO only mice were not assessed. Mice were allowed to recover for 3 days post-surgery and maintained on ibuprofen during that time. In contrast to the IV administration of liposomes, this technique targeted CNS-resident perivascular and meningeal macrophages. Following ICV depletion of perivascular macrophages, mice were then infected with 2×10^5 PFU VSV intranasally and monitored for signs of illness; control mice were infected with VSV only. Six days post-infection, mice were euthanized and perfused with ~30 mL PBS. Tissue was homogenized and subjected to Percoll fractionation for flow cytometry. Naïve (uninfected) mice are not shown; refer to Fig. 2 and Fig. 5.

Fig. 25A demonstrates that microglia were not depleted by ICV-LIPO treatment; in fact, microglia in the ICV-LIPO+VSV animals expanded more than microglia from VSV-only mice (panels panels a-b, quantified in Fig. 25B) . Microglial activation was also significantly increased as evidenced by upregulation of MHC I and/or CD11c (panels c-d, also quantified in Fig. 25B). These results indicated that microglial activation and proliferation were independent of perivascular or meningeal macrophages in response to VSV infection. The lack of microglial depletion was consistent with previous reports on the specificity of this technique (Polfliet et al., 2001a).

Infiltration of leukocytes (Fig. 25A, panels a-b, region R3) and lymphocytes (Fig. 25A, panels e-h) was also markedly enhanced in mice depleted of perivascular macrophages. Granulocytes (Gr-1$^+$, Fig. 25A panels i-j) were also found at a high frequency in the CNS of clodronate-treated mice. These cell types were quantified in Fig. 25B-C.

By 6 days post-infection, the VSV-only mice were morbid, (Fig. 25D), although two of the moribund mice had no detectable virus remaining in their brains. This suggests that the observed morbidity may be related to the inflammatory response and not to the cytopathic activity of the virus. Mice given ICV clodronate exhibited no evidence of illness and were not moribund at this time. The lack of virus in the brain indicates successful viral clearance (Fig. 25D) and corresponds well with animal health.

Based on the health and infiltration of lymphocytes, we predicted that antigen presentation would remain intact in ICV-LIPO mice. Fig. 26 shows that APC function was intact in both VSV and ICV-LIPO mice. This confirms that macrophages are not required for antigen presentation, and that the APC is not a brain-resident cell type sensitive to clodronate-mediated depletion.

These data from the ICV-LIPO study is highly consistent with the MAFIA model of macrophage depletion, where mice exhibited enhanced infiltrate, viral clearance, and survival relative to VSV-only controls and exhibited fewer symptoms of infection. Thus, it is possible that macrophages contribute to the pathogenesis seen in VSV-infected animals, which is plausible given their pro-inflammatory nature.

A

VSV   ICV-LIPO+VSV

a R2 R3
        27
   63
CD11b
CD45

b   46
     46

c 0   5

   33   62
CD11c
MHC I

d 0   18

   0   82

e 1   3
   46   50
VSV-N
CD49d

f 0   3
   22   75

g 0   3
   9   88
CD4
CD45

h 0   5
   5   90

i 0   13
   8   79
Gr-1
CD45

j 0   27
   5   68

B Microglia (CD45$^{(low/int)}$CD11b^{+})

■ Uninfected
□ VSV
▨ ICV-LIPO+VSV

Cells (x10^4)/mouse

Total   Class I$^+$ CD11c$^+$

C CD45^{high} Infiltrate

■ Uninfected
□ VSV
▨ ICV-LIPO+VSV

Cells (x10^4)/mouse

Total   Gr-1   CD8   CD8+Tet+   CD4+   CD11c+

D

PFU/gram Brain (x10^2)

• VSV
● ICV-LIPO+VSV

VSV   ICV-LIPO+VSV

Fig. 25., Continued. *Impact of systemic depletion of perivascular macrophages on microglia and*

infiltrating leukocytes.

CB6F1 mice were depleted of perivascular macrophages by surgical administration of 8 µL clodronate-

liposomes into the left lateral ventricle of the brain (intracerebroventricular injection, ICV). Mice were

allowed to recover from surgery for 3 days, then intranasally infected with VSV. Six days post-infection,

mice were euthanized and brain tissues were harvested. **A.** Multicolour flow cytometry was performed on

brains from VSV-infected (left column, panels a, c, e, g) and ICV-LIPO+VSV mice (right column, panels

b, d, f, h). **B.** Quantitation of data presented for microglia (a, b) and microglia-gated (c, d) populations. **C.**

Quantitation of data presented for infiltrating leukocytes (a, b) and CD8 (e, f) or CD45^{high} (g, h) gated

leukocytes. Note that depletion of perivascular macrophages with ICV-LIPO did not deplete microglia, but

markedly reduced infiltrating antigen-specific CD8$^+$ and CD4$^+$ lymphocytes. These data are representative

of four mice per group. **D.** Depletion of perivascular macrophages/microglia does not inhibit viral

clearance.
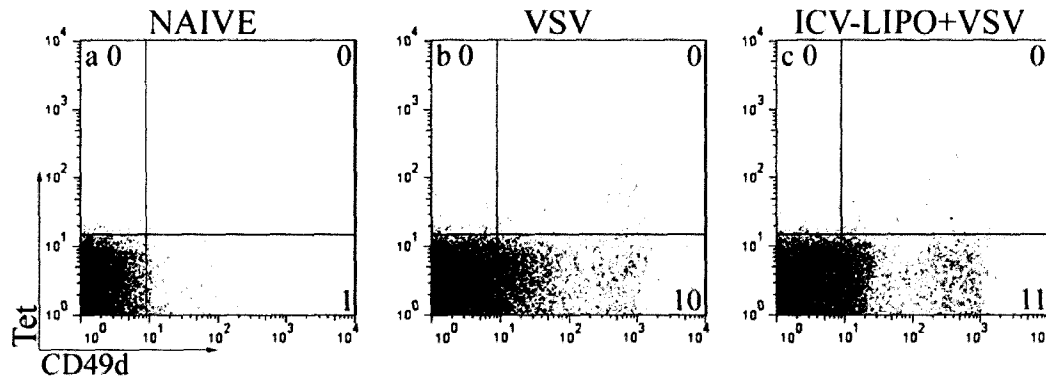
Fig. 26. *Antigen preservation is preserved in mice depleted of perivascular macrophages.*

CB6F1 mice were depleted of perivascular macrophages by surgical administration of 8 µL clodronate-liposomes into the left lateral ventricle of the brain (intracerebroventricular injection, ICV). Mice were allowed to recover from surgery for 3 days, then intranasally infected with VSV. Six days post-infection, cervical lymph nodes (CLN) were harvested from animals and subjected to multicolour flow cytometry. Cells were stained for antigen-specific (Tet⁺) CD8⁺ T cells that coexpressed CD49d (panels a-c). These data are representative of four mice per group.

Protein Array Results for ICV-LIPO+VSV Mice

We also assayed protein cytokine production in ICV-LIPO treated mice. These mice were harvested in a separate experiment from previously reported arrays, although normalisation across the assays was possible. Brain tissues from four ICV-LIPO mice were harvested and treated identically to naïve, VSV, and DT+VSV brains used for protein arrays. In these experiments, two cytokines, SCF and TECK, were significantly inhibited in ICV-LIPO+VSV mice relative to VSV-only controls (Fig. 27). Again, several cytokines were dysregulated to a lesser extent (25-50%) in ICV-LIPO treated mice relative to VSV-only controls (Table 4). Almost all upregulated cytokines were chemotactic for granulocytes or monocyte/macrophages, although two were mitogenic (bFGF, basic fibroblast growth factor; IL-12p40/p70). It should be noted that IL-12p70, also assayed separately, did not increase in ICV-LIPO infected mice; therefore, it is likely that most of the increased levels noted for the heterodimer are due to the IL-12p40 subunit. Axl, which is structurally similar to Dtk, was also found to be increased. It typically forms part of the BBB and is cleaved by MMPs in response to hyperosmotic stress. Downregulated cytokines included VEGF R1, VEGF R2, and VEGF-D. Although VEGF receptors were increased, no increase in their ligand (VEGF) was noted. IL-9 and RANTES, which both increased in VSV infection, were suppressed in ICV-LIPO treated mice to naïve levels. Expression of Fas ligand was also suppressed to near-basal levels, which may reflect the loss of infiltrating T cells noted in this model.

Table 4: Perivascular Macrophage-dependent Cytokine Changes (25-50%)				
Cytokine	VSV	ICV-LIPO+VSV	% Change	General Function(s)
CTACK	1.22	1.73	40%	chemotactic
bFGF	0.99	1.37	40%	mitogenic
MCP1(CCL2)	1.41	1.94	40%	chemotactic
IL-12 p40/p70	1.53	2.09	40%	mitogenic
Lymphotactin	1.33	1.79	30%	chemotactic
LIX(CXCL5)	1.41	1.87	30%	chemotactic
MIP-2	1.01	1.34	30%	chemotactic
Eotaxin-2	1.26	1.67	30%	chemotactic
TPO	1.18	1.50	30%	platelet differentiation
Thymus CK-1	1.14	1.44	30%	chemotactic
Axl	0.87	1.10	30%	BBB integrity
VEGF R1	1.04	0.78	-30%	adhesion
IL-9	0.97	0.72	-30%	mitogenic
RANTES	1.42	1.01	-30%	chemotactic adhesion
HGF R	1.29	0.89	-30%	haematopoietic
VEGF-D	1.31	0.88	-30%	adhesion
Fas Ligand	1.11	0.73	-30%	cytotoxicity
VEGF R2	1.58	0.94	-40%	adhesion
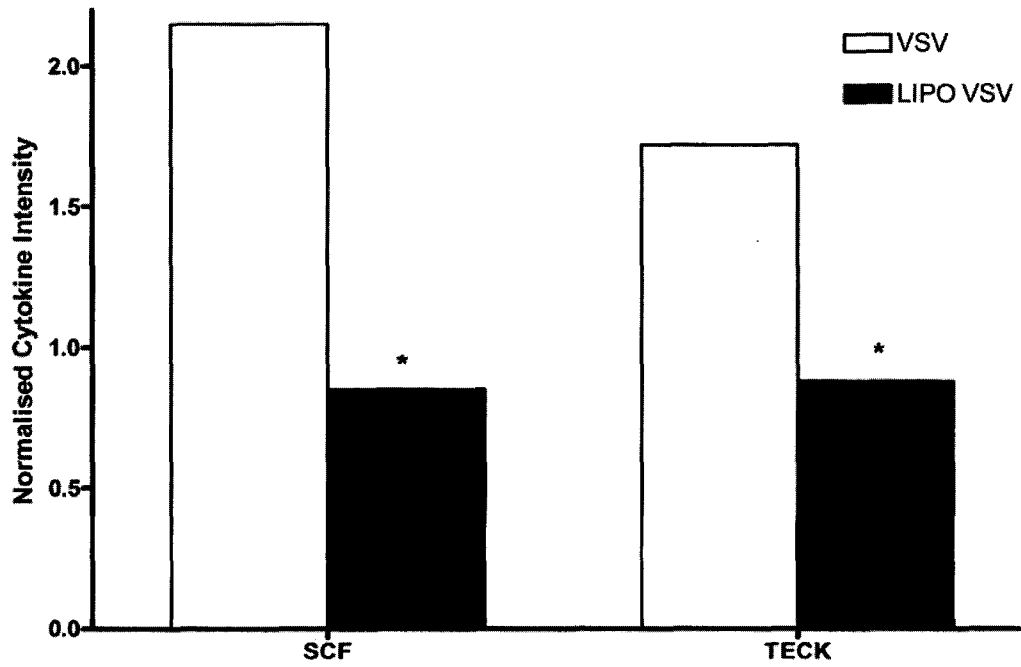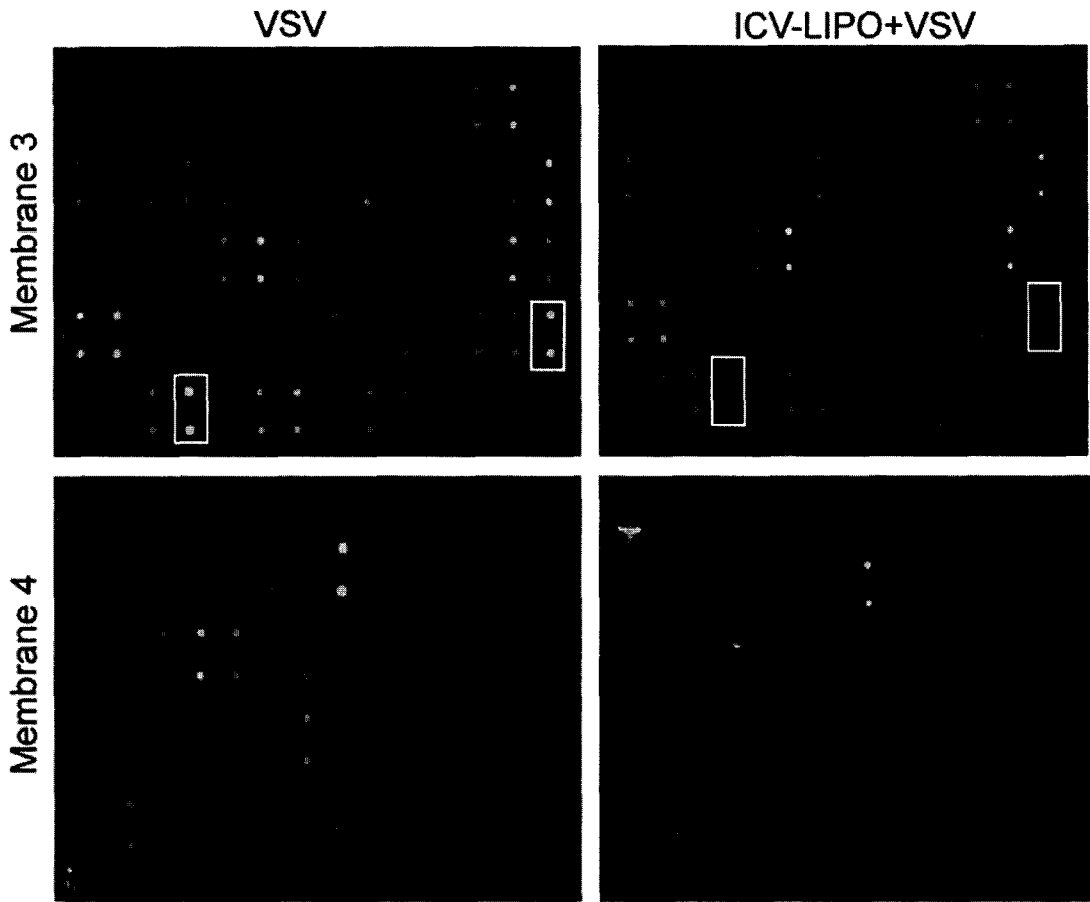
Fig. 27., Continued. *Protein Cytokine Array Results for ICV-LIPO treated, VSV-infected mice.*

CB6F1 mice were depleted of perivascular macrophages by surgical administration of 8 μL clodronate-liposomes into the left lateral ventricle of the brain (intracerebroventricular injection, ICV). Mice were allowed to recover from surgery for 3 days, then intranasally infected with VSV. Seven days post-infection, mice were euthanized and brain tissues were harvested. For VSV-only mice, brain tissues were harvested 8 days post-infection and snap-frozen using liquid nitrogen before assays for cytokines were performed. Tissues from VSV and ICV-LIPO+VSV groups were pooled (25 mg tissue/mouse, 4-5 mice/group). Protein extracts were prepared in the presence of a protease inhibitor cocktail (Calbiochem) and protein concentrations adjusted to 250 μg/mL prior to use with RayBiotech Cytokine Arrays. Protein spots were revealed with Streptavidin-IR 800CW (Li-Cor Odyssey) and scanned on the Odyssey Imaging system. (A) Protein Arrays are depicted with background correction (maximal fluorescence intensity is shown as white). Significantly altered cytokines are boxed. (B) Quantitation of fluorescence signals: a 3-pixel background was subtracted from the integrated fluorescence intensity of each spot and results were normalised. Cytokines demonstrating a 50% increase or decrease in expression relative to naïve control mice were identified. Asterisks indicate statistical significance (α=0.05, GraphPad Prism 4).

Discussion

These sets of experiments offered disparate results, despite having the same aim: to deplete macrophages. The MAFIA model allowed us to selectively deplete cells that expressed the CSF-1 receptor, which is primarily expressed by cells of the monocyte/macrophage lineage, including immature precursors in the bone marrow (Rettenmier et al., 1988; Rothwell and Rohrschneider, 1987). Although the c-fms gene is expressed in both macrophages and DCs (Rieser et al., 1998), Burnett et al. demonstrated that it is expressed at nearly tenfold lower levels in DCs (Burnett et al., 2004), which may explain the relative preservation of DCs following dimeriser treatment. We have made similar observations about DCs in our initial studies of MAFIA mice (data not shown). Microglia were not depleted by treatment with AP20187, which indicates that it may not effectively cross the blood-brain barrier. This idea is supported by historical observations that large molecules in excess of 500 Da do not cross the blood-brain barrier successfully; the molecular weight of AP20187 is 1428.8 Da (Ariad Pharmaceuticals, Cambridge, MA). Dimeriser treatment did not inhibit activation of microglia as defined by cellular expansion and/or upregulation of MHC II, which indicates that microglial activation was independent of peripheral macrophages. This is also consistent with failure of AP20187 to cross the blood-brain barrier. To confirm that successful depletion of monocyte/macrophage lineage cells had occurred, we also observed the bone marrow and spleens for characteristic blanching (Steel et al., 2008). Flow cytometric analysis performed on bone marrow and peritoneal exudate cells (PECs) revealed that normal MAFIA bone marrow contained a prominent population of $CD45^{high}CD11b^+$ cells which expressed Gr-1 and were approximately one-third $EGFP^{low/int}$. VSV infection resulted in the selective disappearance of $Gr-1^+EGFP^{low/int}$ cells from the bone marrow, whereas prior dimeriser treatment resulted in expansion of $Gr-1^+EGFP^{low/int}$ cells. In contrast, $CD45^{high}CD11b^+$ cells in the peritoneum were exclusively macrophages. Two macrophage populations based on EGFP expression were present in the normal peritoneum. Macrophages with high EGFP expression were dramatically reduced by VSV infection and this loss was exacerbated by prior dimeriser treatment. Although the number of $EGFP^{low/int}$ macrophages was also reduced by virus infection, this population expanded in mice depleted of macrophages. These results also correspond well with our previously published work in the MAFIA model which showed depletion of $EGFP^{high}$ cells and a

corresponding compensatory increase in granulocytes in the absence of viral infection (Steel et al., 2008). Leukocytes isolated from VSV infected brains included a significant population of CD45^{high}CD11b$^+$ cells as well as a small but detectable infiltrate of CD11c$^+$ DCs. These results were consistent with our previously reported studies that showed a surprising expansion of CD11b$^+$ cells in the periphery following AP20187 treatment, which we attributed to an immature macrophage or granulocyte phenotype resulting from a compensatory precursor haematopoietic response in the spleen and bone marrow. Further analysis studies demonstrated that these cells were most likely neutrophils because they expressed a CD45^{high}CD11b$^+$F4/80$^-$Gr-1$^+$ phenotype, consistent with the work of Reiss et al. who demonstrated that neutrophils were the first cell population to infiltrate the virally infected CNS (Bi et al., 1995a; Ireland and Reiss, 2006). Mature neutrophils do not express CSF-1 receptor (Hume et al., 2002) and would be expected to be insensitive to AP20187 treatment. It seems likely that these cells emigrated from the bone marrow to infiltrate the brain and contribute to the granulocytic response seen in this organ. This view is consistent with the accumulation of CD45^{high}EGFP$^{low/int}$ cells in the brains of mice depleted of macrophages. As previously noted, we did not detect pDCs, B cells or NK cells in VSV-infected brains. Although the CD11b- infiltrate was minimal, CD8$^+$ T cells were abundant, suggesting that lymphocytes upregulated CD11b on activation. This observation was confirmed by back-gating analysis in Fig. 12. As noted in the previous studies, a significant percentage of CD8$^+$ T cells were antigen-specific, though not all. The specificity of the remaining activated T cells remains to be determined. Despite their dual functionality as APCs and effector cells, mice rendered deficient of peripheral macrophages mounted a normal innate and adaptive antiviral immune response in the CNS. This also implies preservation of peripheral DCs in dimeriser treated mice because depletion of these cells markedly inhibited antiviral immunity and viral clearance in the DTRTg model. Thus, peripheral depletion of macrophages failed to suppress the inflammatory response in the brain because the predominant myeloid cell type infiltrating the brain was neutrophils and not macrophages. As noted previously, low expression of the transgene in DCs apparently prevented significant loss of these essential APCs resulting in normal cellular expansion and CNS penetration of CD8$^+$VSV-N T cells.

MGBG does not directly kill target cells; rather, it blocks maturation of monocytes into macrophages. This mechanism is therefore unique as a depletion strategy, because it should not induce a compensatory proliferation of haematopoietic precursors noted in the MAFIA model. Specifically, MGBG inhibits S-adenosyl L-methionine decarboxylase, which catalyzes the synthesis of spermidine (McGrath and Hadlock, 2007). Spermidine is a naturally-occurring polyamine, while MGBG is a synthetic polyamine with similar activity. With regard to immunity, spermidine has been shown to kill lymphocytes at concentrations above 100 μM *in vitro* (Swanson and Gibbs, 1980) and was inhibitory to concanavalin-A and LPS-stimulated lymphoproliferation *in vivo* (Ishizuka et al., 1982) but increased production of the T-cell mitogen IL-2. Spermidine has also been demonstrated to be inhibitory to monocyte maturation and differentiation into macrophages (Kaczmarek et al., 1992; Messina et al., 1992; Zhang et al., 2000). Although initially inhibition of spermidine production by MGBG would appear to be proinflammatory, it should be noted that the drug likely acts as a biochemical competitor and replaces the actions of spermidine in immunoregulation. Treatment of mice with MGBG prior to viral infection caused a marked loss of microglia in the CNS and inhibited activation of remaining cells as determined by upregulation of MHC I/II, and the expression of the negative regulator PD-1 was increased nearly twofold in MGBG-treated mice. MGBG may therefore also block maturation of microglia if it is capable of crossing the blood-brain barrier. Due to its relative size (MW=282 Da), it is likely that MGBG is directly responsible for the alterations in microglia noted during this experiment, although studies demonstrating its capacity to penetrate the blood-brain barrier have not been reported. In addition to inhibition of microglia, MGBG-treated mice showed a reduction in the absolute numbers of infiltrating CD45^{high} leukocytes, with a small decrease in the number of infiltrating granulocytes (Gr-1^{+}) and antigen-specific CD8^{+} lymphocytes. The remaining CD11b^{+} leukocytes were not further phenotyped; however, it is likely that the bulk of depletion occurred in this heterogeneous population. A loss of CD11b^{+} macrophages was anticipated, and these data reflects successful inhibition of monocyte/macrophage differentiation. This conclusion is also supported by the observation that MGBG-treated mice showed significantly less VSV-induced morbidity relative to untreated controls, which may indicate a loss of tissue-destructive inflammation. The loss of antigen-specific CD8^{+} response was somewhat surprising, given that these cells were not reported to be targets of

MGBG; however, research indicates that the natural analogue spermidine has inhibitory effects on lymphoproliferation as well. Thus, the inhibition of antigen-specific $CD8^+$ T cells may also be a direct result of MGBG treatment. Although the results from this experiment are preliminary, it is possible that MGBG may provide a good model for observing the role of microglia in the CNS. If directly infused into the CNS (intracerebroventricular administration), MGBG may selectively inhibit CNS-resident leukocytes. Additional studies would be required to determine the efficacy of this technique and whether MGBG subsequently leaked into the peripheral immune system.

Depletion by liposome-encapsulated clodronate requires functional maturation of phagocytic cells (van Rooijen and van Nieuwmegen, 1984) and active phagocytosis. Intravenous administration of clodronate-encapsulated liposomes into naïve MAFIA mice suppressed the inflammatory response in the brain. Thus, the global influx of blood-derived leukocytes ($CD45^{high}$) was dramatically diminished. As noted previously, this infiltrate was composed primarily of neutrophils ($CD45^{high}CD11b^+F4/80^-Gr-1^+$), T cells and relatively small numbers of DCs. For reasons that are not clear, neutrophils do not appear to be depleted by clodronate despite their phagocytic activity (Qian et al., 1994) and were therefore unavailable to infiltrate the VSV infected brain. Their diminished numbers in the brain suggests that they may lack the ability to penetrate the blood-brain barrier. The total number T cells ($CD4^+$ and $CD8^+$) detected in the brain were reduced including the $CD8^+$ T cell subset specific for VSV, despite a normal $CD8^+$ T cell response in the draining CLN. This implies that the impaired infiltrate of leukocytes in the encephalitic brain may reflect a failure of leukocyte extravasation across the blood-brain barrier or lack of permeability as noted in the DTRTg model. The impaired IFN-γ response may reflect the diminished numbers of T cells that infiltrated the brains of mice depleted of macrophages if T cells represent the cellular source of this cytokine; however, this interpretation would conflict with the DTRTg model, which demonstrated a robust IFN-γ response in the absence of infiltrating T cells. The effects of clodronate were not limited solely to macrophages but also depleted marginal ($CD8^-$) DCs in the spleen (Leenen et al., 1998), which may explain the reduction in lymphocytic infiltrate. In some experiments, we detected a population of $CD11c^-PDCA-1^+$ cells whose function remains to be elucidated. Clodronate treatment was associated with increased morbidity/mortality that did not correlate with impaired viral clearance in the CNS.

Early studies demonstrate that when given intracerebroventricularly (ICV), macrophages in the perivascular spaces and meninges were susceptible to liposome-mediated depletion, while microglial cells remained intact (Polfliet et al., 2001a). This may reflect differences in basal phagocytic activity. It is also important to note that the liposomes used in this study were mannosylated, which has been demonstrated to improve blood-brain barrier permeability (Polfliet et al., 2001a). Flow cytometric analysis showed a markedly inhibited infiltrate of leukocytes, particularly a loss of macrophages and granulocytes. However, we also noted a loss of both CD8$^+$ and CD4$^+$ T cells despite a weak VSV-induced response in virally infected controls. These data appears very similar to the DT+VSV depletion model in that the leukocyte infiltrate was broadly inhibited. The loss of a T cell infiltrate was unexpected because clodronate delivered into the brain did not deplete macrophages or DCs in the draining CLN and therefore should not have inhibited accumulation of antigen-specific T cells in the CNS. Consistent with reports that microglia are not depleted by clodronate, the activation and proliferation of these parenchymal-resident leukocytes remained normal in these studies. Overtly, the mice in this group appeared healthier than VSV-only cohorts. This led us to think that inflammation, a generally destructive process, would be suppressed in these mice. Therefore, investigation of the cytokine profile was also interesting. In this model, similar to the DT+VSV model, many chemotactic cytokines were upregulated, including the T-cell chemokines Lymphotactin and CTACK. However, it was upregulated to a much lesser extent in ICV-LIPO+VSV mice than in DT+VSV mice. Chemokines involved in neutrophil, granulocyte, and monocyte/macrophage recruitment continued to be expressed at slightly elevated levels. Again, these findings indicate that the failure of leukocyte infiltration was not due to cytokine dysregulation, and further imply that these cytokines are not dependent on perivascular macrophages. IL-12p40/p70, but not IL-12p70, was increased in response to ICV-LIPO treatment. The IL-12p40 subunit is antagonistic to the heterodimer and has been shown to exert protective effects in CNS infections (Bi et al., 1995b; Chesler and Reiss, 2002; Komatsu et al., 1997). The increased expression of Axl in the ICV-LIPO group could have a few potential sources. This protein forms part of the BBB and is cleaved by MMPs in response to hyperosmotic stress. Such stress might have been induced during the surgical administration of clodronate-liposomes, but this response may also reflect an immune-mediated difference in response to the viral infection. Notably, VEGF receptors were inhibited in this

model. Although the VEGF ligand is primarily responsible for proliferation of vascular endothelial cells, it also plays a critical role in vascular permeability (Brown et al., 1992; Clauss et al., 1990; Connolly, 1991) and may promote monocyte migration (Clauss et al., 1990). The loss of the receptors from the vascular endothelium may therefore be partially responsible for the failure of leukocyte infiltration. In this model, a few unusual cytokines were found to be altered relative to VSV-only controls, including thrombopoeitin (TPO) and basic fibroblast growth factor (bFGF). Both these cytokines may be involved in wound healing and may reflect the surgical administration of clodronate liposomes into the CNS. These preliminary studies suggest perivascular/meningeal macrophages provide some nonredundant function essential for enhancing permeability of the blood-brain barrier, similar to DCs in the DTRTg model. Taken together, the loss of cellular infiltrate despite a robust cytokine response and normal response in the draining cervical lymph nodes (in the ICV-clodronate model) imply that disruption of the blood-brain barrier may require an interaction between perivascular/meningeal macrophages and infiltrating DCs. This view is further supported by the observation that CD11c$^+$ DCs also reside in the perivascular spaces and may have been depleted by the direct CNS infusion of clodronate liposomes as they were also susceptible to DT-mediated depletion (Fig. 7). This population of DCs may be especially critical to modulating the integrity of the blood-brain barrier.

Because each of these depletion strategies employs a unique mechanism of action, we were able to evaluate several facets of macrophage-mediated immunity. In striking contrast to the AP20187 conditional ablation model, intravenous administration of liposome-encapsulated clodronate into naïve MAFIA mice suppressed the inflammatory response in the brain. The different outcome achieved with clodronate versus dimeriser may reflect the different populations targeted by these treatments. In the MAFIA model, AP20187 dimeriser targets macrophages with high *c-fms* activity and leaves relatively intact cells with low expression levels of the transgene such as DCs and immature and mature granulocytes. Marked differences between the intravenous and intracerebroventricular models of clodronate administration were also apparent. Intravenous injection of clodronate liposomes affects diverse tissues, such as the spleen, liver, and bone marrow (van Rooijen, 2006), while the effects of ICV-administered clodronate are localised to the CNS (Polfliet et al., 2001a). Functional differences between routes of injection (intraperitoneal versus

intravenous) have been reported. Depletion of peripheral DCs in the DTRTg model or perivascular/meningeal macrophages in the ICV-clodronate model results in similarly impaired innate and adaptive antiviral immune responses. Perivascular and/or meningeal macrophages apparently do not function as APCs in the brain because depletion of these cells does not inhibit infiltration of antigen-specific $CD8^+$ T cells into the CNS (Galea et al., 2007b). How these different cell populations regulate leukocyte infiltration is currently unknown. It should be noted that none of these depletion strategies are exclusive to a particular cell or lineage; they are all cross-reactive to some extent. This complicates the data analysis and interpretation of results, but some general trends can be noted. Systemic depletion of macrophages did not inhibit viral clearance, regardless of the mechanism employed. Loss of dendritic cells, whether in the periphery or possibly in the perivascular spaces, results in the maintained integrity of the blood-brain barrier with resultant failure of peripheral leukocyte infiltration into the CNS. Further studies will be required to delineate how these distinct macrophage populations regulate blood-brain barrier permeability and enhance viral encephalitis.

Taken together, these results demonstrated that a population of DCs that is neither myeloid nor lymphoid drove antigen presentation in the CLN in response to CNS infections. Furthermore, myeloid DCs, lymphoid DCs, or both played a key role in modulating BBB integrity and subsequent leukocyte extravasation into the brain parenchyma. Microglia alone or in combination with IFN-γ were insufficient to mediate viral clearance in the CNS; these studies further confirmed $CD8^+$ T cells as the primary mediators of viral clearance. Macrophages did not contribute to antiviral immunity as APCs or in viral clearance, but appeared to exacerbate CNS injury in response to viral infection.

CHAPTER VII

CONCLUSIONS AND FUTURE DIRECTIONS

The studies presented in this work investigated the roles of resident microglia as well as peripheral dendritic cells and macrophages in the adaptive immune response to acute viral infections of the central nervous system. We began by characterising the normal cellular and cytokine response to VSV infection in the CNS. As previously reported, the peak of infection occurred between 6-8 days post-infection, which varied somewhat with mouse strain and gender. At this time, the leukocyte response was characterised by an expansion of resident microglia and an infiltrate of peripheral leukocytes which consisted largely of granulocytes, macrophages, and T cells. In the encephalitic brain, microglia upregulated surface molecules including MHC I/II and CD11c, which implied that they may be able to serve as a resident antigen-presenting population within the CNS. However, we have no direct evidence that these cells function as APCs for VSV T cells. Future studies should address this capacity. *In vitro* antigen-presentation assays have been performed in other models of CNS infections and demyelinating, recurrent models of infection and generally show little to no antigen-presenting capacity; however, *in vivo* experiments are lacking. The complexity of the adaptive immune response *in vivo* is poorly represented in cell culture models where crucial cytokines and accessory cells may not be present to fully activate T cells. Therefore, *in vivo* experiments should be utilised, and could be performed with highly purified adoptively transferred T cells derived from syngeneic mice intravenously injected into lethally-irradiated recipient mice. Brain-resident microglia are typically protected from irradiation and could continue to serve as antigen-presenting cells. This technique carries a risk of failure: the adoptively transferred T cells may not be sufficient to rescue mice from fatal encephalitis. This risk could be mediated by performing the adoptive transfer early during viral infection (~ 3 days post-infection), at a time when microglia have upregulated appropriate antigen-presenting markers but at which mice are still asymptomatic. The role of granulocytes during viral infection remains unclear and also requires extended study. These cells are typically the first to infiltrate the CNS in response to infection, and have been reported to produce a tremendous variety of cytokines/chemokines, including several that may alter BBB permeability (elastase,

collagenase, metalloproteinases) and aid in subsequent recruitment of lymphocytes. However, these cells also fail to penetrate the CNS with DT treatment, indicating that they alone are insufficient to initiate BBB breakdown and leukocyte infiltration. The role of granulocytes during VSV infection could be easily addressed with antibody depletion studies *in vivo*. Finally, the cytokine profiles we observed by protein array did not match well with RNase protection assays that had been previously reported; these results bear further investigation. RNA-based PCR arrays are available for a wide variety of cytokines/chemokines (SA Biosciences) and should be performed in tandem with protein detection methods (ELISA or protein cytokine arrays) on the same samples to determine whether the discrepancy in results is due to dysregulation of mRNA or protein, or whether our preliminary results are erroneous. Using these methods, it is also possible and critically important to determine the cellular origin of dysregulated cytokines; mRNA and protein-based assays can be performed on specific cell populations that have been highly purified by magnetic bead sorting and/or fluorescence-activated cell sorting (FACS) for cell populations that represent likely cytokine/chemokine sources (microglia, astroglia, perivascular macrophages). Microglia can be detected and FACS purified by endogenous expression of EGFP in either the MAFIA model or a CD11b/DTRTg mouse strain available from Jackson Laboratories. Astroglia may similarly be purified from FVB/N-Tg[GFAPGFP]14Mes/J mice, which express EGFP under the control of the glial fibrillary acidic protein promoter in astrocytes. Perivascular macrophages require *in vitro* labelling with CD206 (mannose receptor, Hycult Biotechnology, clone MR5D3). This molecule is exclusively expressed on PVM and not microglia or blood-derived monocytes/macrophages even in the inflamed brain (Galea et al., 2005). Additional markers for macrophages (CD11b or F4/80) would be required, although endogenous EGFP expression could be used for the CD11b/DTRTg or MAFIA mouse strains. Together, these additional studies will help clarify the cellular and cytokine responses to viral infection. Following these assays, it would be important to evaluate the *in vivo* contributions of these cytokines/chemokines to antiviral immunity by using antibody-mediated cytokine depletion.

The loss of peripheral classical APCs (DCs) with diphtheria toxin treatment was anticipated to result in a failure in the activation and expansion of T cells. We performed experiments in which we conditionally ablated this peripheral APC population, and observed a failure in proliferation and activation

of T cells. However, these results were confounded somewhat by a surprising broad-spectrum inhibition of leukocyte infiltration into the CNS following viral infection. The concurrent loss of infiltrating myeloid cells was surprising, and did not match our predictions. Further evaluation of this model in the experiments described herein point to a general failure of leukocytes to extravasate across the blood-brain barrier and penetrate the CNS following viral infection. These findings need to be extended with additional studies of BBB integrity, which can be evaluated with Evans' blue staining of brain parenchyma (or, alternatively, FITC-dextran). To determine whether peripheral DCs are required for disruption of the BBB, splenic CD8$^+$ T N15Tg (VSV-specific) T cells isolated from VSV-infected (intraperitoneal infection) N15Tg mice would be labelled with CFSE and infused into VSV-infected (CNS) DTRTg mice with intact or depleted peripheral DC populations. This model would also determine the extent to which activated CD8$^+$ VSV-N T cells undergo further cell division in the absence (control) or presence of viral antigen in the CNS. It may also be important to demonstrate that DCs residing in the perivascular spaces are not sensitive to DT-mediated depletion; this can be readily accomplished with immunohistochemistry in the CD11c/DTRTg model. Our results also implied that DCs may produce MMP-3 in response to viral infection: this should be directly evaluated by immunohistochemistry and/or confocal microscopy. It is also critical to confirm that MMP-3 is a key regulator of BBB integrity. Strains of MMP knockout mice have been described as recently as 2005, but do not appear to be commercially available. Chemical means of MMP-3 inhibition are relatively simpler and can be achieved by administration of select TIMPs (tissue inhibitors of metalloproteinases).

Additional observations of chemokines involved in regulation of the BBB are recommended; particularly the matrix metalloproteinases (MMPs) and their inhibitors (TIMPs, tissue inhibitors of metalloproteinases) by both RNA and protein detection methods, which include but are not limited to ELISA assays, protein cytokine arrays, and RNA-based arrays. It was surprising that so few cytokines/chemokines appeared to be dysregulated based on the protein cytokine array; these results also need to be confirmed with tandem mRNA/protein methods as previously described. Furthermore, the cellular source of IFN-γ in the CNS remains to be confirmed; immunohistochemistry and/or confocal microscopy are recommended approaches due to difficulty in isolation and purification of microglia.

Our macrophage depletion models provided consistent results, despite differences in depletion mechanisms and target cell populations. The CD11b/DTRTg mouse strain may allow a more specific depletion of target macrophages than was achieved by the techniques described herein. In this strain, expression of the simian diphtheria toxin receptor is driven by the integrin α-M (CD11b) promoter, which is active in cells of the macrophage and microglial lineages. Based on our studies, most macrophage depletion techniques are cross-reactive with granulocyte or DC populations. Therefore, it would be critical to first verify the specificity of this model with regard to depletion of macrophage subpopulations, with subsequent focus on perivascular macrophages and microglia in the CNS. Given that DT does not cross the BBB effectively, it is unlikely that peripheral (intraperitoneal or intravenous) administration of DT would deplete microglia. However, it is possible that direct infusion of DT into the CNS of transgenic mice might provide a novel means of depleting microglial populations, which would allow us to evaluate antiviral immunity in the absence of this population and clarify the contribution of microglia to antiviral immunity in the CNS. A potential drawback to this mouse model is that we observed a prevalent upregulation of CD11b on leukocytes infiltrating the CNS; administration of DT may therefore deplete activated leukocytes in addition to target macrophage populations. However, careful timing of administration may reduce these effects, given that the serum half-life of DT is relatively short. It would be critical to observe the repopulation kinetics of macrophage populations in this mouse model to determine whether it would be possible to selectively deplete macrophages and maintain depletion for the required 6-8 day duration of the experiment without adversely affecting activated/infiltrating leukocyte populations.

The MAFIA model of macrophage depletion would also benefit from additional study in CNS infections. Microglial activation and proliferation appeared enhanced in our studies, but only rudimentary phenotyping was performed. Additional flow cytometry with extended markers and functional indicators (such as IFN-γ secretion) for microglial activation and kinetic studies would greatly improve the understanding of this model. Additional studies directed toward the cytokine response (either RNA or protein arrays) may shed new light on the molecular mechanisms underlying enhanced microglial and lymphocyte activation and viral clearance.

Of the techniques employed here for macrophage depletion or inhibition, only administration of MGBG appeared to have a significant inhibitory effect on resident microglia. It may be possible to selectively inhibit microglia in future studies by modifying the dose, route, or timing of MGBG administration. Additional studies with this technique are recommended to conclusively determine whether macrophage infiltration into the CNS was inhibited; adoptive transfer of CFSE-labelled monocytes followed by flow cytometry should demonstrate functional impairment of monocyte-macrophage differentiation and penetration into the brain parenchyma. Additionally, it is crucial to determine whether the observed microglial inhibition resulted in impaired IFN-γ production, which can be evaluated with ELISPOT assasys.

In summary, these studies provided several new insights into regulation of the immune response to acute viral infections and allowed us to develop a working model for the primary antiviral immune response in the CNS. In the immunocompetent mouse, VSV successfully infects the CNS via the olfactory nerve and spreads caudally throughout the brain. Shortly after infection, microglia become activated and proliferate, and may secrete IFN-γ. During early infection (3 days post-infection), an unidentified DC subtype (neither lymphoid nor myeloid) acquires antigen and migrates to the CLN to globally activate T cells. These T cells, along with macrophages and granulocytes, home toward the infected CNS via chemokine/cytokine chemotaxis. However, macrophages are not required and appear to exacerbate pathogenesis. Extravasation across the BBB is dependent on lymphoid DCs, myeloid DCs, or both and may be MMP-3 dependent. Additional stimulation from perivascular cells or microglia may be required for full antiviral activity in the CNS. Once these cells have penetrated into the parenchyma of the brain, CD8$^+$ T cells mediate viral clearance in conjuction with IFN-γ, resulting in mouse survival and recovery.

LITERATURE CITED

2003. 13: Dendritic cells from laboratory to clinic (Clinical Immunology Group). Immunology 110 Suppl 1:47-51.

2006. Research Highlights. Nat Immunol 7:361-361.

2008. ADULT_ATLAS_07.jpg. New York, NY: The Gene Expression Nervous System Atlas (GENSAT) Project. p Adult mouse brain (section 7).

Abbas AK, Sharpe AH. 2005. Dendritic cells giveth and taketh away. Nat Immunol 6:227-228.

Ackman JB, Siddiqi F, Walikonis RS, LoTurco JJ. 2006. Fusion of microglia with pyramidal neurons after retroviral infection. J Neurosci 26:11413-11422.

Agnihotri R, Crawford HC, Haro H, Matrisian LM, Havrda MC, Liaw L. 2001. Osteopontin, a novel substrate for matrix metalloproteinase-3 (stromelysin-1) and matrix metalloproteinase-7 (matrilysin). J Biol Chem 276:28261-28267.

Aloisi F. 2001. Immune function of microglia. Glia 36:165-179.

Aloisi F, Ria F, Penna G, Adorini L. 1998. Microglia are more efficient than astrocytes in antigen processing and in Th1 but not Th2 cell activation. J Immunol 160:4671-4680.

Andersson EC, Christensen JP, Marker O, Thomsen AR. 1994. Changes in cell adhesion molecule expression on T cells associated with systemic virus infection. J Immunol 152:1237-1245.

Andoniou CE, van Dommelen SL, Voigt V, Andrews DM, Brizard G, Asselin-Paturel C, Delale T, Stacey KJ, Trinchieri G, Degli-Esposti MA. 2005. Interaction between conventional dendritic cells and natural killer cells is integral to the activation of effective antiviral immunity. Nat Immunol 6:1011-1019.

Andrews DM, Scalzo AA, Yokoyama WM, Smyth MJ, Degli-Esposti MA. 2003. Functional interactions between dendritic cells and NK cells during viral infection. Nat Immunol 4:175-181.

Archambault AS, Sim J, Gimenez MA, Russell JH. 2005. Defining antigen-dependent stages of T cell migration from the blood to the central nervous system parenchyma. Eur J Immunol 35:1076-1085.

Baghestanian M, Hofbauer R, Kiener HP, Bankl HC, Wimazal F, Willheim M, Scheiner O, Fureder W, Muller MR, Bevec D and others. 1997. The c-kit ligand stem cell factor and anti-IgE promote expression of monocyte chemoattractant protein-1 in human lung mast cells. Blood 90:4438-4449.

Bailey SL, Schreiner B, McMahon EJ, Miller SD. 2007. CNS myeloid DCs presenting endogenous myelin peptides 'preferentially' polarize CD4(+) T(H)-17 cells in relapsing EAE. Nat Immunol 8:172-180.

Barchet W, Cella M, Odermatt B, Asselin-Paturel C, Colonna M, Kalinke U. 2002. Virus-induced interferon alpha production by a dendritic cell subset in the absence of feedback signaling in vivo. J Exp Med 195:507-516.

Barna M, Komatsu T, Bi Z, Reiss CS. 1996. Sex differences in susceptibility to viral infection of the central nervous system. J Neuroimmunol 67:31-39.

Battegay M, Bachmann MF, Burhkart C, Viville S, Benoist C, Mathis D, Hengartner H, Zinkernagel RM. 1996. Antiviral immune responses of mice lacking MHC class II or its associated invariant chain. Cell Immunol 167:115-121.

Bechmann I, Galea I, Perry VH. 2007. What is the blood-brain barrier (not)? Trends in Immunology 28:5-11.

Beck G, Habicht GS, Benach JL, Miller F. 1986. Interleukin 1: a common endogenous mediator of inflammation and the local Shwartzman reaction. J Immunol 136:3025-3031.

Bergmann CC, Parra B, Hinton DR, Chandran R, Morrison M, Stohlman SA. 2003. Perforin-mediated effector function within the central nervous system requires IFN-gamma-mediated MHC up-regulation. J Immunol 170:3204-3213.

Bi Z, Barna M, Komatsu T, Reiss C. 1995a. Vesicular stomatitis virus infection of the central nervous system activates both innate and acquired immunity. J Virol 69:6466-6472.

Bi Z, Quandt P, Komatsu T, Barna M, Reiss CS. 1995b. IL-12 promotes enhanced recovery from vesicular stomatitis virus infection of the central nervous system. J Immunol 155:5684-5689.

Binder GK, Griffin DE. 2001. Interferon-gamma-mediated site-specific clearance of alphavirus from CNS neurons. Science 293:303-306.

Binder GK, Griffin DE. 2003a. Immune-mediated clearance of virus from the central nervous system. Microbes Infect 5:439-448.

Binder GK, Griffin DE. 2003b. Immune-mediated clearance of virus from the central nervous system. Microbes Infect 5:439-448.

Bjorck P. 2001. Isolation and characterization of plasmacytoid dendritic cells from Flt3 ligand and granulocyte-macrophage colony-stimulating factor-treated mice. Blood 98:3520-3526.

Brown LF, Yeo KT, Berse B, Yeo TK, Senger DR, Dvorak HF, van de Water L. 1992. Expression of vascular permeability factor (vascular endothelial growth factor) by epidermal keratinocytes during wound healing. J Exp Med 176:1375-1379.

Broxmeyer HE, Kim CH, Cooper SH, Hangoc G, Hromas R, Pelus LM. 1999. Effects of CC, CXC, C, and CX3C chemokines on proliferation of myeloid progenitor cells, and insights into SDF-1-induced chemotaxis of progenitors. Ann NY Acad Sci 872:142-163.

Buch T, Heppner FL, Tertilt C, Heinen TJ, Kremer M, Wunderlich FT, Jung S, Waisman A. 2005. A Cre-inducible diphtheria toxin receptor mediates cell lineage ablation after toxin administration. Nat Methods 2:419-426.

Buckler CE, Baron S. 1966. Antiviral action of mouse interferon in heterologous cells. J Bacteriol 91:231-235.

Bullard DC, Hu X, Schoeb TR, Axtell RC, Raman C, Barnum SR. 2005. Critical Requirement of CD11b (Mac-1) on T Cells and Accessory Cells for Development of Experimental Autoimmune Encephalomyelitis. J Immunol 175:6327-6333.

Bulloch K, Miller MM, Gal-Toth J, Milner TA, Gottfried-Blackmore A, Waters EM, Kaunzner UW, Liu K, Lindquist R, Nussenzweig MC and others. 2008. CD11c/EYFP transgene illuminates a discrete network of dendritic cells within the embryonic, neonatal, adult, and injured mouse brain. J Comp Neurol 508:687-710.

Burnett SH, Kershen EJ, Zhang J, Zeng L, Straley SC, Kaplan AM, Cohen DA. 2004. Conditional macrophage ablation in transgenic mice expressing a Fas-based suicide gene. J Leukoc Biol 75:612-623.

Candelario-Jalil E, Yang Y, Rosenberg GA. 2009. Diverse roles of matrix metalloproteinases and tissue inhibitors of metalloproteinases in neuroinflammation and cerebral ischemia. Neuroscience 158:983-994.

Caraux A, Lu Q, Fernandez N, Riou S, Di Santo JP, Raulet DH, Lemke G, Roth C. 2006. Natural killer cell differentiation driven by Tyro3 receptor tyrosine kinases. Nat Immunol 7:747-754.

Chesler DA, Reiss CS. 2002. IL-12, while beneficial, is not essential for the host response to VSV encephalitis. J Neuroimmunol 131:92-97.

Christensen JE, Andreasen SO, Christensen JP, Thomsen AR. 2001. CD11b expression as a marker to distinguish between recently activated effector CD8(+) T cells and memory cells. Int Immunol 13:593-600.

Ciavarra RP, Buhrer K, Van Rooijen N, Tedeschi B. 1997. T cell priming against vesicular stomatitis virus analyzed in situ: red pulp macrophages, but neither marginal metallophilic nor marginal zone macrophages, are required for priming CD4+ and CD8+ T cells. J Immunol 158:1749-1755.

Ciavarra RP, Burgess DH. 1988. Antigen-presenting B cells: efficient uptake and presentation by activated B cells for induction of cytotoxic T lymphocytes against vesicular stomatitis virus. Cell Immunol 114:27-40.

Ciavarra RP, Stephens A, Nagy S, Sekellick M, Steel C. 2006. Evaluation of Immunological Paradigms in a Virus Model: Are Dendritic Cells Critical for Antiviral Immunity and Viral Clearance? J Immunol 177:492-500.

Ciavarra RP, Taylor L, Greene AR, Yousefieh N, Horeth D, van Rooijen N, Steel C, Gregory B, Birkenbach M, Sekellick M. 2005. Impact of macrophage and dendritic cell subset elimination on antiviral immunity, viral clearance and production of type 1 interferon. Virology 342:177-189.

Ciavarra RP, Tedeschi B. 1994. Priming antiviral cytotoxic T lymphocytes: requirement for CD4+ cells is dependent on the antigen presenting cell in vivo. Cell Immunol 157:132-143.

Claassen IJ, Osterhaus AD, Claassen E. 1995. Antigen detection in vivo after immunization with different presentation forms of rabies virus antigen: involvement of marginal metallophilic macrophages in the uptake of immune-stimulating complexes. Eur J Immunol 25:1446-1452.

Claassen IJ, Osterhaus AD, Poelen M, Van Rooijen N, Claassen E. 1998. Antigen detection in vivo after immunization with different presentation forms of rabies virus antigen, II. Cellular, but not humoral, systemic immune responses against rabies virus immune-stimulating complexes are macrophage dependent. Immunology 94:455-460.

Clauss M, Gerlach M, Gerlach H, Brett J, Wang F, Familletti PC, Pan YC, Olander JV, Connolly DT, Stern D. 1990. Vascular permeability factor: a tumor-derived polypeptide that induces endothelial cell and monocyte procoagulant activity, and promotes monocyte migration. J Exp Med 172:1535-1545.

Colonna M, Trinchieri G, Liu YJ. 2004. Plasmacytoid dendritic cells in immunity. Nat Immunol 5:1219-1226.

Connolly DT. 1991. Vascular permeability factor: a unique regulator of blood vessel function. J Cell Biochem 47:219-223.

Constantinescu CS, Frei K, Wysocka M, Trinchieri G, Malipiero U, Rostami A, Fontana A. 1996. Astrocytes and microglia produce interleukin-12 p40. Ann NY Acad Sci 795:328-333.

Cosenza-Nashat MA, Kim MO, Zhao ML, Suh HS, Lee SC. 2006. CD45 isoform expression in microglia and inflammatory cells in HIV-1 encephalitis. Brain Pathol 16:256-265.

Dalod M, Salazar-Mather TP, Malmgaard L, Lewis C, Asselin-Paturel C, Briere F, Trinchieri G, Biron CA. 2002. Interferon alpha/beta and interleukin 12 responses to viral infections: pathways regulating dendritic cell cytokine expression in vivo. J Exp Med 195:517-528.

Delhaye S, Paul S, Blakqori G, Minet M, Weber F, Staeheli P, Michiels T. 2006. Neurons produce type I interferon during viral encephalitis 10.1073/pnas.0602460103. Proc Natl Acad Sci USA 103:7835-7840.

Devi S, Laning J, Luo Y, Dorf ME. 1995. Biologic activities of the beta-chemokine TCA3 on neutrophils and macrophages. J Immunol 154:5376-5383.

Dimier-Poisson I, Aline F, Bout D, Mevelec MN. 2006. Induction of protective immunity against toxoplasmosis in mice by immunization with Toxoplasma gondii RNA. Vaccine 24:1705-1709.

Dong Y, Benveniste EN. 2001. Immune function of astrocytes. Glia 36:180-190.

Doyle HA, Murphy JW. 1999. Role of the C-C chemokine, TCA3, in the protective anticryptococcal cell-mediated immune response. J Immunol 162:4824-4833.

eBioscience I. 2009. eBioscience BestProtocols: ELISA, Ready-SET-Go! Pretitrated Antibody Sets.

Ernst D, Chambers S, Chronopoulou E, Elia J, Ember J, Huang Z, Luan F-J, Maecker H, Qi G, Sepulveda H and others. 2006. BD™ ELISPOT Assays for Cells That Secrete Biological Response Modifiers. In: Gilette L, Ernst D, editors. Techniques for Immune Function Analysis Application Handbook. San Diego, CA: BD Biosciences. p 109-121.

Fabriek BO, Van Haastert ES, Galea I, Polfliet MM, Dopp ED, Van Den Heuvel MM, Van Den Berg TK, De Groot CJ, Van Der Valk P, Dijkstra CD. 2005. CD163-positive perivascular macrophages in the human CNS express molecules for antigen recognition and presentation. Glia 51:297-305.

Farina C, Aloisi F, Meinl E. 2007. Astrocytes are active players in cerebral innate immunity. Trends in Immunology 28:138-145.

Fife BT, Kennedy KJ, Paniagua MC, Lukacs NW, Kunkel SL, Luster AD, Karpus WJ. 2001. CXCL10 (IFN-gamma-inducible protein-10) control of encephalitogenic CD4+ T cell accumulation in the central nervous system during experimental autoimmune encephalomyelitis. J Immunol 166:7617-7624.

Fischer H-G, Reichmann G. 2001. Brain Dendritic Cells and Macrophages/Microglia in Central Nervous System Inflammation. J Immunol 166:2717-2726.

Fischer HG, Bonifas U, Reichmann G. 2000. Phenotype and functions of brain dendritic cells emerging during chronic infection of mice with Toxoplasma gondii. J Immunol 164:4826-4834.

Fitzgerald-Bocarsly P. 2002. Natural interferon-alpha producing cells: the plasmacytoid dendritic cells. Biotechniques Suppl:16-20, 22, 24-29.

Flugel A, Bradl M, Kreutzberg GW, Graeber MB. 2001. Transformation of donor-derived bone marrow precursors into host microglia during autoimmune CNS inflammation and during the retrograde response to axotomy. J Neurosci Res 66:74-82.

Ford AL, Goodsall AL, Hickey WF, Sedgwick JD. 1995. Normal adult ramified microglia separated from other central nervous system macrophages by flow cytometric sorting. Phenotypic differences defined and direct ex vivo antigen presentation to myelin basic protein- reactive CD4+ T cells compared. J Immunol 154:4309-4321.

Forger JM, 3rd, Bronson RT, Huang AS, Reiss CS. 1991. Murine infection by vesicular stomatitis virus: initial characterization of the H-2d system. J Virol 65:4950-4958.

Galea I, Bechmann I, Perry VH. 2007a. What is immune privilege (not)? Trends in Immunology 28:12-18.

Galea I, Bernardes-Silva M, Forse PA, van Rooijen N, Liblau RS, Perry VH. 2007b. An antigen-specific pathway for CD8 T cells across the blood-brain barrier. J Exp Med 204:2023-2030.

Galea I, Palin K, Newman TA, Van Rooijen N, Perry VH, Boche D. 2005. Mannose receptor expression specifically reveals perivascular macrophages in normal, injured, and diseased mouse brain. Glia 49:375-384.

Gearing AJ, Beckett P, Christodoulou M, Churchill M, Clements JM, Crimmin M, Davidson AH, Drummond AH, Galloway WA, Gilbert R and others. 1995. Matrix metalloproteinases and processing of pro-TNF-alpha. J Leukoc Biol 57:774-777.

Getts DR, Terry RL, Getts MT, Muller M, Rana S, Shrestha B, Radford J, Van Rooijen N, Campbell IL, King NJ. 2008. Ly6c+ "inflammatory monocytes" are microglial precursors recruited in a pathogenic manner in West Nile virus encephalitis. J Exp Med 205:2319-2337.

Ghendler Y, Hussey RE, Witte T, Mizoguchi E, Clayton LK, Bhan AK, Koyasu S, Chang HC, Reinherz EL. 1997. Double-positive T cell receptor(high) thymocytes are resistant to peptide/major histocompatibility complex ligand-induced negative selection. Eur J Immunol 27:2279-2289.

Glabinski AR, Ransohoff RM. 1999. Sentries at the gate: chemokines and the blood-brain barrier. J Neurovirol 5:623-634.

Gobet R, Cerny A, Ruedi E, Hengartner H, Zinkernagel RM. 1988. The role of antibodies in natural and acquired resistance of mice to vesicular stomatitis virus. Exp Cell Biol 56:175-180.

Griffin DE. 2003. Immune responses to RNA-virus infections of the CNS. Nat Rev Immunol 3:493-502.

Gronowitz JS, Kallander CF, Hagberg H, Persson L. 1984. Deoxythymidine-kinase in cerebrospinal fluid: a new potential "marker" for brain tumours. Acta Neurochir (Wien) 73:1-12.

Gropp E, Shanabrough M, Borok E, Xu AW, Janoschek R, Buch T, Plum L, Balthasar N, Hampel B, Waisman A and others. 2005. Agouti-related peptide-expressing neurons are mandatory for feeding. Nat Neurosci 8:1289-1291.

Gurney KJ, Estrada EY, Rosenberg GA. 2006. Blood-brain barrier disruption by stromelysin-1 facilitates neutrophil infiltration in neuroinflammation. Neurobiol Dis 23:87-96.

Hart MN, Fabry Z. 1995. CNS antigen presentation. Trends Neurosci 18:475-481.

Hatterer E, Davoust N, Didier-Bazes M, Vuaillat C, Malcus C, Belin M-F, Nataf S. 2006. How to drain without lymphatics? Dendritic cells migrate from the cerebrospinal fluid to the B-cell follicles of cervical lymph nodes. Blood 107:806-812.

Havenith CE, Askew D, Walker WS. 1998. Mouse resident microglia: isolation and characterization of immunoregulatory properties with naive CD4+ and CD8+ T-cells. Glia 22:348-359.

Hestdal K, Jacobsen SE, Ruscetti FW, Dubois CM, Longo DL, Chizzonite R, Oppenheim JJ, Keller JR. 1992. In vivo effect of interleukin-1 alpha on hematopoiesis: role of colony-stimulating factor receptor modulation. Blood 80:2486-2494.

Hickey WF. 2001. Basic principles of immunological surveillance of the normal central nervous system. Glia 36:118-124.

Hornung V, Guenthner-Biller M, Bourquin C, Ablasser A, Schlee M, Uematsu S, Noronha A, Manoharan M, Akira S, de Fougerolles A and others. 2005. Sequence-specific potent induction of IFN-alpha by short interfering RNA in plasmacytoid dendritic cells through TLR7. Nat Med 11:263-270.

Howard M, O'Garra A. 1992. Biological properties of interleukin 10. Immunol Today 13:198-200.

Hume DA, Ross IL, Himes SR, Sasmono RT, Wells CA, Ravasi T. 2002. The mononuclear phagocyte system revisited. J Leukoc Biol 72:621-627.

Huneycutt BS, Plakhov IV, Shusterman Z, Bartido SM, Huang A, Reiss CS, Aoki C. 1994. Distribution of vesicular stomatitis virus proteins in the brains of BALB/c mice following intranasal inoculation: an immunohistochemical analysis. Brain Res 635:81-95.

Ireland DD, Reiss CS. 2006. Gene expression contributing to recruitment of circulating cells in response to vesicular stomatitis virus infection of the CNS. Viral Immunol 19:536-545.

Ishizuka M, Takeuchi T, Umezawa H. 1982. Studies of the Effect of Spermidine in Enhancing Cellular Immunity. Proc Jpn Acad Ser B Phys Biol Sci 58:327-330.

Janeway CA, National Center for Biotechnology Information (U.S.), National Institutes of Health (U.S.). 2001. Immunobiology 5: the immune system in health and disease. 5th ed. New York Bethesda, MD.: Garland Pub. ;NCBI.

Juedes AE, Ruddle NH. 2001. Resident and Infiltrating Central Nervous System APCs Regulate the Emergence and Resolution of Experimental Autoimmune Encephalomyelitis. J Immunol 166:5168-5175.

Jung S, Unutmaz D, Wong P, Sano G, De los Santos K, Sparwasser T, Wu S, Vuthoori S, Ko K, Zavala F and others. 2002. In vivo depletion of CD11c(+) dendritic cells abrogates priming of CD8(+) T cells by exogenous cell-associated antigens. Immunity 17:211-220.

Kaczmarek L, Kaminska B, Messina L, Spampinato G, Arcidiacono A, Malaguarnera L, Messina A. 1992. Inhibitors of polyamine biosynthesis block tumor necrosis factor-induced activation of macrophages. Cancer Res 52:1891-1894.

Karman J, Chu HH, Co DO, Seroogy CM, Sandor M, Fabry Z. 2006. Dendritic cells amplify T cell-mediated immune responses in the central nervous system. J Immunol 177:7750-7760.

Katz-Levy Y, Neville KL, Girvin AM, Vanderlugt CL, Pope JG, Tan LJ, Miller SD. 1999. Endogenous presentation of self myelin epitopes by CNS-resident APCs in Theiler's virus-infected mice. J Clin Invest 104:599-610.

Kawanokuchi J, Mizuno T, Takeuchi H, Kato H, Wang J, Mitsuma N, Suzumura A. 2006. Production of interferon-gamma by microglia. Mult Scler 12:558-564.

Kelsall BL, Biron CA, Sharma O, Kaye PM. 2002. Dendritic cells at the host-pathogen interface. Nat Immunol 3:699-702.

Kim CH, Broxmeyer HE. 1999. Chemokines: signal lamps for trafficking of T and B cells for development and effector function. J Leukoc Biol 65:6-15.

Kim CH, Pelus LM, White JR, Applebaum E, Johanson K, Broxmeyer HE. 1998. CK beta-11/macrophage inflammatory protein-3 beta/EBI1-ligand chemokine is an efficacious chemoattractant for T and B cells. J Immunol 160:2418-2424.

Kim WK, Alvarez X, Fisher J, Bronfin B, Westmoreland S, McLaurin J, Williams K. 2006. CD163 identifies perivascular macrophages in normal and viral encephalitic brains and potential precursors to perivascular macrophages in blood. Am J Pathol 168:822-834.

Komatsu T, Barna M, Reiss CS. 1997. Interleukin-12 promotes recovery from viral encephalitis. Viral Immunol 10:35-47.

Komatsu T, Bi Z, Reiss CS. 1996. Interferon-gamma induced type I nitric oxide synthase activity inhibits viral replication in neurons. J Neuroimmunol 68:101-108.

Komatsu T, Ireland DD, Chung N, Dore A, Yoder M, Shoshkes Reiss C. 1999. Regulation of the BBB during viral encephalitis: roles of IL-12 and NOS. Nitric Oxide 3:327-339.

Kronin V, Wu L, Gong S, Nussenzweig MC, Shortman K. 2000. DEC-205 as a marker of dendritic cells with regulatory effects on CD8 T cell responses. Int Immunol 12:731-735.

Krug A, French AR, Barchet W, Fischer JA, Dzionek A, Pingel JT, Orihuela MM, Akira S, Yokoyama WM, Colonna M. 2004. TLR9-dependent recognition of MCMV by IPC and DC generates coordinated cytokine responses that activate antiviral NK cell function. Immunity 21:107-119.

Kundig TM, Hengartner H, Zinkernagel RM. 1993. T cell-dependent IFN-gamma exerts an antiviral effect in the central nervous system but not in peripheral solid organs. J Immunol 150:2316-2321.

Lai C, Gore M, Lemke G. 1994. Structure, expression, and activity of Tyro 3, a neural adhesion-related receptor tyrosine kinase. Oncogene 9:2567-2578.

Lalancette-Hebert M, Gowing G, Simard A, Weng YC, Kriz J. 2007. Selective ablation of proliferating microglial cells exacerbates ischemic injury in the brain. J Neurosci 27:2596-2605.

Lauterbach H, Zuniga EI, Truong P, Oldstone MB, McGavern DB. 2006. Adoptive immunotherapy induces CNS dendritic cell recruitment and antigen presentation during clearance of a persistent viral infection. J Exp Med 203:1963-1975.

Lawson LJ, Perry VH, Dri P, Gordon S. 1990. Heterogeneity in the distribution and morphology of microglia in the normal adult mouse brain. Neuroscience 39:151-170.

Leenen PJ, Radosevic K, Voerman JS, Salomon B, van Rooijen N, Klatzmann D, van Ewijk W. 1998. Heterogeneity of mouse spleen dendritic cells: in vivo phagocytic activity, expression of macrophage markers, and subpopulation turnover. J Immunol 160:2166-2173.

Lees JR, Archambault AS, Russell JH. 2006. T-cell trafficking competence is required for CNS invasion. J Neuroimmunol 177:1-10.

Lipscomb MF, Masten BJ. 2002. Dendritic cells: immune regulators in health and disease. Physiol Rev 82:97-130.

Lu L, Hsieh M, Oriss TB, Morel PA, Starzl TE, Rao AS, Thomson AW. 1995. Generation of DC from mouse spleen cell cultures in response to GM-CSF: immunophenotypic and functional analyses. Immunology 84:127-134.

Lu L, Woo J, Rao AS, Li Y, Watkins SC, Qian S, Starzl TE, Demetris AJ, Thomson AW. 1994. Propagation of dendritic cell progenitors from normal mouse liver using granulocyte/macrophage colony-stimulating factor and their maturational development in the presence of type-1 collagen. J Exp Med 179:1823-1834.

Lu Q, Lemke G. 2001. Homeostatic regulation of the immune system by receptor tyrosine kinases of the Tyro 3 family. Science 293:306-311.

Lund JM, Alexopoulou L, Sato A, Karow M, Adams NC, Gale NW, Iwasaki A, Flavell RA. 2004. Recognition of single-stranded RNA viruses by Toll-like receptor 7. Proc Natl Acad Sci USA 101:5598-5603.

Mack CL, Vanderlugt-Castaneda CL, Neville KL, Miller SD. 2003. Microglia are activated to become competent antigen presenting and effector cells in the inflammatory environment of the Theiler's virus model of multiple sclerosis. J Neuroimmunol 144:68-79.

Marvaldi JL, Lucas-Lenard J, Sekellick MJ, Marcus PI. 1977. Cell killing by viruses. IV. Cell killing and protein synthesis inhibition by vesicular stomatitis virus require the same gene functions. Virology 79:267-280.

Masurier C, Pioche-Durieu C, Colombo BM, Lacave R, Lemoine FM, Klatzmann D, Guigon M. 1999. Immunophenotypical and functional heterogeneity of dendritic cells generated from murine bone marrow cultured with different cytokine combinations: implications for anti-tumoral cell therapy. Immunology 96:569-577.

Matyszak MK, Perry VH. 1996. The potential role of dendritic cells in immune-mediated inflammatory diseases in the central nervous system. Neuroscience 74:599-608.

McGrath MS, Hadlock KG; 2007 29 March. Methods for Treating Viral Infections Using Polyamine Analogs.

McMenamin PG. 1999. Distribution and phenotype of dendritic cells and resident tissue macrophages in the dura mater, leptomeninges, and choroid plexus of the rat brain as demonstrated in wholemount preparations. J Comp Neurol 405:553-562.

Megjugorac NJ, Young HA, Amrute SB, Olshalsky SL, Fitzgerald-Bocarsly P. 2004. Virally stimulated plasmacytoid dendritic cells produce chemokines and induce migration of T and NK cells. J Leukoc Biol 75:504-514.

Mendez-Fernandez YV, Hansen MJ, Rodriguez M, Pease LR. 2005. Anatomical and Cellular Requirements for the Activation and Migration of Virus-Specific CD8+ T Cells to the Brain during Theiler's Virus Infection. J Virol 79:3063-3070.

Messina L, Spampinato G, Arcidiacono A, Malaguarnera L, Pagano M, Kaminska B, Kaczmarek L, Messina A. 1992. Polyamine involvement in functional activation of human macrophages. J Leukoc Biol 52:585-587.

Miller DW. 1999. Immunobiology of the blood-brain barrier. J Neurovirol 5:570-578.

Miller SD, McMahon EJ, Schreiner B, Bailey SL. 2007. Antigen Presentation in the CNS by Myeloid Dendritic Cells Drives Progression of Relapsing Experimental Autoimmune Encephalomyelitis. Ann NY Acad Sci 1103:179-191.

Morris MM, Dyson H, Baker D, Harbige LS, Fazakerley JK, Amor S. 1997. Characterization of the cellular and cytokine response in the central nervous system following Semliki Forest virus infection. J Neuroimmunol 74:185-197.

Muller U, Steinhoff U, Reis LF, Hemmi S, Pavlovic J, Zinkernagel RM, Aguet M. 1994. Functional role of type I and type II interferons in antiviral defense. Science 264:1918-1921.

Nag S. 2003. Blood-Brain Barrier Permeability Using Tracers and Immunohistochemistry. The blood-brain barrier: biology and research protocols. Totowa, NJ: Humana Press. p 133-145.

Nair A, Hunzeker J, Bonneau RH. 2007. Modulation of microglia and CD8(+) T cell activation during the development of stress-induced herpes simplex virus type-1 encephalitis. Brain Behav Immun 21:791-806.

Nakamura S, Sung SS, Bjorndahl JM, Fu SM. 1989. Human T cell activation. IV. T cell activation and proliferation via the early activation antigen EA 1. J Exp Med 169:677-689.

Nelson PT, Soma LA, Lavi E. 2002. Microglia in diseases of the central nervous system. Ann Med 34:491-500.

Neumann H. 2001. Control of glial immune function by neurons. Glia 36:191-199.

Newman TA, Galea I, van Rooijen N, Perry VH. 2005. Blood-derived dendritic cells in an acute brain injury. J Neuroimmunol 166:167-172.

Noe V, Fingleton B, Jacobs K, Crawford HC, Vermeulen S, Steelant W, Bruyneel E, Matrisian LM, Mareel M. 2001. Release of an invasion promoter E-cadherin fragment by matrilysin and stromelysin-1. J Cell Sci 114:111-118.

Nussenzweig MC, Steinman RM, Witmer MD, Gutchinov B. 1982. A monoclonal antibody specific for mouse dendritic cells. Proc Natl Acad Sci USA 79:161-165.

Oehen S, Odermatt B, Karrer U, Hengartner H, Zinkernagel R, Lopez-Macias C. 2002. Marginal zone macrophages and immune responses against viruses. J Immunol 169:1453-1458.

Olson JK, Miller SD. 2004. Microglia Initiate Central Nervous System Innate and Adaptive Immune Responses through Multiple TLRs. J Immunol 173:3916-3924.

Pardridge WM. 1999. Blood-brain barrier biology and methodology. J Neurovirol 5:556-569.

Parra B, Hinton DR, Marten NW, Bergmann CC, Lin MT, Yang CS, Stohlman SA. 1999. IFN-gamma is required for viral clearance from central nervous system oligodendroglia. J Immunol 162:1641-1647.

Pashenkov M, Teleshova N, Kouwenhoven M, Smirnova T, Jin YP, Kostulas V, Huang YM, Pinegin B, Boiko A, Link H. 2002. Recruitment of dendritic cells to the cerebrospinal fluid in bacterial neuroinfections. J Neuroimmunol 122:106-116.

Patterson CE, Lawrence DM, Echols LA, Rall GF. 2002. Immune-mediated protection from measles virus-induced central nervous system disease is noncytolytic and gamma interferon dependent. J Virol 76:4497-4506.

Perry VH. 1998. A revised view of the central nervous system microenvironment and major histocompatibility complex class II antigen presentation. J Neuroimmunol 90:113-121.

Persidsky Y. 1999. Model systems for studies of leukocyte migration across the blood - brain barrier. J Neurovirol 5:579-590.

Persidsky Y, Ghorpade A, Rasmussen J, Limoges J, Liu XJ, Stins M, Fiala M, Way D, Kim KS, Witte MH and others. 1999. Microglial and astrocyte chemokines regulate monocyte migration through the blood-brain barrier in human immunodeficiency virus-1 encephalitis. Am J Pathol 155:1599-1611.

Plakhov IV, Arlund EE, Aoki C, Reiss CS. 1995. The earliest events in vesicular stomatitis virus infection of the murine olfactory neuroepithelium and entry of the central nervous system. Virology 209:257-262.

Pogue SL, Preston BT, Stalder J, Bebbington CR, Cardarelli PM. 2004. The receptor for type I IFNs is highly expressed on peripheral blood B cells and monocytes and mediates a distinct profile of differentiation and activation of these cells. J Interferon Cytokine Res 24:131-139.

Polfliet MM, Goede PH, van Kesteren-Hendrikx EM, van Rooijen N, Dijkstra CD, van den Berg TK. 2001a. A method for the selective depletion of perivascular and meningeal macrophages in the central nervous system. J Neuroimmunol 116:188-195.

Polfliet MM, Zwijnenburg PJ, van Furth AM, van der Poll T, Dopp EA, Renardel de Lavalette C, van Kesteren-Hendrikx EM, van Rooijen N, Dijkstra CD, van den Berg TK. 2001b. Meningeal and perivascular macrophages of the central nervous system play a protective role during bacterial meningitis. J Immunol 167:4644-4650.

Ponomarev ED, Novikova M, Maresz K, Shriver LP, Dittel BN. 2005a. Development of a culture system that supports adult microglial cell proliferation and maintenance in the resting state. J Immunol Methods 300:32-46.

Ponomarev ED, Shriver LP, Maresz K, Dittel BN. 2005b. Microglial cell activation and proliferation precedes the onset of CNS autoimmunity. J Neurosci Res 81:374-389.

Pozzi LA, Maciaszek JW, Rock KL. 2005. Both dendritic cells and macrophages can stimulate naive CD8 T cells in vivo to proliferate, develop effector function, and differentiate into memory cells. J Immunol 175:2071-2081.

Prat A, Biernacki K, Wosik K, Antel JP. 2001. Glial cell influence on the human blood-brain barrier. Glia 36:145-155.

Prieto J, Beatty PG, Clark EA, Patarroyo M. 1988. Molecules mediating adhesion of T and B cells, monocytes and granulocytes to vascular endothelial cells. Immunology 63:631-637.

Probst HC, Tschannen K, Odermatt B, Schwendener R, Zinkernagel RM, Van Den Broek M. 2005. Histological analysis of CD11c-DTR/GFP mice after in vivo depletion of dendritic cells. Clin Exp Immunol 141:398-404.

Probst HC, van den Broek M. 2005. Priming of CTLs by lymphocytic choriomeningitis virus depends on dendritic cells. J Immunol 174:3920-3924.

Puddington L, Bevan MJ, Rose JK, Lefrancois L. 1986. N protein is the predominant antigen recognized by vesicular stomatitis virus-specific cytotoxic T cells. J Virol 60:708-717.

Pulendran B, Lingappa J, Kennedy MK, Smith J, Teepe M, Rudensky A, Maliszewski CR, Maraskovsky E. 1997. Developmental pathways of dendritic cells in vivo: distinct function, phenotype, and localization of dendritic cell subsets in FLT3 ligand-treated mice. J Immunol 159:2222-2231.

Qian Q, Jutila MA, Van Rooijen N, Cutler JE. 1994. Elimination of mouse splenic macrophages correlates with increased susceptibility to experimental disseminated candidiasis. J Immunol 152:5000-5008.

Raivich G, Moreno-Flores MT, Moller JC, Kreutzberg GW. 1994. Inhibition of posttraumatic microglial proliferation in a genetic model of macrophage colony-stimulating factor deficiency in the mouse. Eur J Neurosci 6:1615-1618.

Randolph GJ, Angeli V, Swartz MA. 2005. Dendritic-cell trafficking to lymph nodes through lymphatic vessels. Nat Rev Immunol 5:617-628.

Reape TJ, Rayner K, Manning CD, Gee AN, Barnette MS, Burnand KG, Groot PH. 1999. Expression and cellular localization of the CC chemokines PARC and ELC in human atherosclerotic plaques. Am J Pathol 154:365-374.

Reichmann G, Schroeter M, Jander S, Fischer HG. 2002. Dendritic cells and dendritic-like microglia in focal cortical ischemia of the mouse brain. J Neuroimmunol 129:125-132.

Reiss CS, Plakhov IV, Komatsu T. 1998. Viral replication in olfactory receptor neurons and entry into the olfactory bulb and brain. Ann NY Acad Sci 855:751-761.

Rettenmier CW, Roussel MF, Sherr CJ. 1988. The colony-stimulating factor 1 (CSF-1) receptor (c-fms proto-oncogene product) and its ligand. J Cell Sci Suppl 9:27-44.

Rieser C, Ramoner R, Bock G, Deo YM, Holtl L, Bartsch G, Thurnher M. 1998. Human monocyte-derived dendritic cells produce macrophage colony-stimulating factor: enhancement of c-fms expression by interleukin-10. Eur J Immunol 28:2283-2288.

Roach T, Slater S, Koval M, White L, Cahir McFarland ED, Okumura M, Thomas M, Brown E. 1997. CD45 regulates Src family member kinase activity associated with macrophage integrin-mediated adhesion. Curr Biol 7:408-417.

Rock RB, Gekker G, Hu S, Sheng WS, Cheeran M, Lokensgard JR, Peterson PK. 2004. Role of microglia in central nervous system infections. Clin Microbiol Rev 17:942-964.

Rosenberg GA. 2002. Matrix metalloproteinases in neuroinflammation. Glia 39:279-291.

Rothlin CV, Ghosh S, Zuniga EI, Oldstone MB, Lemke G. 2007. TAM receptors are pleiotropic inhibitors of the innate immune response. Cell 131:1124-1136.

Rothwell NJ. 1991. Functions and mechanisms of interleukin 1 in the brain. Trends Pharmacol Sci 12:430-436.

Rothwell VM, Rohrschneider LR. 1987. Murine c-fms cDNA: cloning, sequence analysis and retroviral expression. Oncogene Res 1:311-324.

Rubin LL, Staddon JM. 1999. The cell biology of the blood-brain barrier. Annu Rev Neurosci 22:11-28.

Santambrogio L, Belyanskaya SL, Fischer FR, Cipriani B, Brosnan CF, Ricciardi-Castagnoli P, Stern LJ, Strominger JL, Riese R. 2001. Developmental plasticity of CNS microglia. Proc Natl Acad Sci USA 98:6295-6300.

Saunders AE, Johnson P. Modulation of immune cell signalling by the leukocyte common tyrosine phosphatase, CD45. Cell Signal 22:339-348.

Schilling M, Besselmann M, Leonhard C, Mueller M, Ringelstein EB, Kiefer R. 2003. Microglial activation precedes and predominates over macrophage infiltration in transient focal cerebral ischemia: a study in green fluorescent protein transgenic bone marrow chimeric mice. Exp Neurol 183:25-33.

Schulz NT, Paulhiac CI, Lee L, Zhou R. 1995. Isolation and expression analysis of tyro3, a murine growth factor receptor tyrosine kinase preferentially expressed in adult brain. Brain Res Mol Brain Res 28:273-280.

Schwob JE, Saha S, Youngentob SL, Jubelt B. 2001. Intranasal inoculation with the olfactory bulb line variant of mouse hepatitis virus causes extensive destruction of the olfactory bulb and accelerated turnover of neurons in the olfactory epithelium of mice. Chem Senses 26:937-952.

Sekellick MJ, Marcus PI. 1979. Persistent infection. II. Interferon-inducing temperature-sensitive mutants as mediators of cell sparing: possible role in persistent infection by vesicular stomatitis virus. Virology 95:36-47.

Serafini B, Columba-Cabezas S, Di Rosa F, Aloisi F. 2000. Intracerebral recruitment and maturation of dendritic cells in the onset and progression of experimental autoimmune encephalomyelitis. Am J Pathol 157:1991-2002.

Serbina N, Pamer EG. 2003. Quantitative studies of CD8+ T-cell responses during microbial infection. Curr Opin Immunol 15:436-442.

Serot JM, Bene MC, Foliguet B, Faure GC. 2000. Monocyte-derived IL-10-secreting dendritic cells in choroid plexus epithelium. J Neuroimmunol 105:115-119.

Serot JM, Foliguet B, Bene MC, Faure GC. 1997. Ultrastructural and immunohistological evidence for dendritic-like cells within human choroid plexus epithelium. Neuroreport 8:1995-1998.

Serot JM, Foliguet B, Bene MC, Faure GC. 1998. Intraepithelial and stromal dendritic cells in human choroid plexus. Hum Pathol 29:1174-1175.

Shaked I, Tchoresh D, Gersner R, Meiri G, Mordechai S, Xiao X, Hart RP, Schwartz M. 2005. Protective autoimmunity: interferon-gamma enables microglia to remove glutamate without evoking inflammatory mediators. J Neurochem 92:997-1009.

Shortman K, Liu YJ. 2002. Mouse and human dendritic cell subtypes. Nat Rev Immunol 2:151-161.

Soilu-Hanninen M, Roytta M, Salmi AA, Salonen R. 1997. Semliki Forest virus infection leads to increased expression of adhesion molecules on splenic T-cells and on brain vascular endothelium. J Neurovirol 3:350-360.

Speth C, Rambach G, Hagleitner M, Konstanzer K, Hollmuller I, Dierich MP, Mohsenipour I, Maier H. 2007. Immune response to retroviral infections of the brain. Front Biosci 12:1508-1519.

Stark GR, Kerr IM, Williams BR, Silverman RH, Schreiber RD. 1998. How cells respond to interferons. Annu Rev Biochem 67:227-264.

Steel CD, Stephens AL, Hahto SM, Singletary SJ, Ciavarra RP. 2008. Comparison of the lateral tail vein and the retro-orbital venous sinus as routes of intravenous drug delivery in a transgenic mouse model. Lab Anim (NY) 37:26-32.

Stichel CC, Luebbert H. 2007. Inflammatory processes in the aging mouse brain: participation of dendritic cells and T-cells. Neurobiol Aging 28:1507-1521.

Stoll G, Jander S. 1999. The role of microglia and macrophages in the pathophysiology of the CNS. Prog Neurobiol 58:233-247.

Stoll G, Jander S, Schroeter M. 1998. Inflammation and glial responses in ischemic brain lesions. Prog Neurobiol 56:149-171.

Sun L, Lee J, Fine HA. 2004. Neuronally expressed stem cell factor induces neural stem cell migration to areas of brain injury. J Clin Invest 113:1364-1374.

Suzuki Y, Claflin J, Wang X, Lengi A, Kikuchi T. 2005. Microglia and macrophages as innate producers of interferon-gamma in the brain following infection with Toxoplasma gondii. Int J Parasitol 35:83-90.

Swanson TL, Gibbs GE. 1980. Inhibition of lymphocyte growth by spermidine in medium containing fetal bovine serum. In Vitro 16:761-766.

Thauland TJ, Koguchi Y, Wetzel SA, Dustin ML, Parker DC. 2008. Th1 and Th2 cells form morphologically distinct immunological synapses. J Immunol 181:393-399.

Town T, Nikolic V, Tan J. 2005. The microglial "activation" continuum: from innate to adaptive responses. J Neuroinflammation 2:24.

Turner DL, Cauley LS, Khanna KM, Lefrancois L. 2007. Persistent Antigen Presentation after Acute Vesicular Stomatitis Virus Infection. J Virol 81:2039-2046.

van den Berg TK, Kraal G. 2005. A function for the macrophage F4/80 molecule in tolerance induction. Trends Immunol 26:506-509.

van Rooijen N. 2006. ClodronateLiposomes.org: Injection.

van Rooijen N, van Nieuwmegen R. 1984. Elimination of phagocytic cells in the spleen after intravenous injection of liposome-encapsulated dichloromethylene diphosphonate. An enzyme-histochemical study. Cell Tissue Res 238:355-358.

Velge-Roussel F, Marcelo P, Lepage AC, Buzoni-Gatel D, Bout DT. 2000. Intranasal immunization with Toxoplasma gondii SAG1 induces protective cells into both NALT and GALT compartments. Infect Immun 68:969-972.

Vicari AP, Figueroa DJ, Hedrick JA, Foster JS, Singh KP, Menon S, Copeland NG, Gilbert DJ, Jenkins NA, Bacon KB and others. 1997. TECK: a novel CC chemokine specifically expressed by thymic dendritic cells and potentially involved in T cell development. Immunity 7:291-301.

Walker DG, Link J, Lue LF, Dalsing-Hernandez JE, Boyes BE. 2006. Gene expression changes by amyloid beta peptide-stimulated human postmortem brain microglia identify activation of multiple inflammatory processes. J Leukoc Biol 79:596-610.

Wang X, Suzuki Y. 2007. Microglia produce IFN-gamma independently from T cells during acute toxoplasmosis in the brain. J Interferon Cytokine Res 27:599-605.

Watanabe T, Yamamoto T, Abe Y, Saito N, Kumagai T, Kayama H. 1999. Differential activation of microglia after experimental spinal cord injury. J Neurotrauma 16:255-265.

Williams K, Alvarez X, Lackner AA. 2001. Central nervous system perivascular cells are immunoregulatory cells that connect the CNS with the peripheral immune system. Glia 36:156-164.

Wrobel CJ, Wright DC, Dedrick RL, Youle RJ. 1990. Diphtheria toxin effects on brain-tumor xenografts. Implications for protein-based brain-tumor chemotherapy. J Neurosurg 72:946-950.

Zhang M, Wang H, Tracey KJ. 2000. Regulation of macrophage activation and inflammation by spermine: a new chapter in an old story. Crit Care Med 28:N60-N66.

APPENDICES

Appendix A. ANTIBODIES

Supplier	Conjugate	Antigen	Clone	Catalogue #	Stock Conc	Working Conc	Working Vol
eBioscience	APC	isotype	eBRG1	17-4301	0.20 mg/mL	0.05 ug/1.E+06 cells	0.25 uL
eBioscience	APC	isotype	n/a	17-4914	0.20 mg/mL	0.05 ug/1.E+06 cells	0.25 uL
eBioscience	APC	CD3e	145-2C11	17-0031	0.20 mg/mL	0.25 ug/1.E+06 cells	1.25 uL
eBioscience	APC	CD11b	M1/70	17-0112	0.20 mg/mL	0.06 ug/1.E+06 cells	0.30 uL
eBioscience	APC	CD11c	N418	17-0114	0.20 mg/mL	0.13 ug/1.E+06 cells	0.65 uL
eBioscience	APC	Gr-1	RB6-8C5	17-5931	0.20 mg/mL	0.10 ug/1.E+06 cells	0.50 uL
eBioscience	APC	MHC II	M5/114.15.2	17-5321	0.20 mg/mL	0.02 ug/1.E+06 cells	0.10 uL
eBioscience	APC	Streptavidin	n/a	17-4317	0.20 mg/mL	0.06 ug/1.E+06 cells	0.30 uL
eBioscience	APC	TCR-b	H57-597	17-5961	0.20 mg/mL	0.06 ug/1.E+06 cells	0.30 uL
eBioscience	Biotin	IL-2	JES6-5H4	13-7021	0.50 mg/mL	2.00 ug/mL	4.00 uL
eBioscience	Biotin	IL-4	BVD6-24G2	13-7042	0.50 mg/mL	2.00 ug/mL	4.00 uL
eBioscience	Biotin	IFN-g	R4-6A2	13-7312	0.50 mg/mL	2.00 ug/mL	4.00 uL
eBioscience	Biotin	GM-CSF	MP1-31G6	13-7332	0.50 mg/mL	2.00 ug/mL	4.00 uL
BD Pharmingen	Biotin	isotype	n/a	11092C	0.50 mg/mL		0.00 uL
eBioscience	Biotin	anti-mouse IgG	polyclonal	13-4013	0.50 mg/mL	0.50 ug/1.E+06 cells	1.00 uL
eBioscience	Biotin	anti-rat IgG	polyclonal	13-4813	0.50 mg/mL	0.10 ug/1.E+06 cells	0.20 uL
BD Pharmingen	Biotin	isotype	R3-34	11012C	0.50 mg/mL		0.00 uL
BD Pharmingen	Biotin	CD3e	145-2C11	01082A	0.50 mg/mL	0.50 ug/1.E+06 cells	1.00 uL
BD Pharmingen	Biotin	CD5	53-7.3	01032A	0.50 mg/mL	0.13 ug/1.E+06 cells	0.25 uL
BD Pharmingen	Biotin	CD8a	53-6.7	553028	0.50 mg/mL	0.25 ug/1.E+06 cells	0.50 uL
BD Pharmingen	Biotin	CD11b	M1/70	01712D	0.50 mg/mL	0.06 ug/1.E+06 cells	0.12 uL
BD Pharmingen	Biotin	CD11c	HL3	09702D	0.50 mg/mL		0.00 uL
BD Pharmingen	Biotin	CD44	IM7	01222D	0.50 mg/mL	0.06 ug/1.E+06 cells	0.12 uL
BD Pharmingen	Biotin	CD45R	RA3-6B2	01122A	0.50 mg/mL	0.06 ug/1.E+06 cells	0.12 uL
BD Pharmingen	Biotin	CD49b	DX5	09942D	0.50 mg/mL	0.13 ug/1.E+06 cells	0.25 uL
eBioscience	Biotin	CD90.2	53-2.1	13-0902	0.50 mg/mL	0.06 ug/1.E+06 cells	0.12 uL
BD Pharmingen	Biotin	CD95	MFL3	28102D	0.50 mg/mL	0.13 ug/1.E+06 cells	0.25 uL
eBioscience	Biotin	CD115	AFS98	13-1152	0.50 mg/mL	0.25 ug/1.E+06 cells	0.50 uL
eBioscience	Biotin	B7-H1	MIH5	13-5982	0.50 mg/mL	0.06 ug/1.E+06 cells	0.12 uL
eBioscience	Biotin	B7-H4	188	13-5972	0.50 mg/mL	0.25 ug/1.E+06 cells	0.50 uL
eBioscience	Biotin	Dendritic Cell Marker	33D1	13-5884	0.50 mg/mL	0.25 ug/1.E+06 cells	0.50 uL
eBioscience	Biotin	F4/80	BM8	13-4801	0.50 mg/mL	0.13 ug/1.E+06 cells	0.26 uL
Caltag	Biotin	F4/80	BM8	RM2915	0.10 mg/mL	0.13 ug/1.E+06 cells	1.25 uL
BD Pharmingen	Biotin	Gr-1	RB6-8C5	553125	0.50 mg/mL	0.13 ug/1.E+06 cells	0.25 uL
eBioscience	Biotin	Gr-1	RB6-8C5	13-5931	0.50 mg/mL	0.13 ug/1.E+06 cells	0.25 uL
BD Pharmingen	Biotin	H-2Ld/H-2Db	28-14-8	06232D	0.50 mg/mL	1.00 ug/1.E+06 cells	2.00 uL
BD Pharmingen	Biotin	H-2Kb	AF6-88.5	06102D	0.50 mg/mL	0.06 ug/1.E+06 cells	0.12 uL
BD Pharmingen	Biotin	I-Ab	KH74	06262D	0.50 mg/mL		0.00 uL
BD Pharmingen	Biotin	ab-TCR	H57-597	01302A	0.50 mg/mL	0.50 ug/1.E+06 cells	1.00 uL

Supplier	Conjugate	Antigen	Clone	Catalogue #	Stock Conc	Working Conc	Working Vol
BD Pharmingen	CyChrome	CD3e	145-2C11	553065	0.20 mg/mL	0.13 ug/1.E+06 cells	0.63 uL
BD Pharmingen	CyChrome	Streptavidin	n/a	554062	0.20 mg/mL		0.00 uL
BD Pharmingen	FITC	isotype	R3-34	554684	0.50 mg/mL		0.00 uL
eBioscience	FITC	CD4	GK1.5	11-0041	0.50 mg/mL	0.25 ug/1.E+06 cells	0.50 uL
eBioscience	FITC	CD8a	53.6.7	11-0081	0.50 mg/mL	0.13 ug/1.E+06 cells	0.26 uL
eBioscience	FITC	CD11b	M1/70	11-0112	0.50 mg/mL	0.25 ug/1.E+06 cells	0.50 uL
BD Pharmingen	FITC	CD11c	HL3	553801	0.50 mg/mL		0.00 uL
eBioscience	FITC	CD19	MB19-1	11-0191	0.50 mg/mL	0.50 ug/1.E+06 cells	1.00 uL
eBioscience	FITC	CD27	LG.7F9	11-0271	0.50 mg/mL	0.06 ug/1.E+06 cells	0.12 uL
eBioscience	FITC	CD49d	R1-2	11-0492	0.50 mg/mL	0.25 ug/1.E+06 cells	0.50 uL
eBioscience	FITC	CD90.2	53-2.1	11-0902	0.50 mg/mL	0.06 ug/1.E+06 cells	0.12 uL
eBioscience	FITC	F4/80	BM8	11-4801	0.50 mg/mL	0.25 ug/1.E+06 cells	0.50 uL
eBioscience	FITC	Gr-1	RB6-8C5	11-5931	0.50 mg/mL	0.13 ug/1.E+06 cells	0.26 uL
eBioscience	FITC	MHC I	34-1-2S	11-5998	0.50 mg/mL	0.13 ug/1.E+06 cells	0.26 uL
eBioscience	FITC	MHC II	M5/114.15.2	11-5321	0.50 mg/mL	0.06 ug/1.E+06 cells	0.12 uL
BD Pharmingen	FITC	a-rat k light chain	MRK-1	10014D	0.50 mg/mL		0.00 uL
eBioscience	FITC	PD-1	J43	11-9985	0.50 mg/mL	0.50 ug/1.E+06 cells	1.00 uL
eBioscience	FITC	Streptavidin	n/a	11-4311	0.50 mg/mL	0.05 ug/1.E+06 cells	0.10 uL
BD Pharmingen	FITC	TCR-Vb 5.1, 5.2	MR9-4	553189	0.50 mg/mL		0.00 uL
Abcam	FITC	TCR-z	G3	11505-500	0.10 mg/mL	1.00 ug/1.E+06 cells	10.00 uL
eBioscience	PE	isotype	eBR2a	12-4321	0.20 mg/mL	0.05 ug/1.E+06 cells	0.25 uL
BD Pharmingen	PE	CD4	GK1.5	09425A	0.20 mg/mL	0.06 ug/1.E+06 cells	0.30 uL
eBioscience	PE	CD5	53-7.3	12-0051	0.20 mg/mL	0.06 ug/1.E+06 cells	0.30 uL
eBioscience	PE	CD8a	53-6.7	12-0081	0.20 mg/mL	0.13 ug/1.E+06 cells	0.65 uL
eBioscience	PE	CD11a	M17/4	12-0111	0.20 mg/mL	0.05 ug/1.E+06 cells	0.25 uL
eBioscience	PE	CD11b	M1/70	12-0112	0.20 mg/mL	0.06 ug/1.E+06 cells	0.30 uL
eBioscience	PE	CD11c	N418	12-0114	0.20 mg/mL	0.25 ug/1.E+06 cells	1.25 uL
eBioscience	PE	CD19	6D5	12-0192	0.20 mg/mL	0.13 ug/1.E+06 cells	0.65 uL
eBioscience	PE	CD25	PC61	12-0251	0.20 mg/mL	0.06 ug/1.E+06 cells	0.30 uL
BD Pharmingen	PE	CD40	3/23	553791	0.20 mg/mL		0.00 uL
eBioscience	PE	CD45R	RA3-6B2	12-0452	0.20 mg/mL	0.25 ug/1.E+06 cells	1.25 uL
eBioscience	PE	CD49d	R1-2	12-0492	0.20 mg/mL	0.50 ug/1.E+06 cells	2.50 uL
eBioscience	PE	CD70	FR70	12-0701	0.20 mg/mL	0.25 ug/1.E+06 cells	1.25 uL
eBioscience	PE	CD80	16-10A1	12-0801	0.20 mg/mL	0.03 ug/1.E+06 cells	0.15 uL
eBioscience	PE	CD137	17B5	12-1371	0.20 mg/mL	0.13 ug/1.E+06 cells	0.63 uL
eBioscience	PE	CD152	UC10-4B9	12-1522	0.20 mg/mL	0.25 ug/1.E+06 cells	1.25 uL
eBioscience	PE	CD154	MR1	12-1541	0.20 mg/mL	0.13 ug/1.E+06 cells	0.63 uL
eBioscience	PE	F4/80	BM8	12-4801	0.20 mg/mL	0.13 ug/1.E+06 cells	0.65 uL
eBioscience	PE	4-1BBL	TKS-1	12-5901	0.20 mg/mL	0.50 ug/1.E+06 cells	2.50 uL
BD Pharmingen	PE	B7-2	GL-1	09275B	0.20 mg/mL	0.06 ug/1.E+06 cells	0.30 uL
eBioscience	PE	B7-DC	TY25	12-5986	0.20 mg/mL	0.06 ug/1.E+06 cells	0.30 uL
eBioscience	PE	B7-H1	MIH5	12-5982	0.20 mg/mL	0.03 ug/1.E+06 cells	0.15 uL
eBioscience	PE	CCR7	4B12	12-1971	0.20 mg/mL	0.80 ug/1.E+06 cells	4.00 uL
BD Pharmingen	PE	Fas	Jo2	554258	0.20 mg/mL		0.00 uL
eBioscience	PE	Granzyme B	16G6	12-8822	0.20 mg/mL	0.13 ug/1.E+06 cells	0.63 uL

Supplier	Conjugate	Antigen	Clone	Catalogue #	Stock Conc	Working Conc	Working Vol
BD Pharmingen	PE	I-Ad	AMS-32.1	553548	0.20 mg/mL		0.00 uL
eBioscience	PE	MHC II	M5/114.15.2	12-5321	0.20 mg/mL	0.01 ug/1.E+06 cells	0.05 uL
eBioscience	PE	IFN-g	XMG1.2	12-7311	0.20 mg/mL	0.13 ug/1.E+06 cells	0.63 uL
eBioscience	PE	IL-2	JES6-5H4	12-7021	0.20 mg/mL	0.50 ug/1.E+06 cells	2.50 uL
eBioscience	PE	IgM	II/41	12-5790	0.20 mg/mL	0.06 ug/1.E+06 cells	0.30 uL
eBioscience	PE	Gr-1	RB6-8C5	12-5931	0.20 mg/mL	0.03 ug/1.E+06 cells	0.15 uL
eBioscience	PE	Streptavidin	n/a	12-4312	0.20 mg/mL	0.05 ug/1.E+06 cells	0.25 uL
BD Pharmingen	PE	TCR-b	H57-597	01305A	0.20 mg/mL	0.25 ug/1.E+06 cells	1.25 uL
BD Pharmingen	PE	gd-TCR	GL3	553178	0.20 mg/mL	0.25 ug/1.E+06 cells	1.25 uL
Southern Biotechnology Associates Inc	PE	CD69	H1.2F3	1715-09	0.50 mg/mL	0.13 ug/1.E+06 cells	0.25 uL
eBioscience	PE-Cy5	isotype	eBR2a	15-4321	0.20 mg/mL	0.05 ug/1.E+06 cells	0.25 uL
eBioscience	PE-Cy5	CD8a	53-6.7	15-0081	0.20 mg/mL	0.10 ug/1.E+06 cells	0.50 uL
eBioscience	PE-Cy5	CD80	16-10A1	15-0801	0.20 mg/mL	0.03 ug/1.E+06 cells	0.15 uL
eBioscience	PE-Cy5	MHC II	M5/114.15.2	15-5321	0.20 mg/mL	0.01 ug/1.E+06 cells	0.05 uL
eBioscience	PE-Cy5	TCR-b	H57-597	15-5961	0.20 mg/mL	0.13 ug/1.E+06 cells	0.65 uL
eBioscience	PE-Cy5.5	isotype	eBR2a	35-4321	0.20 mg/mL	0.05 ug/1.E+06 cells	0.25 uL
eBioscience	PE-Cy5.5	CD4	RM4-5	35-0042	0.20 mg/mL	0.10 ug/1.E+06 cells	0.50 uL
eBioscience	PE-Cy5.5	CD45R	RA3-6B2	35-0452	0.20 mg/mL	0.10 ug/1.E+06 cells	0.50 uL
eBioscience	PE-Cy7	isotype	eBR2a	25-4321	0.10 mg/mL	0.03 ug/1.E+06 cells	0.25 uL
eBioscience	PE-Cy7	CD8a	53-6.7	25-0081	0.20 mg/mL	0.25 ug/1.E+06 cells	1.25 uL
eBioscience	PE-Cy7	CD11c	N418	25-0114	0.20 mg/mL	0.25 ug/1.E+06 cells	1.25 uL
eBioscience	PE-Cy7	CD45	30-F11	25-0451	0.20 mg/mL	0.06 ug/1.E+06 cells	0.30 uL
eBioscience	PE-Cy7	CD49b	DX5	25-5971	0.20 mg/mL	0.25 ug/1.E+06 cells	1.25 uL
Biolegend	PE-Cy7	CD86	PO3	105115	0.20 mg/mL	0.13 ug/1.E+06 cells	0.65 uL
eBioscience	PE-Cy7	Streptavidin	n/a	25-4317	0.20 mg/mL	0.05 ug/1.E+06 cells	0.25 uL
eBioscience	unconjugated	IL-2	JES6-1A12	14-7022	0.50 mg/mL	2.00 ug/mL	4.00 uL
eBioscience	unconjugated	IL-4	11B11	14-7041	0.50 mg/mL	2.00 ug/mL	4.00 uL
eBioscience	unconjugated	IFN-g	AN-18	14-7313	0.50 mg/mL	2.00 ug/mL	4.00 uL
BD Pharmingen	unconjugated	CD3z	1z3A1	554241	0.50 mg/mL		0.00 uL
eBioscience	unconjugated	CD11c	N418	14-0114	0.50 mg/mL	1.00 ug/1.E+06 cells	2.00 uL
BD Pharmingen	unconjugated	CD16/32	2.4G2	01241A	0.50 mg/mL		0.00 uL
eBioscience	unconjugated	CD16/32	93	14-0161	0.50 mg/mL	0.25 ug/1.E+06 cells	0.50 uL
eBioscience	unconjugated	CD45R	RA3-6B2	14-0452	0.50 mg/mL	0.50 ug/1.E+06 cells	1.00 uL
BD Pharmingen	unconjugated	H-2Kk	36-7-5	06181D	0.50 mg/mL		0.00 uL
eBioscience	unconjugated	MHC I	34-1-2S	14-5998	0.50 mg/mL	1.00 ug/1.E+06 cells	2.00 uL
BD Pharmingen	unconjugated	H-2Dd	34-2-12	06131D	0.50 mg/mL		0.00 uL
		Ser-4					#DIV/0!
		ERTR9					#DIV/0!
Miltenyi Biotech	PE	PDCA-1	JF05-1C2.4.1	130-091-962			2.00 uL
eBioscience	unconjugated	GFP	polyclonal	14-6758	0.20 mg/mL		0.00 uL
Sigma	unconjugated	ERGIC		E1031	0.50 mg/mL	0.50 ug/1.E+06 cells	1.00 uL
Sigma	Biotin	anti-rabbit IgG	polyclonal	B7389	0.90 mg/mL	0.50 ug/1.E+06 cells	0.56 uL
eBioscience	APC	CD11b	M1/70	12-0112	0.20 mg/mL	0.25 ug/1.E+06 cells	1.25 uL
eBioscience	APC	MHC II	M5/114.15.2	15-5321	0.20 mg/mL	0.01 ug/1.E+06 cells	0.05 uL

Appendix B. CYTOKINES/CHEMOKINES

Cytokine/Chemokine	Biological Role	Cellular source(s) in CNS
Axl	BBB component, neuronal growth	Neurons, Vascular endothelium
bFGF	neuroprotective	Astrocytes, Microglia
CRG-2	T cell chemotactic, NK cell chemotactic	Astrocytes, Microglia
CTACK	T cell chemotactic	Unknown
CXCL16	T cell chemotactic	Astrocytes
Dtk	Neuronal growth	Neurons
Eotaxin	Eosinophil chemotactic	Unknown
Eotaxin-2	Eosinophil chemotactic	Unknown
Fas Ligand	Apoptotic	Glia, BBB, neurons
Fcγ RIIB	Antigen clearance	Microglia
Fractalkine	T cell chemotactic, monocyte chemotactic	Microglia
GM-CSF	Macrophage mitogenic	Astrocytes
HGF R	Leukocyte mitogenic	Microglia, Macrophages
IFN γ	Antiviral, T cell mitogenic	Microglia
IGFBP-2	Glucose regulation, growth inhibition	Astrocytes
IGFBP-3	Glucose regulation, growth inhibition	Astrocytes
IGFBP-5	Glucose regulation, growth inhibition	Astrocytes
IGFBP-6	Glucose regulation, growth inhibition	Astrocytes
IGF-I	Glucose regulation, general growth factor, neuroprotective	
IGF-II	Glucose regulation, general growth factor, neuroprotective	
IL-1 beta	Proinflammatory	Microglia
IL-10	Cytokine suppression, T cell inhibition	Microglia
IL-12 p40/p70	T cell mitogenic	Astrocytes, Microglia
IL-12 p70	T cell mitogenic	Astrocytes, Microglia
IL-2	T cell mitogenic	Microglia
IL-3	Eosinophil chemotactic, Granulocyte mitogenic, Monocyte mitogenic	Microglia
IL-6	T cell mitogenic	Astrocytes, Microglia
IL-9	T cell mitogenic	Astrocytes, Microglia
LIX	Granulocyte chemotactic	Unknown
L-Selectin	Adhesion	Vascular endothelium
Lymphotactin	T cell chemotactic	Unknown
MCP1	Macrophage chemotactic	Astrocytes, Microglia
MIG	T cell chemotactic	Microglia
MIP-1α	Neutrophil chemotactic	Astrocytes, Microglia
MIP-3α	T cell chemotactic	Astrocytes
MMP-2	BBB regulation	Microglia
MMP-3	BBB regulation	Microglia
Osteopontin	Monocyte-macrophage differentiation	Unknown
Pro-MMP-9	BBB regulation	Microglia
RANTES	T cell chemotactic, granulocyte chemotactic, monocyte adhesion,	Astrocytes, Microglia
SCF	Granulocyte chemotactic, Leukocyte mitogenic	Neurons
sTNF RI	Blocks TNF-α	Unknown
sTNF RII	Blocks TNF-α	Unknown
TARC	T cell maturation	Unknown

Cytokine/Chemokine	Biological Role	Cellular source(s) in CNS
TECK	Macrophage chemotactic, DC chemotactic, T cell maturation	Thymic DCs
Thymus CK-1	B cell chemotactic	Unknown
TNFα	Proinflammatory, antiviral	Astrocytes, Microglia
TPO	platelet differentiation	Unknown
VCAM-1	Adhesion	Vascular endothelium
VEGF	Adhesion	Vascular endothelium
VEGF R1	Adhesion	Vascular endothelium
VEGF R2	Adhesion	Vascular endothelium
VEGF R3	Adhesion	Vascular endothelium
VEGF-D	Adhesion	Vascular endothelium

Appendix C. COPYRIGHT INFORMATION FOR REPRINT OF PUBLICATION IN

DISSERTATION

**ELSEVIER LICENSE
TERMS AND CONDITIONS**

Apr 26, 2010

This is a License Agreement between Christina D Steel ("You") and Elsevier ("Elsevier") provided by Copyright Clearance Center ("CCC"). The license consists of your order details, the terms and conditions provided by Elsevier, and the payment terms and conditions.

All payments must be made in full to CCC. For payment instructions, please see information listed at the bottom of this form.

Supplier	Elsevier Limited The Boulevard,Langford Lane Kidlington,Oxford,OX5 1GB,UK
Registered Company Number	1982084
Customer name	Christina D Steel
Customer address	2511 E Little Creek #26
	Norfolk, VA 23518
License Number	2416790658463
License date	Apr 26, 2010
Licensed content publisher	Elsevier
Licensed content publication	Virology
Licensed content title	Peripheral dendritic cells are essential for both the innate and adaptive antiviral immune responses in the central nervous system
Licensed content author	Christina D. Steel, Suzanne M. Hahto, Richard P. Ciavarra
Licensed content date	25 April 2009
Volume number	387
Issue number	1
Pages	10
Type of Use	Thesis / Dissertation
Portion	Full article
Format	Print
You are an author of the Elsevier article	Yes
Are you translating?	No
Order Reference Number	
Expected publication date	May 2010
Elsevier VAT number	GB 494 6272 12
Permissions price	0.00 USD

Value added tax 0.0%	0.00 USD
Total	0.00 USD

Terms and Conditions

INTRODUCTION

1. The publisher for this copyrighted material is Elsevier. By clicking "accept" in connection with completing this licensing transaction, you agree that the following terms and conditions apply to this transaction (along with the Billing and Payment terms and conditions established by Copyright Clearance Center, Inc. ("CCC"), at the time that you opened your Rightslink account and that are available at any time at http://myaccount.copyright.com).

GENERAL TERMS

2. Elsevier hereby grants you permission to reproduce the aforementioned material subject to the terms and conditions indicated.

3. Acknowledgement: If any part of the material to be used (for example, figures) has appeared in our publication with credit or acknowledgement to another source, permission must also be sought from that source. If such permission is not obtained then that material may not be included in your publication/copies. Suitable acknowledgement to the source must be made, either as a footnote or in a reference list at the end of your publication, as follows:

"Reprinted from Publication title, Vol /edition number, Author(s), Title of article / title of chapter, Pages No., Copyright (Year), with permission from Elsevier [OR APPLICABLE SOCIETY COPYRIGHT OWNER]." Also Lancet special credit - "Reprinted from The Lancet, Vol. number, Author(s), Title of article, Pages No., Copyright (Year), with permission from Elsevier."

4. Reproduction of this material is confined to the purpose and/or media for which permission is hereby given.

5. Altering/Modifying Material: Not Permitted. However figures and illustrations may be altered/adapted minimally to serve your work. Any other abbreviations, additions, deletions and/or any other alterations shall be made only with prior written authorization of Elsevier Ltd. (Please contact Elsevier at permissions@elsevier.com)

6. If the permission fee for the requested use of our material is waived in this instance, please be advised that your future requests for Elsevier materials may attract a fee.

7. Reservation of Rights: Publisher reserves all rights not specifically granted in the combination of (i) the license details provided by you and accepted in the course of this licensing transaction, (ii) these terms and conditions and (iii) CCC's Billing and Payment terms and conditions.

8. License Contingent Upon Payment: While you may exercise the rights licensed immediately upon issuance of the license at the end of the licensing process for the transaction, provided that you have disclosed complete and accurate details of your proposed use, no license is finally effective unless and until full payment is received from

you (either by publisher or by CCC) as provided in CCC's Billing and Payment terms and conditions. If full payment is not received on a timely basis, then any license preliminarily granted shall be deemed automatically revoked and shall be void as if never granted. Further, in the event that you breach any of these terms and conditions or any of CCC's Billing and Payment terms and conditions, the license is automatically revoked and shall be void as if never granted. Use of materials as described in a revoked license, as well as any use of the materials beyond the scope of an unrevoked license, may constitute copyright infringement and publisher reserves the right to take any and all action to protect its copyright in the materials.

9. Warranties: Publisher makes no representations or warranties with respect to the licensed material.

10. Indemnity: You hereby indemnify and agree to hold harmless publisher and CCC, and their respective officers, directors, employees and agents, from and against any and all claims arising out of your use of the licensed material other than as specifically authorized pursuant to this license.

11. No Transfer of License: This license is personal to you and may not be sublicensed, assigned, or transferred by you to any other person without publisher's written permission.

12. No Amendment Except in Writing: This license may not be amended except in a writing signed by both parties (or, in the case of publisher, by CCC on publisher's behalf).

13. Objection to Contrary Terms: Publisher hereby objects to any terms contained in any purchase order, acknowledgment, check endorsement or other writing prepared by you, which terms are inconsistent with these terms and conditions or CCC's Billing and Payment terms and conditions. These terms and conditions, together with CCC's Billing and Payment terms and conditions (which are incorporated herein), comprise the entire agreement between you and publisher (and CCC) concerning this licensing transaction. In the event of any conflict between your obligations established by these terms and conditions and those established by CCC's Billing and Payment terms and conditions, these terms and conditions shall control.

14. Revocation: Elsevier or Copyright Clearance Center may deny the permissions described in this License at their sole discretion, for any reason or no reason, with a full refund payable to you. Notice of such denial will be made using the contact information provided by you. Failure to receive such notice will not alter or invalidate the denial. In no event will Elsevier or Copyright Clearance Center be responsible or liable for any costs, expenses or damage incurred by you as a result of a denial of your permission request, other than a refund of the amount(s) paid by you to Elsevier and/or Copyright Clearance Center for denied permissions.

LIMITED LICENSE

The following terms and conditions apply only to specific license types:

15. **Translation**: This permission is granted for non-exclusive world **English** rights only unless your license was granted for translation rights. If you licensed translation rights you may only translate this content into the languages you requested. A professional translator must perform all translations and reproduce the content word for word preserving the integrity of the article. If this license is to re-use 1 or 2 figures then permission is granted for

non-exclusive world rights in all languages.

16. **Website**: The following terms and conditions apply to electronic reserve and author websites:

Electronic reserve: If licensed material is to be posted to website, the web site is to be password-protected and made available only to bona fide students registered on a relevant course if:

This license was made in connection with a course,

This permission is granted for 1 year only. You may obtain a license for future website posting,

All content posted to the web site must maintain the copyright information line on the bottom of each image,

A hyper-text must be included to the Homepage of the journal from which you are licensing at http://www.sciencedirect.com/science/journal/xxxxx or the Elsevier homepage for books at http://www.elsevier.com , and

Central Storage: This license does not include permission for a scanned version of the material to be stored in a central repository such as that provided by Heron/XanEdu.

17. **Author website** for journals with the following additional clauses:

All content posted to the web site must maintain the copyright information line on the bottom of each image, and

he permission granted is limited to the personal version of your paper. You are not allowed to download and post the published electronic version of your article (whether PDF or HTML, proof or final version), nor may you scan the printed edition to create an electronic version,

A hyper-text must be included to the Homepage of the journal from which you are licensing at http://www.sciencedirect.com/science/journal/xxxxx , As part of our normal production process, you will receive an e-mail notice when your article appears on Elsevier's online service ScienceDirect (www.sciencedirect.com). That e-mail will include the article's Digital Object Identifier (DOI). This number provides the electronic link to the published article and should be included in the posting of your personal version. We ask that you wait until you receive this e-mail and have the DOI to do any posting.

Central Storage: This license does not include permission for a scanned version of the material to be stored in a central repository such as that provided by Heron/XanEdu.

18. **Author website** for books with the following additional clauses:

Authors are permitted to place a brief summary of their work online only.

A hyper-text must be included to the Elsevier homepage at http://www.elsevier.com

All content posted to the web site must maintain the copyright information line on the bottom of each image

You are not allowed to download and post the published electronic version of your chapter, nor may you scan the printed edition to create an electronic version.

Central Storage: This license does not include permission for a scanned version of the material to be stored in a central repository such as that provided by Heron/XanEdu.

19. **Website** (regular and for author): A hyper-text must be included to the Homepage of the journal from which you are licensing at http://www.sciencedirect.com/science/journal

/xxxxx. or for books to the Elsevier homepage at http://www.elsevier.com

20. **Thesis/Dissertation**: If your license is for use in a thesis/dissertation your thesis may be submitted to your institution in either print or electronic form. Should your thesis be published commercially, please reapply for permission. These requirements include permission for the Library and Archives of Canada to supply single copies, on demand, of the complete thesis and include permission for UMI to supply single copies, on demand, of the complete thesis. Should your thesis be published commercially, please reapply for permission.

21. **Other Conditions**: None

VITA

Christina Dawn Steel
May 2010

Address
Department of Microbiology & Molecular Cell Biology
Eastern Virginia Medical School
700 W. Olney Rd.
Norfolk, VA 23507

Areas of Interest
Teaching: Biology, Immunology, Microbiology, Biochemistry, Chemistry.

Education
Ph.D., Biomedical Sciences (2010) Eastern Virginia Medical School/ Old Dominion University, Norfolk, VA: Dissertation Title: Cellular Immunity in Mouse Models of Viral Encephalitis, Awarded May 2010
B.S., B.A., Biology, Foreign Language (2001) Radford University, Radford, VA

Teaching Experience
Tidewater Community College, Division of Mathematics and Sciences, Norfolk, VA (Spring 2009-Spring 2010) Adjunct Faculty. Taught Introductory Biology (101).
Old Dominion University, Department of Chemistry and Biochemistry, Norfolk, VA (Fall 2001-Fall 2003) Graduate Teaching Assistant. Taught Introductory Chemistry Laboratories (101-115).
Radford University, Supplemental Instruction, Radford, VA (Jan 1998-Spring 2001) Supplemental Instruction (SI) Assistant Supervisor. Trained and supervised SI leaders in relevant science courses, also served as a SI leader for Biology.

Research Experience
Eastern Virginia Medical School: 2004-2009, Graduate Research Assistant to Dr. Richard Ciavarra on Antiviral Immunity in Murine Models
Old Dominion University: 2002-2003, Graduate Research Assistant to Dr. X. Nancy Xu, on Multidrug Resistance in *Pseudomonas aeruginosa*

Selected Journal Publications
Ciavarra, R.P., et al. 2005. Impact of macrophage and dendritic cell subset elimination on antiviral immunity, viral clearance and production of type 1 interferon. Virology 342:177-89.
Ciavarra, R.P., et al. 2006. Evaluation of immunological paradigms in a virus model: are dendritic cells critical for antiviral immunity and viral clearance? J Immunol 177:492-500.
Steel, C.D., et al. 2008. Comparison of the lateral tail vein and the retro-orbital venous sinus as routes of intravenous drug delivery in a transgenic mouse model. Lab Anim (NY) 37:26-32.
Steel, C.D., S.M. Hahto, and R.P. Ciavarra. 2009. Peripheral dendritic cells are essential for both the innate and adaptive antiviral immune responses in the central nervous system. Virology 387:117-26.
Steel C, Kim W-K, Sanford L, Wellman L, Burnett S, Rooijen Nv, Ciavarra R. 2010. Distinct macrophage subpopulations regulate viral encephalitis but not viral clearance in the CNS. J Neuroimmunol *Accepted for Publication May 18, 2010.*